VIBRATION ANALYSIS OF NON-UNIFORM SHAFT-ROTOR SYSTEM

A THESIS SUBMITTED IN PARTIAL FULFILLMENT

OF THE REQUIREMENTS FOR THE DEGREE OF

MASTER OF TECHNOLOGY (RESEARCH)

IN

MECHANICAL ENGINEERING

BY

P. M. G. BASHIR ASDAQUE
611ME105

Under the guidance
Of

Prof. R. K. Behera

DEPARTMENT OF MECHANICAL ENGINEERING
NATIONAL INSTITUTE OF TECHNOLOGY
ROURKELA
2014

National Institute of Technology
Rourkela

CERTIFICATE

This is to certify that the thesis entitled, **"VIBRATION ANALYSIS OF NON-UNIFORM SHAFT-ROTOR SYSTEM"** submitted by **Mr. P. M. G. Bashir Asdaque** in partial fulfilment of the requirements for the award of ***Master of Technology (Res)*** degree in ***Mechanical Engineering*** with specialization in *Machine Design and Analysis* during session 2012- 2014 at the National Institute of Technology, Rourkela (Deemed University) is an authentic work carried out by him under my supervision and guidance. To the best of my knowledge, the matter embodied in the thesis has not been submitted to any other University / Institute for the award of any degree or diploma.

Prof. R. K. Behera

Date:

Dept. of Mechanical Engg.

Rourkela

National Institute of Technology

Rourkela, Odisha

Acknowledgement

I express my deep sense of gratitude and reverence to my thesis supervisor Dr. R. K. Behera, Associate Professor, Mechanical Engineering Department, National Institute of Technology, Rourkela, for introducing the topic and giving me an opportunity to conduct the present work under his guidance. His invaluable encouragement, helpful suggestions and supervision throughout the course of this work and providing valuable department facilities helped me a lot for the completion of this thesis.

I express my sincere thanks to Prof. S. K. Sarangi, Director, NIT Rourkela for creating healthy environment in the campus and giving freedom to use the facilities available in the institute for this study.

I would like to thank Prof. K. P. Maity, Head of the Department, Prof. T. Roy, Prof. H. Roy, Prof. J. Srinivas, Prof. S. K. Panda and other faculty and staff members of the department for their help and cooperation for completing the thesis.

I would also like to thank Mr. Alok Biswal, Mr. Pavan Kishore, Mr. Alok Jha, Mr. Irshad Khan, Mr. Jakeer Shaikh, Mr. Sourabh Chandrakar, Mr. Raj Kamal, Mr. Abhinav Khare and well-wishers who are involved directly or indirectly in successful completion of the present work.

I would like to thanks my parents for their strong support and encouragement without which the thesis would not have reached the complete stage.

Last but not the least I would like to thank my fellow post graduate friends and seniors who are involved directly or indirectly in my endeavour.

(P. M. G. Bashir Asdaque)

ABSTRACT

Rotor dynamics is the study of the behaviour of the machines resulting from excitations originating from its rotating elements, and has a very important role to play throughout the fast-growing mechanical and industrial world. Shafts or circular cross-section beams are important parts of rotating systems and their geometries play important role in rotor dynamics. Therefore, there is a need to consider the dynamic characteristics of special shaft-rotor systems with disks and shafts whose radii are functions of their length. The procedures for the determination of the deflection slope, shear force and bending moment at the extremities of the shaft are used and the dynamics of shaft-rotor system are considered. Conventional frequency response method is used for the computation of resonance, critical speed or whirling frequency. For particular lengths and rotational speeds, the response of the system is determined for the establishment of the dynamic characteristics. Several types of such shaft-rotors are analysed as examples. Hollow tapered shaft-rotors with uniform thickness and uniform bore are also considered.

Critical speeds or whirling frequency conditions are computed using transfer matrix method and then the results are compared with the results obtained using FEA. A dynamic model of the profiled shaft-rotor system is presented. The equation of motion of the rotating non-uniform shaft is derived using Lagrangian approach together with the finite-element method. The shaft-rotor components with circular cross-section are discretized into a number of finite shaft elements with 8 degrees of freedom each. Euler-Bernoulli beam theory has been used for both the methods. For particular shaft-lengths and rotating speeds, response of the hollow-tapered shaft-rotor system is determined for the establishment of dynamic characteristics. Effects of shaft lengths and rotational speeds on frequency response are shown by bode plots. Step responses of the systems are also plotted simultaneously.

Contents

LIST OF TABLES

LIST OF FIGURES

Nomenclature

English Symbols

C(x)	Compliance per unit of length (function)
L(x)	Inertia per unit of length (function)
L	Length of shaft
E	Modulus of elasticity
F(s)	System model matrix
$M_y(x, s)$	Bending moment in x–y plane (function)
$Q_y(x, s)$	Shear force (function)
Y(x, s)	Vertical deflection of shaft (function)
I(x)	Mass moment of inertia (function)
J	Shaft polar moment of inertia
R_0	Beginning radius of the shaft element
R_i	Inner radius of the shaft element
R_1	End radius of the shaft element
m	Mass of the disk attached at free end
$[M]$	Mass matrix
$[G]$	Gyroscopic matrix
$[K]$	Stiffness matrix
$[M_d^T]$	Translational mass matrix for disk
$[M_d^R]$	Rotational mass matrix for disk
$[G_d]$	Gyroscopic matrix for disk
$[M_e^T]$	Translational mass matrix for shaft element
$[M_e^R]$	Rotational mass matrix for shaft element
$[G_e]$	Gyroscopic matrix for element
$[K_e]$	Stiffness matrix for shaft element
$[Q^e]$	External force matrix
$A(x)$	Cross-sectional area (function)
$I_D(x)$	Diametral inertia (function)
$I_P(x)$	Polar inertia (function)

Greek Symbols

ρ	Material density
Ω	Shaft–rotor rotational speed
Γ(s)	Wave propagation factor (function)
$[\phi]$	Rotational shape function matrix
ω	Rotational speed in rpm
Θ(x, s)	Slope of the shaft (function)
[Ψ]	Matrix of translation displacement
[Φ]	Matrix of rotation displacement

Subscripts

p	profiled
n	non-uniform bore
u	uniform bore
T, t	translational
R, r	rotational
d	disk

Superscripts

e	element
s	system

CHAPTER-1

INTRODUCTION

1.1 Background

Rotor dynamics [1] is the study of the behaviour of the machines resulting from excitations originating from its rotating elements. It plays a very important role throughout the fast-growing mechanical and industrial world. This is different from structural vibrations analysis because of the gyroscopic moments, and the possibility of whirling instability. Rotating machinery find its applications in turbo-machines, power stations, machine tools, automobiles and aerospace. The interaction of the rotating machines with their surroundings is of great importance due to the fact that if these machines are not operating at the correct speeds, vibration may occur and ultimately cause failure of the machines. Shaft is a major component of any rotating system, used to transmit torque and rotation. Hence the study shaft-rotor systems have been the concern of researchers for more than a century, and will continue to persist as an active area of research and analysis in near future. Geometry of shaft is of the main concern during the study of any rotating system. Most research work related to shaft-rotor systems considered uniform cylindrical shaft elements for study and analysis of rotating systems.

Many investigations in linear rotor dynamics deal with the problems of unbalance, natural and transient vibrations. Analytical methods can be used to analyse the simple shaft-rotor systems. . In this regard, transfer matrix method (TMM) has been widely used. Whalley and Ameer [2] used frequency response analysis for profiled shafts to study dynamic response of distributed-lumped shaft rotor system. They studied the system behaviour in terms of frequency response for the shafts with diameters which are functions of their lengths. They derived an analytical method which uses Euler-Bernoulli beam theory in combination with TMM. However, complex shaft-rotor systems normally used in plants and industries are not amenable to exact analysis. Therefore, it is necessary to follow some approximate methods to study the dynamic behaviour of complex rotor systems. Powerful approximation methods, such as the finite element method, are available for analysing complex structures.

Frequency response of any rotating machine is influenced by many vital parameters such as; shaft geometry including length, hollowness, rotor-speed etc.

1.2 Motivation and Objective

The geometry of shaft plays very important role in dynamic analysis of shaft-rotor systems. Most of the papers on rotor dynamics consider linear shaft with uniform cylindrical geometry.

The present work focuses on non-uniform shaft-rotors. Objective of this work is to find the frequency response of shaft-rotor systems where shafts' radii are functions of their lengths, i.e., the cross-sectional area will change continuously with increasing shaft-rotor-length. Euler-Bernoulli beam theory has been considered for the shaft vibration analysis. Multi-disk, multi-profiled including convergent-divergent type of shaft, hollow profiled and hollow tapered shaft-rotor systems are analysed here. Numerical examples are provided for better understanding and general applicability of TMM and FEM. Effects of rotational speeds, shaft length and hollowness are also discussed.

Shafts are the important parts of the rotating machines and are employed hugely in aeronautics, industries and power plants. Shaft geometry is one of the vital parameters that affect the response of the shaft-rotor system. In the present work, axisymmetric non-uniform shafts are considered. The shafts' radii are the function of their lengths, and hence the cross-section varies according to the length of the shaft. The main purpose of the present work is to study different such shaft-rotor systems with respect to the shaft lengths and rotor speeds and their effects on the response of the system.

1.3 Transfer matrix method (Myklestad-Prohl Technique)

A general method that can be used for computation of frequency response of uniform and variable stiffness was developed by N.O Myklestad and M.A Prohl [3, 4]. The method was initially developed for uncoupled bending vibrations, but later it was extended for coupled and uncoupled problems. In present research Myklestad method will be developed for computation of frequency response of members with variable stiffness.

Myklestad method can be thought of as an extension to the Holzer method that is used for the solution of torsional vibration problems. However, solution of flexural vibration

problems is difficult since it involves computation of four elastic parameters namely deflection, slope, bending moment and shear force for each length segment of the shaft.

1.4 Frequency Response

The term frequency response refers to steady state response of a system for a given input. The response of the system is analysed over a certain range of shaft speeds resulting in magnitude and phase with frequency. The response of a given system can be studied for different configurations by varying the system parameters. The transfer function that gives the relation between input (force) and output (displacement), is a complex quantity and can be represented by magnitude and phase angle with frequency (shaft rotational speed). In the current work Bode plot technique is used to obtain the response from the given transfer function. Bode diagram is represented by two plots, one giving magnitude versus frequency and the other the phase angle versus frequency. Both the diagrams are plotted on logarithmic scale. The unit of magnitude is generally dB (decibel) and that of phase in degree.

1.5 Laplace Transform

Partial and ordinary differential equations describe certain quantities which vary with time, such as the current in electrical circuit, the oscillations of vibrating members, flow of pipes or heat conduction through conductor. These equations are generally coupled with initial and boundary conditions that describe the state of system at time t=0.
A powerful technique for solving these engineering problems is the use of Laplace transform, which transforms the original differential equation into elementary algebraic equations. Later this can then be simply transformed once again into the solution of the original problem. This technique is generally known as the "Laplace transform method."

1.6 Finite element method

The main rule that involved in finite element method is "divide and analyse". The greatest unique feature which separates finite element method from other existing methods is "it divides the given domain into a set of sub domains, called finite

elements". Any geometric shape that allows the computation of the solution or its approximation, or provides necessary relations among the values of the solution at selected points called 'nodes' of the sub domain, qualifies as finite element. Division of the domain into elements is called mesh. Approximate solutions of these finite elements give rise to the solution of the given geometry which is also an approximate solution.

The approximate solution can only become exact when

1. Division of the given domain into infinite number of sub domains or elements
2. The expression for the primary variable must contain a complete set of polynomials (infinite terms).

1.7 Outline of the thesis

The research presented in this thesis gives a framework on the study of the shaft-rotors with non-uniform geometries. The investigation as outlined in this thesis is broadly divided into six chapters. The thesis work is outlined as follows;

Chapter 1: This chapter gives a brief introduction to the thesis work and summarizes the importance, motivation of the present investigation.

Chapter 2: This chapter contains detailed relevant literature review on various aspects of vibration analysis of shaft-rotor systems. Most of the earlier and present vital researches carried out by various scientists and researchers have been represented in details. This chapter is divided into different sections emphasizing; transfer matrix method for vibration analysis, Finite element approach in rotor dynamics, various configurations of shaft-rotors including hollowness and research work done on non-rotating non-uniform beams.

Chapter 3: This chapter elaborates a complete description of the transfer matrix method for frequency response computations of the non-uniform shaft-rotors used by Whalley and Ameer [2]. Complete matrix expressions and hence the computation of transfer function is explained in detail.

Chapter 4: This chapter outlines the details of the finite element approach on vibration analysis of non-uniform shaft-rotors. Element matrices formulation is presented in detail. Lagrangian approach is used as governing equation.

Chapter 5: This chapter elaborates the detailed discussions on the results obtained from the analytical approach of Whalley and Ameer [2] and finite element analysis as outlined in chapters 3 and 4. The theoretical expression for different arrangements and configurations of the shaft-rotor systems has been found out by considering different shaft profile values, shaft lengths and rotor speeds. Further, method has been extended for finding frequency response of hollow shaft-rotors. Step responses for such systems are also plotted. Numerical example on hollow tapered shaft has been presented for ease of understanding. The results obtained are compared with the results of Whalley and Ameer [2].

Chapter 6: This chapter summarizes the important conclusions drawn from the observations discussed in the chapter 5 along with some suggestions for applying the present work in various fields of real applications. This chapter also contains the scope for further research work.

CHAPTER-2

LITRETURE REVIEW

2.1 Introduction

Rotating machines began manufacturing in significant numbers concurrently with the development hydraulic power in the early 1800s and steam turbines in late 1800s. The first dynamics problem encountered was critical speed where the vibration produced by rotor unbalance is magnified by resonance with the first natural frequency of the system. Rankine analysed the critical speed phenomenon in 1869 and it was only partially correct. The resulting design philosophy was to keep running speeds below the first critical speed. Rotor dynamics and stability of shaft-rotor systems has been the concern of engineers and scientists for more than a century, and it will continue to persist as an active area of research and study in coming future. Shaft geometries are one of the basic concerns for the researchers. Jeffcott [5] provided a very basic model of a shaft-rotor system. Initially, he made three assumptions for his model: (i) Zero damping is associated with the rotor, (ii) Axially symmetric rotor, and the important one is (iii) The rotor carries a point mass. Later, the model was expanded to take care of damping. In general, two methods, namely transfer matrix method and finite element method are used for vibration analysis of shaft-rotor systems. Dunkerley [6] published an article in which he showed the whirling speeds of a uniform shaft rotating on simple supports are same as its natural frequencies of lateral vibration. Dunkerley suggested that any unbalance of rotating shaft would excite the natural frequencies to produce critical speeds with large, synchronous whirling amplitudes. Dunkerley gave a simple formula for calculating whirling speeds of shafts with several disks spaced at different locations along the length of the shaft. The formula neglects the effect of gyroscopic moments, but still it was being used in some machine design textbooks in late 1960s. Dunkerley's formula is given by,

$$\frac{1}{\omega_{cr}^2} = \frac{1}{\omega_1^2} + \frac{1}{\omega_2^2} \tag{2.1.1}$$

where ω_1 and ω_2 are the whirl speeds of the shaft with disks 1 and 2 alone, respectively, and ω_{cr} is the critical speed with all disks installed. The literature reviewed in this chapter are grouped into three sections namely,

- Transfer matrix method as a tool for vibration analysis,
- Finite element method as a tool for vibration analysis, and
- Vibration analysis of non-rotating non-uniform beams.

2.2 Transfer matrix method as a tool for vibration analysis

Basic idea of transfer matrix method was first put forth by Holzer for finding natural frequencies of torsional systems. Later it was adapted by Myklestad [3,7] for computing natural frequencies of airplane wing, coupled in bending and torsion. In this approach the shaft is divided into a set of longitudinal sections with the distributed mass of each, concentrated at the section end. Thereafter, the boundary conditions for the bending moment–shear force and inertia loading are equated until parity is achieved, again by way of iteration. This resolution identifies the critical speed in that this is the only possible origin for the maximisation of the deflection, in the absence of additional external loading. Prohl [4] applied it to rotor-bearing systems and included gyroscopic moments in his computations. Lund [8] used complex variables as the next significant advancement in the method and showed it could be applied to more general formulations of bearing forces. Lund showed how system damping could be accounted for including self-exciting influences, such as oil whip and internal frictions. From the above developments, the method came to be known as "The Transfer Matrix Method" (TMM). The design of shaft-rotor systems includes computation of the critical or whirling speed, which is an essential design parameter. Whenever the critical frequency is found, the operational conditions below the lowest or fundamental critical are normally considered. An improved method for calculating critical speeds and rotor stability of turbo machinery is investigated by Murphy and Vance [9]. In their work, they shown that complex variable can be employed in transfer matrix programs when damping and cross coupling are included in rotor bearing system and it may lead to loss of accuracy in the computation of critical speeds. They show that by rearranging the calculations performed in transfer matrix program, one can derive characteristic polynomial for a complex rotor-bearing. A mathematical model, developed by Marhomy *et al*. [10] in which method of R-H stability criterion was applied to both the characteristics equations of the translational and rotational modes of motion and the stability regions were represented graphically. Hsieh *et al.* [11] developed a modified

transfer matrix method for analysing the coupling lateral and torsional vibrations of the symmetric rotor-bearing system with an external torque. They modelled rotating shaft as Timoshenko beam and considered a continuous system concept rather than the conventional "lumped system" concept.

Whalley and Ameer [2] used frequency response analysis for profiled shafts to study dynamic response and transient response of distributed-lumped shaft rotor system. They studied the system behaviour in terms of frequency response for the shafts with diameters which are functions of their lengths. They derived an analytical method which uses Euler-Bernoulli beam theory in combination with transfer matrix method (TMM). Frequency response and transient response of the system for an impulse of 1N is determined in terms of critical speed for various values of shaft speed and shaft lengths by minimising mass, inertia etc.

2.3 Finite element method as a tool for vibration analysis

On the other hand, there are large number of numerical applications of finite element techniques for the calculation of whirling and the computation of maximum dynamic magnitude. In this regard, Ruhl and Booker [12] modelled the distributed parameter turbo rotor systems using a finite element method (FEM), which may be considered as the beginning of finite element modelling in rotor dynamics. Thorkildsen [13] was the first to include rotary inertia and gyroscopic moments in the finite element model. Nelson and McVaugh [14] reduced large number of eigenvalues and eigenvectors identified, following finite element analysis, and the erroneous modes of vibration predicted were eliminated. Nelson [15] again formulated the equations of motion for a uniform rotating shaft element using deformation shape functions developed from Timoshenko beam theory including the effects of translational and rotational inertia, gyroscopic moments, bending and shear deformation and axial load. Chen and Ku [16] used a three nodal C ° Timoshenko beam finite element to analyse the natural whirl speeds of a rotating shaft with different end conditions. The Timoshenko model was extended by Ozguven and Ozkan [17] to include effects such as transverse and rotary inertia, gyroscopic moments, axial load, internal hysteretic, viscous damping, and shear deformations in a single model. Zorzi and Nelson [18] provided a finite element model for a multi-disk rotor bearing system. The model was based on Euler-Bernoulli beam

theory. Rouch and Kao [19] presented a comprehensive approach to the linearized analysis of rotor-bearing systems including matrix reduction techniques; to accurately assess the dynamic behaviour of a rotor-bearing system for four type of analysis namely undamped critical speed, synchronous response, damped eigen value or stability analysis and transient integration of system equations. Kim and Lee [20] developed a powerful matrix reduction technique to analyse rotor-bearing systems by using the modal data of the isotropic undamped stationary parts, which gives significant reductions in computation time and core size. Kalita and Kakoty [21] studied the dynamic behaviour of Timoshenko beam supported on hydrodynamic bearings incorporating internal damping using finite element model. Khulief and Mohiuddin [22] developed a finite element dynamic model for a rotor-bearing system. The model included gyroscopic moments and anisotropic bearings. Reduced order model using modal truncation was obtained. Khulief and Al-Naserb [23] derived equation of motion of the rotating drill string using Lagrangian approach together with the finite-element method. The drill string components with circular cross-section were discretized into a number of finite shaft elements with 12 degrees of freedom each. Modal transformations were invoked to obtain a reduced order modal form of the dynamic equations. They integrated developed model into a computational scheme to calculate the modal characteristics and to perform time-response analysis of the drill string system. Forrai [24] studied the stability analysis of symmetrical rotor bearing systems with internal damping by using finite element method. By the analysis, it was proved that the whirling motion of the rotor system becomes unstable at all speeds beyond the critical speed of instability. It was found that the rotor stability is improved by increasing the damping provided in the bearings. Aleyassin [25, 26] worked on computation of irrational characteristic determinant of the system model by the dynamics stiffness matrix method (DSMM). He compared the results obtained to the transfer matrix method (TMM) and discussed about the accuracy of the results. Aleyassin proved the equivalence of the characteristic determinant in TMM and the DSMM and clarified that TMM is more accurate method. Various papers were published for conical or tapered shaft-rotors. Lee *et al.* [27] investigated the forced response analysis of an undamped distributed parameter rotating shaft by using a modal analysis technique. Their shaft model included rotary inertia and gyroscopic effects, and various boundary conditions. They presented a study of the resulting non-self-adjoint eigenvalue problem and its characteristics in the case of rotor dynamics. In

addition to the modal analysis, they applied the Galerkin's method to analyse the forced response of an undamped gyroscopic system. Both methods were illustrated in a numerical example and the results are compared and discussed. Katz *et al.* [28] investigated the dynamic behaviour of a rotating shaft subjected to a constant velocity moving load. The Euler-Bernoulli, Rayleigh and Timoshenko beam theories were used to model the rotating shaft. The modal analysis method and an integral transformation method were employed in their study, for the case of a shaft with simply supported boundary conditions. The influence of parameters such as rotational speed of the shaft, the axial velocity of the load and the dimensions of the shaft were discussed for each shaft model. The results were presented and compared with then available solutions of a non-rotating beam subjected to a moving load. Katz [29] investigated the dynamic response of a rotating shaft subjected to an axially, constant-velocity, moving and rotating load. He studied the dynamic behaviour of high-speed linear bearings. Considering slender shaft, they used Rayleigh beam theory to model the rotating shaft. Modal analysis and integral transformation methods were employed to develop analytical expressions for the transient response of the shaft with simply supported boundary conditions. Numerical results were presented, discussed and compared with the then available solutions. They observed that by changing model parameters, it is possible to describe dynamic behaviour of different types of linear bearings and other mechanical elements. Ku [30] presented a C^0-class Timoshenko beam finite element model to analyse the dynamic characteristics of a rotor-bearing system with internal damping. Numerical results were compared with the then published works in order to demonstrate the accuracy of finite element model of the rotor-bearing system. His findings indicated that hysteretic internal damping results in the destabilisation of forward precessional modes at all spin speeds, whereas viscous internal damping results in the destabilisation of forward precessional modes only when the spin speed becomes higher than the critical speed. He observed that for any kind of internal damping, the backward precessional modes are always stable. Greenhill *et al.* [31] derived equation of motion for a conical beam finite element form Timoshenko beam theory and include effects of translational and rotational inertia, gyroscopic moments, bending and shear deformation, axial load and internal damping. Genta and Gugliotta [32] analysed element with hollow or annular cross-section based on Timoshenko beam theory having two degrees of freedom at each node. Agostini and Souza [33] worked on the vibration analysis of vertical rotors including gravitational and gyroscopic effects. They obtained

forward and backward modes separately through the implementation in MATLAB of complex modal analysis in conjunction with the finite elements method. They compared numerical simulations with the existing literature and found it to be satisfactory. Gmur and Rodrigues [34] presented the first forward and backward natural frequencies of a hollow tapered shaft with simply supported conditions rotating at 10000 rpm. Mohiuddin and Khulief [35] derived equations of coupled bending and torsional motion of the rotating shaft using the Lagrangian approach. They derived conical beam finite element for vibration analysis of rotating shafts including shear deformations and rotary inertia. The finite beam element has ten degrees of freedom and accounts for linear tapering. Explicit expressions for the element mass, stiffness, and gyroscopic matrices are derived using consistent mass formulation. They compared their findings with exact solutions, and with other numerical results available in the literature. Again Mohiuddin and Khulief [36] derived a finite element model of a tapered rotating cracked shaft for modal analysis and dynamic modelling of a rotor-bearing systems, based on Timoshenko beam theory i.e., included shear deformation and rotary inertia. Edney *et al* [37] developed two tapered beam finite elements as part of a study of the shock response of rotor-bearing systems. In one of the finite element, a linear approximation is used for the geometrical properties yielding closed form expressions for the element matrices. Scaling factors are also incorporated to compensate for errors introduced by the linear approximation. While for other element, exact expressions are used with a numerical integration. They included translational and rotational inertia, gyroscopic moment, axial torque, shear deformation, viscous and hysteretic material damping and mass eccentricity for analysis. They proved that applied torque has little effect on the predicted whirl speeds unless the rotor is very slender. However, it has a destabilizing effect on some of the modes. Many examples on dynamics and vibration analyses are provided in [38, 39, and 40].

2.4 Vibration analysis of non-rotating non-uniform beams

Many researchers carried out vibration analysis of non-rotating non-uniform shafts. Mehmet *et al.* [41] investigated an isotropic beam which has a variable cross-section. They reduced the governing equation to an ordinary differential equation in spatial coordinate for a family of cross-section geometries with exponentially varying width. Three different types of boundary conditions associated with simply supported,

clamped and free ends were applied and studied. Results show that the non-uniformity in the cross-section influences the natural frequencies and the mode shapes. Tong *et al.* [42] presented an analytical solution for free and forced vibrations of non-uniform Timoshenko beams. As an approximation the non-homogeneous beam with variable cross-section is replaced by a number of homogeneous stepped beams with constant cross-section. They also proved that as the number of the stepped beams increases the results converge to the exact solutions of the original beams.

Abrate [43] presented an efficient procedure to analyse the free vibration of non-uniform beams with general shape and arbitrary boundary conditions. He presented simple formulas for predicting the fundamental natural frequency of non-uniform beams with various end support conditions. The natural frequencies are determined by solving a simple transcendental equation. Rosa and Auciello [44] examined the dynamic behaviour of beams with linearly varying cross-section, in the presence of rotationally and axially flexible ends. The equation of motion is solved in terms of Bessel functions. Attarnejad *et al.* [45] introduced new functions, namely basic displacement functions (BDFs) and studied free transverse vibration of non-prismatic beams from a mechanical point of view. They developed dynamic shape functions in terms of BDFs. The new shape functions developed by them were dependent on the circular frequency, configuration of the element and physical properties such as mass density and modulus of elasticity. Differential transform method was employed to obtain BDFs via solving the governing differential equation for transverse motion of non-prismatic beams. They carried out free vibration analysis for five numerical examples including beams with linear mass and inertia, linear mass and fourth order inertia, second order mass and fourth order inertia, tapered beam with non-classical boundary conditions and exponentially varying area and inertia. It was observed that the results were in good agreement with the previously published ones in the literature. Grossi and Bhat [46] presented a note which dealt with the approximate determination of frequency coefficients of linearly tapered beams with ends elastically restrained against rotation, using two approaches namely the modified Rayleigh-Schmidt method and the characteristic orthogonal polynomials method. They concluded that the use of a set of orthogonal polynomials in the Rayleigh-Ritz method is a quite simple procedure, and provides not only the determination of the values of the fundamental frequency coefficient but also the values corresponding to higher modes. Auciello and Ercolano [47] determined the free-vibration frequencies of tapered beams in the most general

possible boundary conditions by means of direct method. Their study was extended to beams, made up of two sections with different cross-sectional variations. The equations of motion were solved by means Ressel function. The natural frequencies were determined using the false position method and symbolic program as roots of the corresponding characteristic equations. Klein [48] investigated the free vibrations of elastic beams with non-uniform characteristics theoretically by a new method. He combined the advantages of finite element approach and of Rayleigh-Ritz analysis. He compared the results with the known analytical results for uniform beams and found good convergence of the method for natural frequencies and modes. He observed that for internal shear forces and bending moments, rate of convergence is less rapid. He conducted experiments with a cantilevered helicopter blade with strong non-uniformities. The theory developed by him adequately predicts natural frequencies and mode shapes. Lee *et al.* [49] developed and presented a systematic solution theory for the non-uniform Euler- Bernoulli beam vibration, including forced and free vibrations, with general elastically restrained boundary conditions. The frequency equation and the dynamic forced response, in closed integral form, are expressed concisely in terms of the fundamental solutions of the system. Lee and Ke [50] presented a simple and efficient method to study the problem of free vibration of a non-uniform Euler-Bernoulli beam with general elastic restraints at boundary points. They derived frequency equation and expressed in concise form, with one set of particularly chosen fundamental solutions of the system. They found that if the closed form fundamental solutions of the system are not available, the approximate fundamental solutions can be obtained through the newly developed algorithm shown to be efficient, convenient and accurate. Finally, they examined several limiting cases of the general system. Laura *et al.* [51] obtained an approximate solution of free and forced vibrations of beams of non-uniform cross-section by using Rayleigh's optimization technique where the mechanical system subjected to harmonic loading is symmetric. They also assumed that the beam is subject to an axial force and presented the results for the buckling problem as well. They compared the analytically determined eigen values with values calculated by the finite element method. Zheng *et al.* [52] analysed the vibration of a multi-span non-uniform beam subjected to a moving load by using modified beam vibration functions as the assumed modes, based on Hamilton’s principle. They presented numerical results for both uniform and non-uniform beams under moving loads of various velocities. They, from examples, observed that this method converges very quickly and good

results are obtained. Dugush and Eisenberger [53] investigated the dynamic behaviour of multi-span non-uniform beams transverse by a moving load at a constant and variable velocity. The continuous beam is modelled using Euler-Bernoulli beam theory. The solution was obtained by using both the modal analysis method and the direct integration method. They obtained the natural frequencies and mode shapes exactly by deriving the exact dynamic stiffness matrices for any polynomial variation of the cross-section along the beam using the exact element method. They expressed mode shapes as infinite polynomial series. They presented numerical examples in order to demonstrate the accuracy and the effectiveness of their study, and the results were compared to previously published results. Esmailzadeh and Ohadi [54] presented two sets of governing equations for transverse vibration of non-uniform Timoshenko beam subjected to both the axial and tangential loads. For the first set, the axial and tangential loads were taken perpendicular to the shearing force, i.e., normal to the cross-section inclined at an angle, while for the second set, the axial force is considered to be tangential to the axis of the beam-column. For each case, there existed a pair of differential equations coupled in terms of the flexural displacement and the angle of rotation due to bending. The two coupled second order governing differential equations were combined into one fourth order ordinary differential equation with variable coefficients. They presented several illustrative examples of uniform and non-uniform beams with various boundary conditions such as clamped supported, elastically supported, and free end mass and pinned end mass. They also investigated the stability analysis for the variation of the natural frequencies of the uniform and non-uniform beams with the axial force. Li [55] proposed an exact approach for free vibration analysis of a non-uniform beam with an arbitrary number of cracks and concentrated masses. He adopted a model of massless rotational spring to describe the local flexibility induced by cracks in the beam. He developed the fundamental solutions and recurrence formulas for determining the mode shape function of vibration of a non-uniform beam with an arbitrary number of cracks and concentrated masses. The main advantage of Li's proposed method is that the eigen value equation of a non-uniform beam with any kind of two end supports, any finite number of cracks and concentrated masses can be conveniently determined from a second order determinant. He observed that the decrease in the determinant order as compared with previously developed procedures leads to significant savings in the computational effort and cost associated with dynamic analysis of non-uniform beams with cracks. He presented numerical

examples to illustrate their proposed method and to study the effect of cracks on the natural frequencies and mode shapes of cracked beams. Kumar and Sujith [56] presented the exact analytical solutions for the longitudinal vibration of rods with non-uniform cross-section. They reduced the equation of motion of axial vibration of a rod with varying cross-section using appropriate transformations to analytically solvable standard differential equations whose form depends upon the specific area variation. They obtained the Solutions for a rod with a polynomial area variation and for a sinusoidal rod. The solutions were obtained in terms of special functions such as Bessel and Neumann as well as trigonometric functions. Simple formulas to predict the natural frequencies of non-uniform rods with various boundary conditions were presented. The natural frequencies of non-uniform rods for several end conditions were calculated, and they discussed their dependence on taper. Li [57] presented an exact approach for free longitudinal vibrations of one-step non-uniform rods with classical and non-classical boundary conditions. He expressed the expression for describing the distribution of mass is arbitrary, and the distribution of longitudinal stiffness as a functional relation with the mass distribution and vice versa. Using appropriate functional transformation, the governing differential equations for free vibrations of one-step non-uniform rods were reduced to analytically solvable differential equations for several functional relations between stiffness and mass. He derived the fundamental solutions that satisfy the normalization conditions and used them to establish the frequency equations for one-step rods with classical and non-classical boundary conditions. He proposed a new exact approach for determining the longitudinal natural frequencies and mode shapes of multi-step non-uniform rods using the fundamental solutions of each step rod and a recurrence formula developed by him. Li demonstrated with the help of numerical examples that the calculated longitudinal natural frequencies and mode shapes are in good agreement with the experimental data and those determined by the finite element method. Irie *et al.* [58] presented an analysis for the vibration and stability of a non-uniform Timoshenko beam subjected to a tangential follower force distributed over the centre line by use of the transfer matrix approach. For this purpose, the governing equations of a beam were written in a coupled set of first-order differential equations by using the transfer matrix of the beam. After the matrix has been determined by numerical integration of the equations, they obtained the eigen values of vibration and the critical flutter loads. They applied this method to beams with linearly, parabolically and exponentially varying depths, subjected to a concentrated, uniformly distributed or

linearly distributed follower force, and the natural frequencies and flutter loads were calculated numerically, from which they studied the effects of the varying cross-section, slenderness ratio, follower force and the stiffness of the supports on them.

2.5 Summary

Most of the previous research work deals with vibration analysis of rotating uniform cross-section shafts and non-rotating non-uniform beams. Objective of the present work is to compute the frequency response for the rotating shafts whose radii are the functions of their length. Bode plots for such shaft-rotor systems, including profiled, multi-disk, multi-profiled and hollow tapered shaft-rotors are found by TMM approach and are compared with the results found from the FEM approach, specially focussing on the effects of shaft-lengths and rotor-speeds. The TMM approach is discussed in chapter-3.

CHAPTER-3

THEORETICAL ANALYSIS BY TRANSFER MATRIX APPROACH

3.1 Introduction

Transfer matrix method or the Myklestad-Prohl technique is an approach to matrix structural analysis that uses a mixed form of the element force-displacement relationship and transfers the structural behaviour parameters and the joint forces and displacement from one end of the structures to other. The best advantage of transfer matrix method is that it produces system of equations to be solved that are quite small in comparison with those produced by the stiffness method. However, the disadvantage is the extensive sequence of operations that are required on a small matrix.

The transfer-matrix method is used whenever there is any possibility that the total system can be broken into a sequence of subsystems that interact only with adjacent subsystems. This method is suitable for line structures such as arches, cables and beams.

For implementing the transfer matrix method, we need a relationship that gives the state of forces and displacements at one end of the element in terms of force and displacement at the other.

3.2 Mathematical Formulation

The system represents distributed lumped model of cantilever shaft carrying rigid disk at its end. Consider a profiled shaft of length ‘l’ is loaded with a concentrated harmonic force and impulse of 1N at its end as shown in the Fig. 3.1.

The cross section area of the shaft is A(x) which is a function of its length. Consequently the stiffness and moment of inertia of the shaft varies with the length. Its young’s modulus is ‘E’ and ‘m’ be the mass per unit length of the shaft.

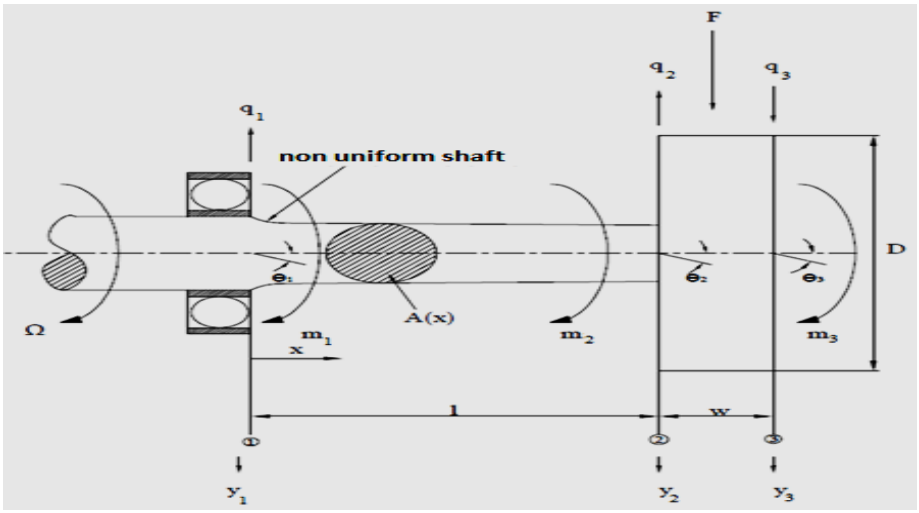

Fig. 3.1 A cantilever non-uniform shaft-rotor system subjected to external excitation at its free end.

A general method that can be used for computation of vibrational frequencies was developed by Prohl [3] and Myklestad [4]. The method extensively used for both coupled and uncoupled bending vibrations. In using this method, the member is divided into number of sufficiently large massless lengths with constant Young's modulus (E) and variable moment of inertia (I).The total mass of segment is converted into lumped masses at the juncture point of each the segment.

The following assumptions are made in deriving the mathematical model.

1. The mass of the shaft is neglected as compared to the disc.
2. Torsional effect of shaft is neglected.
3. Effect of bearing elements is also neglected.
4. The initial displacement and initial velocity at time t = 0 are assumed to be zero.
5. The material is isotropic and homogeneous.

3.3 Modelling of vibrating shaft

Relation between input-output state vectors for a shaft-rotor system

Consider a segment dx of the shaft subjected to transverse vibration as shown in the free body Fig. 3.2. The deflection, slope, bending moment and shear force at both the ends of a segment is determined from differential equation of motion of a vibrating shaft. Examining various quantities involved in the segment of length dx, we can apply Newton's second law of motion to obtain equation of motion.

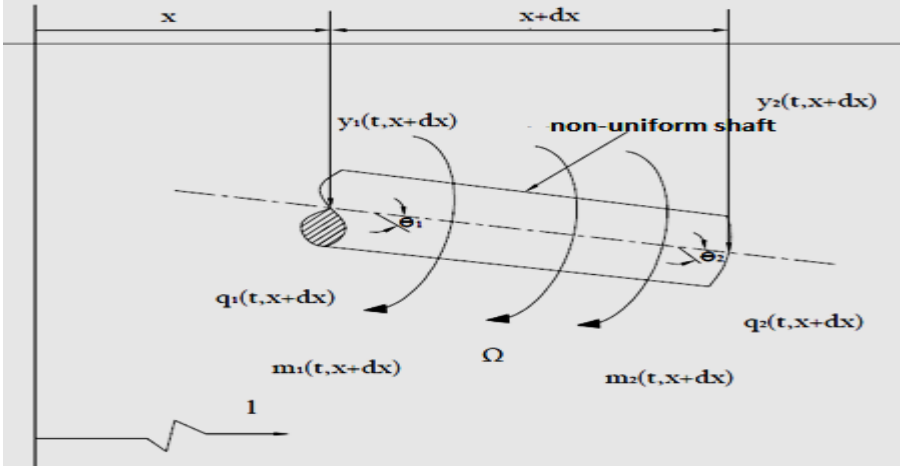

Fig. 3.2 Lateral vibration of shaft element.

From Fig. 3.2, we have

y1, y2 (x, t) - Vertical downward deflection at station 1 & 2

θ1, θ2(x, t) - Slope of the shaft at station 1& 2.

m1, m2(x, t) - Bending moment at station 1&2.

q1, q2(x, t) - Shear force at station 1 & 2.

I(x) - Moment of inertia at a distance 'x' from the bearing end.

The bending moment- shear force relation is given by,

$$q_y = \frac{dM_y}{dx}. \tag{3.3.1}$$

From the simple beam theory, one can have

$$M_y = -EI(x)\frac{d^2y}{dx^2}, \text{ and} \tag{3.3.2}$$

$$q_y = -EI(x)\frac{d^3y}{dx^3} \tag{3.3.3}$$

From Newton's second law of motion, one can write

$$\frac{\partial q_y}{\partial x} = -\rho A(x)\frac{\partial^2 y}{\partial t^2}. \tag{3.3.4}$$

Velocity at any point x is given by,

$$v_y = \frac{\partial y}{\partial t}. \tag{3.3.5}$$

Hence equation (3.3.4) becomes,

$$\frac{\partial q_y}{\partial x} = -\rho A(x)\frac{\partial v_y}{\partial t}. \tag{3.3.6}$$

On differentiating (3.3.3) w r t time and substituting from (3.3.5) gives

$$\frac{\partial q_y}{\partial t} = -EI(x)\frac{\partial^3 v_y}{\partial x^3}. \tag{3.3.7}$$

Let mass per unit length of the shaft is given by,

$$\rho A(x) = L(x). \tag{3.3.8}$$

Let the shaft compliance per unit length given by,

$$\frac{1}{EI(x)} = c(x). \tag{3.3.9}$$

Now taking Laplace of equation (3.3.7) one can get

$$s.Q_y(x,s) = -EI(x)\frac{d^3V_y}{dx^3},$$

$$\text{Or } \frac{d^3V_y}{dx^3} = -s.c(x).Q_y(x,s). \tag{3.3.10}$$

Taking Laplace of equation (3.3.6) with respect to time,

$$\frac{dQ_y}{dx} = -s.\rho A(x).V_y(x,s), \tag{3.3.11}$$

$$\text{or } \frac{dQ_y}{dx} = -s.L(x).V_y(x,s). \tag{3.3.12}$$

Differentiating equation (3.3.10) with respect to x,

$$\frac{d^4V_y}{dx^4} = -s.c(x).\frac{dQ_y}{dx}. \tag{3.3.13}$$

Using equation (3.3.12), equation (3.3.13) can be written as,

$$\frac{d^4V_y}{dx^4} = s.c(x).L(x).V(x,s). \tag{3.3.14}$$

$$\therefore \frac{d^4V_y}{dx^4} - s^2c(x).L(x).V(x,s) = 0. \tag{3.3.15}$$

Eq. (3.3.15) can be written in the form of,

$$\frac{d^4V_y}{dx^4} - \Gamma^2(x).V = 0 \tag{3.3.16}$$

$$\text{where } \Gamma(x) = s.\sqrt{c(x).L(x)}. \tag{3.3.17}$$

Equation (15) is known as Euler-Bernoulli beam equation. The solution of equation (3.3.16) will be

$$V_y(x,s) = A.\sinh x\sqrt{\Gamma(x)} + B.\cosh x\sqrt{\Gamma(x)} + C.\sin x\sqrt{\Gamma(x)} + D.\cos x\sqrt{\Gamma(x)}. \tag{3.3.18}$$

Since $Y(x,s) = L\{y(x,t)\}$ be the vertical deflection of the shaft, transformed with initial zero condition is,

$$Y(x,s) = \frac{A}{s}.\sinh x\sqrt{\Gamma(x)} + \frac{B}{s}.\cosh x\sqrt{\Gamma(x)} + \frac{C}{s}.\sin x\sqrt{\Gamma(x)} + \frac{D}{s}.\cos x\sqrt{\Gamma(x)}. \tag{3.3.19}$$

Differentiating equation (3.3.19) with respect to x, we get the slope as

$$\frac{dY(x,s)}{dx} = \begin{pmatrix} \frac{A}{s}.\sqrt{\Gamma(x)}.\cosh x\sqrt{\Gamma(x)} + \frac{B}{s}.\sqrt{\Gamma(x)}.\sinh x\sqrt{\Gamma(x)} + \frac{C}{s}.\sqrt{\Gamma(x)}.\cos x\sqrt{\Gamma(x)} \\ -\frac{D}{s}.\sqrt{\Gamma(x)}.\sin x\sqrt{\Gamma(x)} \end{pmatrix}. \tag{3.3.20}$$

For bending moment differentiating equation (3.3.20) with respect to x & multiply by – EI(x), equation (3.3.20) become

$$-EI(x).\frac{d^2Y(x,s)}{dx^2}=\frac{-EI(x)\Gamma(x)}{s}\begin{pmatrix}A.\sinh x\sqrt{\Gamma(x)}+B.\cosh x\sqrt{\Gamma(x)}-C.\sin x\sqrt{\Gamma(x)}\\-D.\cos x\sqrt{\Gamma(x)}\end{pmatrix} \quad (3.3.21)$$

For shear force one can differentiate equation (3.3.21) with respect to x, to obtain

$$-EI(x).\frac{d^3Y(x,s)}{dx^3}=\frac{-EI(x)\Gamma(x)\sqrt{\Gamma(x)}}{s}\begin{pmatrix}A\cosh x\sqrt{\Gamma(x)}+B\sinh x\sqrt{\Gamma(x)}\\-C\cos x\sqrt{\Gamma(x)}-D\sin x\sqrt{\Gamma(x)}\end{pmatrix} \quad (3.3.22)$$

Since,

$$-EI(x)\frac{d^2y}{dx^2}=M, \text{ and} \quad (3.3.23)$$

$$-EI(x)\frac{d^3y}{dx^3}=Q. \quad (3.3.24)$$

Applying boundary conditions to equations (3.3.19) through (3.3.22)

i.e. at $x=0, Y=Y_1, \theta=\theta_1, M_y=M_{y1} \& Q_y=Q_{y1}$

we obtain,

$$Y_1=\frac{B+D}{s}, \quad (3.3.25)$$

$$\theta_1=\frac{\sqrt{\Gamma(0)}}{s}(A+C), \quad (3.3.26)$$

$$M_1=EI(0)\frac{\Gamma(0)}{s}(D-B) \text{ and} \quad (3.3.27)$$

$$Q_1=\frac{\Gamma(0)\sqrt{\Gamma(0)}}{s}EI(0)(C-A). \quad (3.3.28)$$

Eqs. (3.3.25) – (3.3.28) can be written in the form of matrix as

$$\begin{bmatrix} Y_1 \\ \theta_1 \\ M_{y1} \\ Q_{y1} \end{bmatrix} = \frac{1}{s}\begin{bmatrix} 0 & 1 & 0 & 1 \\ \sqrt{\Gamma(0)} & 0 & \sqrt{\Gamma(0)} & 0 \\ 0 & -EI(0)\Gamma(0) & 0 & EI(0)\Gamma(0) \\ -EI(0)\Gamma(0)\sqrt{\Gamma(0)} & 0 & EI(0)\Gamma(0)\sqrt{\Gamma(0)} & 0 \end{bmatrix}\begin{bmatrix} A \\ B \\ C \\ D \end{bmatrix}. \tag{3.3.29}$$

The values of A, B, C and D can be obtained by inverting equation (3.3.29) to get

$$\begin{bmatrix} A \\ B \\ C \\ D \end{bmatrix} = s\begin{bmatrix} 0 & 1 & 0 & 1 \\ \sqrt{\Gamma(0)} & 0 & \sqrt{\Gamma(0)} & 0 \\ 0 & -EI(0)\Gamma(0) & 0 & EI(0)\Gamma(0) \\ -EI(0)\Gamma(0)\sqrt{\Gamma(0)} & 0 & EI(0)\Gamma(0)\sqrt{\Gamma(0)} & 0 \end{bmatrix}^{-1}\begin{bmatrix} Y_1 \\ \theta_1 \\ M_{y1} \\ Q_{y1} \end{bmatrix}.$$

This can be written further as

$$[W]=[X]^{-1}[S].$$

Consider now the inverse of matrix [X].

$$[X]=\frac{adjX}{|X|}=\frac{CF^T}{|X|}$$

Where CF^T is transpose of the cofactor matrix.

$$C_{11}=(-1)^{1+1}\begin{bmatrix} 0 & \sqrt{\Gamma(0)} & 0 \\ -EI(0)\Gamma(0) & 0 & EI(0)\Gamma(0) \\ 0 & EI(0)\Gamma(0)\sqrt{\Gamma(0)} & 0 \end{bmatrix}=0.$$

$$C_{12}=(-1)1+2\begin{bmatrix} \sqrt{\Gamma(0)} & \sqrt{\Gamma(0)} & 0 \\ 0 & 0 & EI(0)\Gamma(0) \\ -EI(0)\Gamma(0)\sqrt{\Gamma(0)} & EI(0)\Gamma(0)\sqrt{\Gamma(0)} & 0 \end{bmatrix}$$

$$\therefore C_{12}=-1\left\{-(EI(0))^2\Gamma^3(0)-(EI(0))^2\Gamma^3(0)\right\}$$

$$\therefore C_{12}=2(EI(0))^2\Gamma^3(0)$$

$$C_{13}=(-1)^{1+3}\begin{bmatrix} \sqrt{\Gamma(0)} & 0 & 0 \\ 0 & -EI(0)\Gamma(0) & EI(0)\Gamma(0) \\ -EI(0)\Gamma(0)\sqrt{\Gamma(0)} & 0 & 0 \end{bmatrix}=0,$$

$$C_{14}=(-1)^{1+4}\begin{bmatrix}\sqrt{\Gamma(0)} & 0 & \sqrt{\Gamma(0)}\\ 0 & \text{-EI}(0)\Gamma(0) & 0\\ \text{-EI}(0)\Gamma(0)\sqrt{\Gamma(0)} & 0 & \text{EI}(0)\Gamma(0)\sqrt{\Gamma(0)}\end{bmatrix}$$

$$\therefore C_{14}=-1\left\{\text{-}(\text{EI}(0))^2\Gamma^3(0)\text{-}(\text{EI}(0))^2\Gamma^3(0)\right\}$$

$$\therefore C_{14}=2(\text{EI}(0))^2\Gamma^3(0)$$

$$C_{21}=(-1)^{2+1}\begin{bmatrix}1 & 0 & 0\\ \text{-EI}(0)\Gamma(0) & 0 & \text{EI}(0)\Gamma(0)\\ 0 & \text{EI}(0)\Gamma(0)\sqrt{\Gamma(0)} & 0\end{bmatrix}$$

$$\therefore C_{21}=-1\left\{\text{-}(\text{EI}(0))^2\Gamma^2(0)\sqrt{\Gamma(0)}\text{-}(\text{EI}(0))^2\Gamma^2(0)\sqrt{\Gamma(0)}\right\}$$

$$\therefore C_{21}=2(\text{EI}(0))^2\Gamma^2(0)\sqrt{\Gamma(0)}$$

$$C_{22}=(-1)^{2+2}\begin{bmatrix}0 & 0 & 1\\ 0 & 0 & \text{EI}(0)\Gamma(0)\\ \text{-EI}(0)\Gamma(0)\sqrt{\Gamma(0)} & \text{EI}(0)\Gamma(0)\sqrt{\Gamma(0)} & 0\end{bmatrix}=0$$

$$C_{23}=(-1)^{2+3}\begin{bmatrix}0 & 1 & 1\\ 0 & \text{-EI}(0)\Gamma(0) & \text{EI}(0)\Gamma(0)\\ \text{-EI}(0)\Gamma(0)\sqrt{\Gamma(0)} & 0 & 0\end{bmatrix}$$

$$\therefore C_{23}=-1\left\{\text{-}(\text{EI}(0))^2\Gamma^2(0)\sqrt{\Gamma(0)}\text{-}(\text{EI}(0))^2\Gamma^2(0)\sqrt{\Gamma(0)}\right\}$$

$$\therefore C_{23}=2(\text{EI}(0))^2\Gamma^2(0)\sqrt{\Gamma(0)}$$

$$C_{24}=(-1)^{2+4}\begin{bmatrix}0 & 1 & 0\\ 0 & \text{-EI}(0)\Gamma(0) & 0\\ \text{-EI}(0)\Gamma(0)\sqrt{\Gamma(0)} & 0 & \text{EI}(0)\Gamma(0)\sqrt{\Gamma(0)}\end{bmatrix}=0$$

$$C_{31}=(-1)^{3+1}\begin{bmatrix}1 & 0 & 1\\ 0 & \Gamma(0) & 0\\ 0 & \text{EI}(0)\Gamma(0)\sqrt{\Gamma(0)} & 0\end{bmatrix}=0$$

$$C_{32}=(-1)^{3+2}\begin{bmatrix} 0 & 0 & 1 \\ \Gamma(0) & \Gamma(0) & 0 \\ -\mathrm{EI}(0)\Gamma(0)\sqrt{\Gamma(0)} & \mathrm{EI}(0)\Gamma(0)\sqrt{\Gamma(0)} & 0 \end{bmatrix}$$

$$\therefore C_{32}=-1\left(\mathrm{EI}(0))^2\Gamma^2(0)+\mathrm{EI}(0))^2\Gamma^2(0)\right)$$

$$\therefore C_{32}=-2\mathrm{EI}(0))^2\Gamma^2(0)$$

$$C_{33}=(-1)^{3+3}\begin{bmatrix} 0 & 1 & 1 \\ \Gamma(0) & 0 & 0 \\ -\mathrm{EI}(0)\Gamma(0)\sqrt{\Gamma(0)} & 0 & 0 \end{bmatrix}=0$$

$$C_{34}=(-1)^{3+4}\begin{bmatrix} 0 & 1 & 0 \\ \Gamma(0) & 0 & \Gamma(0) \\ -\mathrm{EI}(0)\Gamma(0)\sqrt{\Gamma(0)} & 0 & \mathrm{EI}(0)\Gamma(0)\sqrt{\Gamma(0)} \end{bmatrix}$$

$$\therefore C_{34}=-1\left(\mathrm{EI}(0))^2\Gamma^2(0)+\mathrm{EI}(0))^2\Gamma^2(0)\right)$$

$$\therefore C_{34}=2(\mathrm{EI}(0))^2\Gamma^2(0)$$

$$C_{41}=(-1)^{4+1}\begin{bmatrix} 1 & 0 & 1 \\ 0 & \sqrt{\Gamma(0)} & 0 \\ -\mathrm{EI}(0)\Gamma(0) & 0 & \mathrm{EI}(0)\Gamma(0) \end{bmatrix}$$

$$\therefore C_{41}=-1\left(\mathrm{EI}(0))^2\Gamma(0)\sqrt{\Gamma(0)}+\mathrm{EI}(0))^2\Gamma(0)\sqrt{\Gamma(0)}\right)$$

$$\therefore C_{41}=-2\left(\mathrm{EI}(0))^2\Gamma(0)\sqrt{\Gamma(0)}\right)$$

$$C_{42}=(-1)^{3+3}\begin{bmatrix} 0 & 0 & 1 \\ \sqrt{\Gamma(0)} & \sqrt{\Gamma(0)} & 0 \\ 0 & 0 & \mathrm{EI}(0)\Gamma(0) \end{bmatrix}=0$$

$$C_{43}=(-1)^{4+3}\begin{bmatrix} 0 & 1 & 1 \\ \sqrt{\Gamma(0)} & 0 & 0 \\ 0 & -\mathrm{EI}(0)\Gamma(0) & \mathrm{EI}(0)\Gamma(0) \end{bmatrix}$$

$$\therefore C_{43}=-1\left(\mathrm{EI}(0))^2\Gamma(0)\sqrt{\Gamma(0)}+\mathrm{EI}(0))^2\Gamma(0)\sqrt{\Gamma(0)}\right)$$

$$\therefore C_{43}=-2\left(\mathrm{EI}(0))^2\Gamma(0)\sqrt{\Gamma(0)}\right)$$

$$C_{44} = (-1)^{4+4}\begin{bmatrix} 0 & 1 & 0 \\ \sqrt{\Gamma(0)} & 0 & \sqrt{\Gamma(0)} \\ 0 & \mathrm{EI}(0)\Gamma(0) & 0 \end{bmatrix} = 0$$

The cofactor matrix will be

$$CF = \begin{bmatrix} 0 & 2(\mathrm{EI}(0))^2\Gamma^3(0) & 0 & 2(\mathrm{EI}(0))^2\Gamma^3(0) \\ 2(\mathrm{EI}(0))^2\Gamma^2(0)\sqrt{\Gamma(0)} & 0 & 2(\mathrm{EI}(0))^2\Gamma^2(0)\sqrt{\Gamma(0)} & 0 \\ 0 & -2\mathrm{EI}(0))^2\Gamma^2(0) & 0 & 2\mathrm{EI}(0))^2\Gamma^2(0) \\ -2\left(\mathrm{EI}(0))^2\Gamma(0)\sqrt{\Gamma(0)}\right) & 0 & 2\left(\mathrm{EI}(0))^2\Gamma(0)\sqrt{\Gamma(0)}\right) & 0 \end{bmatrix}$$

and

$$\mathrm{CF}^{\mathrm{T}} = \begin{bmatrix} 0 & 2(\mathrm{EI}(0))^2\Gamma^2(0)\sqrt{\Gamma(0)} & 0 & -2\left(\mathrm{EI}(0))^2\Gamma(0)\sqrt{\Gamma(0)}\right) \\ 2(\mathrm{EI}(0))^2\Gamma^3(0) & 0 & -2\mathrm{EI}(0))^2\Gamma^2(0) & 0 \\ 0 & 2(\mathrm{EI}(0))^2\Gamma^2(0)\sqrt{\Gamma(0)} & 0 & 2\left(\mathrm{EI}(0))^2\Gamma(0)\sqrt{\Gamma(0)}\right) \\ 2(\mathrm{EI}(0))^2\Gamma^3(0) & 0 & 2\mathrm{EI}(0))^2\Gamma^2(0) & 0 \end{bmatrix}$$

$$|X| = X_{11}CF_{11} + X_{12}CF_{12} + X_{13}CF_{13} + X_{14}CF_{14}$$

$$\therefore |X| = 4(\mathrm{EI}(0))^2\Gamma^3(0)$$

$$\therefore \mathrm{X}^{-1} = \begin{bmatrix} 0 & \dfrac{1}{2\sqrt{\Gamma(0)}} & 0 & \dfrac{-\mathrm{C}(0)}{2\Gamma(0)\sqrt{\Gamma(0)}} \\ \dfrac{1}{2} & 0 & \dfrac{-\mathrm{C}(0)}{2\Gamma(0)} & 0 \\ 0 & \dfrac{1}{2\sqrt{\Gamma(0)}} & 0 & \dfrac{\mathrm{C}(0)}{2\Gamma(0)\sqrt{\Gamma(0)}} \\ \dfrac{1}{2} & 0 & \dfrac{\mathrm{C}(0)}{2\Gamma(0)} & 0 \end{bmatrix}$$

$$\therefore \begin{bmatrix} \mathrm{A} \\ \mathrm{B} \\ \mathrm{C} \\ \mathrm{D} \end{bmatrix} = \mathrm{s}\begin{bmatrix} 0 & \dfrac{1}{2\sqrt{\Gamma(0)}} & 0 & \dfrac{-\mathrm{C}(0)}{2\Gamma(0)\sqrt{\Gamma(0)}} \\ \dfrac{1}{2} & 0 & \dfrac{-\mathrm{C}(0)}{2\Gamma(0)} & 0 \\ 0 & \dfrac{1}{2\sqrt{\Gamma(0)}} & 0 & \dfrac{\mathrm{C}(0)}{2\Gamma(0)\sqrt{\Gamma(0)}} \\ \dfrac{1}{2} & 0 & \dfrac{\mathrm{C}(0)}{2\Gamma(0)} & 0 \end{bmatrix}\begin{bmatrix} \mathrm{Y}_1 \\ \theta_1 \\ \mathrm{M}_{y1} \\ \mathrm{Q}_{y1} \end{bmatrix}$$

$$\therefore A = \frac{s}{2\sqrt{\Gamma(0)}}.\theta_1 - \frac{c(0)s}{2\Gamma(0)\sqrt{\Gamma(0)}}.Q_1, \tag{3.3.30}$$

$$B = \frac{s}{2}.Y_1 - \frac{c(0)s}{2\Gamma(0)}.M_{y1}, \tag{3.3.31}$$

$$C = \frac{s}{2\sqrt{\Gamma(0)}}.\theta_1 - \frac{c(0)s}{2\Gamma(0)\sqrt{\Gamma(0)}}.Q_{y1} \text{ and} \tag{3.3.32}$$

$$D = \frac{s}{2}.Y_1 + \frac{c(0)s}{2\Gamma(0)}.M_{y1}. \tag{3.3.33}$$

Substituting the values of A, B, C and D in equation (3.3.19) through (3.3.22) and applying the boundary conditions,

i.e. at x='l',Y=Y_2, θ=θ_2, M_y=M_{y2} & Q_y=Q_{y2} one can write

$$Y_2 = \left(\begin{array}{l} \left(\frac{s}{2\sqrt{\Gamma(0)}}.\theta_1 - \frac{c(0)s}{2\Gamma(0)\sqrt{\Gamma(0)}}.Q_{y1} \right) \sinhl\sqrt{\Gamma(l)} + \left(\frac{s}{2}.Y_1 - \frac{c(0)s}{2\Gamma(0)}.M_{y1} \right) \coshl\sqrt{\Gamma(l)} \\ + \left(\frac{s}{2\sqrt{\Gamma(0)}}.\theta_1 - \frac{c(0)s}{2\Gamma(0)\sqrt{\Gamma(0)}}.Q_{y1} \right) \sinl\sqrt{\Gamma(l)} + \frac{s}{2}.Y_1 + \frac{c(0)s}{2\Gamma(0)}.M_{y1}\cosl\sqrt{\Gamma(l)} \end{array} \right). \tag{3.3.34}$$

$$\theta_2 = \left(\begin{array}{l} \left(\frac{s}{2}.\theta_1 - \frac{c(0)s}{2\Gamma(0)}.Q_{y1} \right) \coshl\sqrt{\Gamma(l)} + \left(\frac{s}{2}.Y_1 - \frac{c(0)\sqrt{\Gamma(0)}s}{2\Gamma(0)}.M_{y1} \right) \sinhl\sqrt{\Gamma(l)} \\ + \left(\frac{s}{2}.\theta_1 - \frac{c(0)s}{2\Gamma(0)}.Q_{y1} \right) \cosl\sqrt{\Gamma(l)} - \left(\frac{s}{2}.Y_1 + \frac{c(0)\sqrt{\Gamma(0)}s}{2\Gamma(0)}.M_{y1} \right) \sinl\sqrt{\Gamma(l)} \end{array} \right). \tag{3.3.35}$$

$$M_{y2} = \left(\begin{array}{l} \left(\frac{s\sqrt{\Gamma(0)}}{2c(0)}.\theta_1 - \frac{s}{2c(l)\sqrt{\Gamma(0)}}.Q_{y1} \right) \sinhl\sqrt{\Gamma(l)} + \left(\frac{s\sqrt{\Gamma(l)}}{2c(0)}.Y_1 - \frac{s}{2}.M_{y1} \right) \coshl\sqrt{\Gamma(l)} \\ - \left(\frac{s\sqrt{\Gamma(0)}}{2c(0)}.\theta_1 - \frac{s}{2\sqrt{\Gamma(0)}}.Q_{y1} \right) \sinl\sqrt{\Gamma(l)} - \left(\frac{s\sqrt{\Gamma(0)}}{2c(0)}.Y_1 + \frac{s}{2}.M_{y1} \right) \cosl\sqrt{\Gamma(l)} \end{array} \right). \tag{3.3.36}$$

$$Q_{y2}=\begin{pmatrix}\left(\frac{s\Gamma(0)}{2c(0)}.\theta_1-\frac{s}{2\Gamma(0)}.Q_{y1}\right)\cosh l\sqrt{\Gamma(1)}+\left(\frac{s\Gamma(0)\sqrt{\Gamma(0)}}{2c(0)}.Y_1-\frac{\sqrt{\Gamma(0)}s}{2}.M_{y1}\right)\sinh l\sqrt{\Gamma(1)}\\+\left(\frac{s\Gamma(0)}{2c(0)}.\theta_1-\frac{s}{2\Gamma(0)}.Q_{y1}\right)\cos l\sqrt{\Gamma(1)}-\left(\frac{s\Gamma(0)\sqrt{\Gamma(0)}}{2c(0)}.Y_1+\frac{\Gamma(0)s}{2}.M_{y1}\right)\sin l\sqrt{\Gamma(1)}\end{pmatrix}. \tag{3.3.37}$$

Now the input & output relation can be obtained from equation (3.3.34)-(3.3.37) in the matrix form as,

$$\begin{Bmatrix}Y_2\\ \theta_2\\ M_{y2}\\ Q_{y2}\end{Bmatrix}=F(s)\begin{Bmatrix}Y_1\\ \theta_1\\ M_{y1}\\ Q_{y1}\end{Bmatrix} \tag{3.3.38}$$

Where F(s) is given by,

$$\begin{bmatrix}\frac{\cos\sqrt{\Gamma(l)}l+\cosh\sqrt{\Gamma(l)}l}{2} & \frac{\sin\sqrt{\Gamma(l)}l+\sinh\sqrt{\Gamma(l)}l}{2\sqrt{\Gamma(l)}}\\ \frac{-\sqrt{\Gamma(0)}(\sin\sqrt{\Gamma(l)}l-\sinh\sqrt{\Gamma(l)}l)}{2} & \frac{\cos\sqrt{\Gamma(l)}l+\cosh\sqrt{\Gamma(l)}l}{2}\\ \frac{\Gamma(0)(\cos\sqrt{\Gamma(l)}l-\cosh\sqrt{\Gamma(l)}l)}{2C(0)} & \frac{\sqrt{\Gamma(0)}(\sin\sqrt{\Gamma(l)}l-\sinh\sqrt{\Gamma(l)}l)}{2C(0)}\\ \frac{-\Gamma(0)\sqrt{\Gamma(0)}(\sin\sqrt{\Gamma(l)}l+\sinh\sqrt{\Gamma(l)}l)}{2C(0)} & \frac{\Gamma(0)(\cos\sqrt{\Gamma(l)}l-\cosh\sqrt{\Gamma(l)}l)}{2C(0)}\end{bmatrix}$$

$$\begin{bmatrix}\frac{C(0)(\cos\sqrt{\Gamma(l)}l-\cosh\sqrt{\Gamma(l)}l)}{2\Gamma(l)} & \frac{C(0)(\sin\sqrt{\Gamma(l)}l-\sinh\sqrt{\Gamma(l)}l)}{2\Gamma(0)\sqrt{\Gamma(0)}}\\ \frac{-C(0)(\sin\sqrt{\Gamma(l)}l+\sinh\sqrt{\Gamma(l)}l)}{2\sqrt{\Gamma(0)}} & \frac{C(0)(\cos\sqrt{\Gamma(l)}l-\cosh\sqrt{\Gamma(l)}l)}{2\Gamma(0)}\\ \frac{\cos\sqrt{\Gamma(l)}l+\cosh\sqrt{\Gamma(l)}l}{2} & \frac{\sin\sqrt{\Gamma(l)}l+\sinh\sqrt{\Gamma(l)}l}{2\sqrt{\Gamma(0)}}\\ \frac{-\sqrt{\Gamma(0)}(\sin\sqrt{\Gamma(l)}l-\sinh\sqrt{\Gamma(l)}l)}{2} & \frac{\cos\sqrt{\Gamma(l)}l+\cosh\sqrt{\Gamma(l)}l}{2}\end{bmatrix}$$

In more simplified way we can write

$$\begin{bmatrix}Y_2 & \theta_2 & M_{y2} & Q_{y2}\end{bmatrix}^T=F(s)\begin{bmatrix}Y_1 & \theta_1 & M_{y1} & Q_{y1}\end{bmatrix}^T \tag{3.3.39}$$

The matrix F(s) is called field transfer matrix that connects state vector on the left and right of the profiled shaft.

For simplification of equation, following trigonometric identities are required.

$$\sin x = x - \frac{x^3}{3!} + \frac{x^5}{5!} - \frac{x^7}{7!} + \text{-------}$$

$$\cos x = 1 - \frac{x^2}{2!} + \frac{x^4}{4!} - \frac{x^6}{6!} + \text{-------}$$

$$\sinh x = x + \frac{x^3}{3!} + \frac{x^5}{5!} + \frac{x^7}{7!} + \text{------}$$

$$\cosh x = 1 + \frac{x^2}{2!} + \frac{x^4}{4!} + \frac{x^6}{6!} + \text{------}.$$

The trigonometric identities in the elements of the field transfer matrix are denoted by following expressions. The series expansion of these identities is given by,

$$f_1 = \frac{1}{2}\left(\cosh \gamma(l) + \cos \gamma(l)\right) = \left(1 + \frac{\gamma^4(l)}{4!} + \frac{\gamma^8(l)}{8!} + \text{------}\right)$$

$$f_2 = \sinh\gamma(l) + \sin\gamma(l) = 2\left(\gamma(l) + \frac{\gamma^5(l)}{5!} + \frac{\gamma^9(l)}{9!} + \text{---}\right)$$

$$f_3 = \cosh\gamma(l) - \cos\gamma(l) = \gamma^2(l) + 2\frac{\gamma^6(l)}{6!} + 2\frac{\gamma^{10}(l)}{10!} + \text{---}$$

$$f_4 = \sinh\gamma(l) - \sin\gamma(l) = 2\left(\frac{\gamma^3(l)}{3!} + \frac{\gamma^7(l)}{7!} + \frac{\gamma^{11}(l)}{11!} + \text{---}\right)$$

$$\gamma(0) = l\sqrt{\Gamma(0)} = l\sqrt{s\sqrt{L(0)c(0)}} = ls^{1/2}\left(L(0).c(0)\right)^{1/2}$$

$$\gamma(1) = ls^{1/2}\left(L(1).c(1)\right)^{1/4}.$$

The lowest frequency of oscillation or whirl would be detected when restricting series expansion of f1, f2, f3 and f4 is restricted to the least number of terms. The accuracy of the results can be increased by increasing the number of terms in the series expansion. Hence the resultant matrix becomes,

$$F(s)=\begin{bmatrix} f_1 & \frac{l}{2\gamma(0)}f_2 & \frac{-c(0)l^2}{2\gamma^2(0)}f_3 & \frac{-c(0)l^3}{2\gamma^3(0)}f_4 \\ \frac{\gamma(0)}{2l}f_4 & f_1 & \frac{-c(0)l}{2\gamma(0)}f_2 & \frac{-c(0)l^2}{2\gamma^2(0)}f_3 \\ \frac{-\gamma^2(0)}{2l^2c(0)}f_3 & \frac{-\gamma(0)}{2cl(0)}f_4 & f_1 & \frac{l}{2\gamma(0)}f_2 \\ \frac{-\gamma^3(0)}{2c(0)l^3}f_2 & \frac{-\gamma^2(0)}{2c(0)l^2}f_3 & \frac{\gamma(0)}{2l}f_4 & f_1 \end{bmatrix}$$

$$F(s)=\begin{bmatrix} 1 & \frac{l\gamma(1)}{\gamma(0)} & \frac{-\gamma^2(1)c(0)l^2}{2\gamma^2(0)} & \frac{-c(0)l^3\gamma^3(1)}{6\gamma^3(0)} \\ \frac{\gamma^3(1)\gamma(0)}{6l} & 1 & \frac{-c(c)l\gamma(1)}{\gamma(0)} & \frac{-\gamma^2(1)c(0)}{2\gamma^2(l)} \\ \frac{-\gamma^2(0)\gamma^2(1)}{2c(0)l^2} & \frac{-\gamma^3(0)\gamma(0)}{6lc(0)} & 1 & \frac{l\gamma(1)}{\gamma(0)} \\ \frac{-\gamma^3(0)\gamma(1)}{l^3c(0)} & \frac{-\gamma^2(c)\gamma^2(1)}{2l^2c(0)} & \frac{\gamma(1)\gamma^3(0)}{6l} & 1 \end{bmatrix}$$

3.4 Disk Modelling

The mathematical modelling of disk involves determination of state vectors at station 2 and 3. Fig. 3.3 depicts detached model of disk from shaft, showing various parameters involved in modelling.

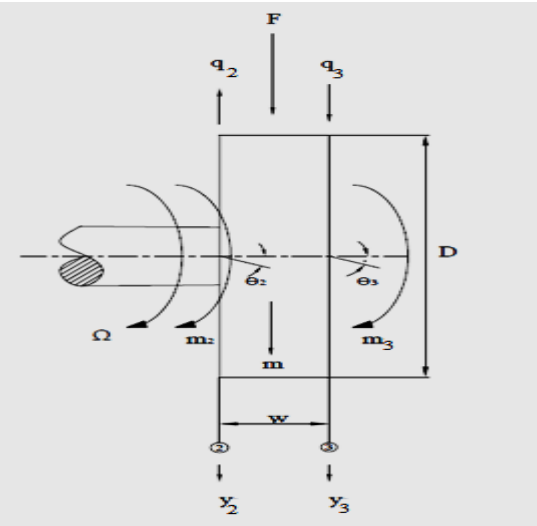

Fig. 3.3 Vibrating disk element

From Fig. 3.3, we have

$y_2(x, t)$, $y_3(x, t)$ - Vertical downward deflections at station 2 & 3.

$\theta_2(x, t)$, $\theta_3(x, t)$ - Slope of the shaft at station 2 & 3.

$m_2(x, t)$, $m_3(x, t)$ - Bending moment at station 2 & 3.

$q_2(x, t)$, $q_3(x, t)$ - Shear force at station 2 & 3.

J –mass moment of inertia of the disk.

The relation between the state vectors at station 2 and station 3 is established by writing continuity and equilibrium equations for the four parameters namely deflection, slope, bending moment and shear force. The disk is assumed to be rigid and hence from continuity conditions, we have

$$y_2(2)=y_3(3) \quad \text{and} \tag{3.4.1}$$

$$\theta_2(2)=\theta_3(3) \tag{3.4.2}$$

Equation (3.4.1) and equation (3.4.2) indicates the displacements and slopes at left and right side of the rigid disk are equal. From the equilibrium conditions moment and shear force can be written as

$$M_{y3}+J\Omega\frac{d\theta_2}{dt}=M_{y2} \text{ and} \tag{3.4.3}$$

$$Q_{y3}=M_{y2}\ddot{y}_2+Q_{y2} \tag{3.4.4}$$

Taking Laplace of equation (3.4.1)-(3.4.4), we get

$$Y_3(s)=Y_2(s), \tag{3.4.5}$$

$$\theta_3(s)=\theta_2(s), \tag{3.4.6}$$

$$M_{y3}=-J\Omega s\theta_2(s)+M_{y2} \text{ and} \tag{3.4.7}$$

$$Q_{y3}=ms^2Y_2+Q_{y2}. \tag{3.4.8}$$

In matrix form, equation (3.4.5) to (3.4.8) can be written as follows,

$$\begin{bmatrix} Y_3 \\ \theta_3 \\ M_{y3} \\ Q_{y3} \end{bmatrix} = \begin{bmatrix} 1 & 0 & 0 & 0 \\ 0 & 1 & 0 & 0 \\ 0 & -J\Omega s & 1 & 0 \\ ms^2 & 0 & 0 & 1 \end{bmatrix} \begin{bmatrix} Y_2 \\ \theta_2 \\ M_{y2} \\ Q_{y2} \end{bmatrix} \quad (3.4.9)$$

$$\therefore \begin{bmatrix} Y_3 & \theta_3 & M_{y3} & Q_{y3} \end{bmatrix}^T = R(s) \begin{bmatrix} Y_2 & \theta_2 & M_{y2} & Q_{y2} \end{bmatrix}^T \quad (3.4.10)$$

The matrix R(s) is called point transfer matrix. The point transfer matrix connects the state vectors on either side of the mass.

3.5 Cantilever Shaft-Rotor System

Consider now the cantilever shaft –rotor system subjected to the external excitation as shown in Fig.3.4. In order to obtain the relation between the state vectors, the shaft and the disk modal matrices are assembled into equation (3.5.1). This equation represents the relation between the state vectors at station 3 and station 1.

$$[Y_3, \theta_3, M_{y3}, Q_{y3}]^T = R(S)\, F(S)\, [Y_1, \theta_1, M_{y1}, Q_{y1}]^T$$

$$= H(s)\, [Y_1, \theta_1, M_{y1}, Q_{y1}]^T \quad (3.5.1)$$

Where H(s) = Transfer matrix which when multiplied to state vector at station ‘n-1’ gives state vector at station ‘n’.

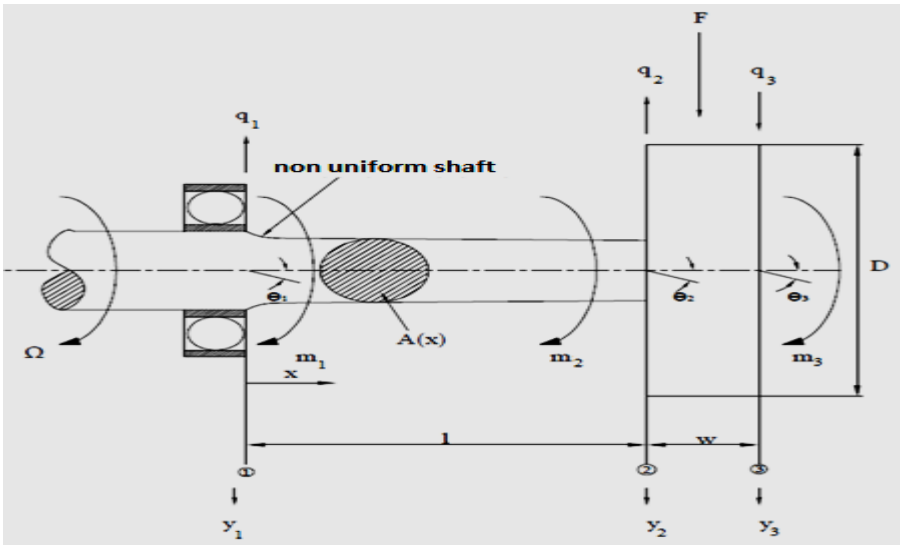

Fig. 3.4 A cantilever shaft-rotor system subjected to external excitation at its end.

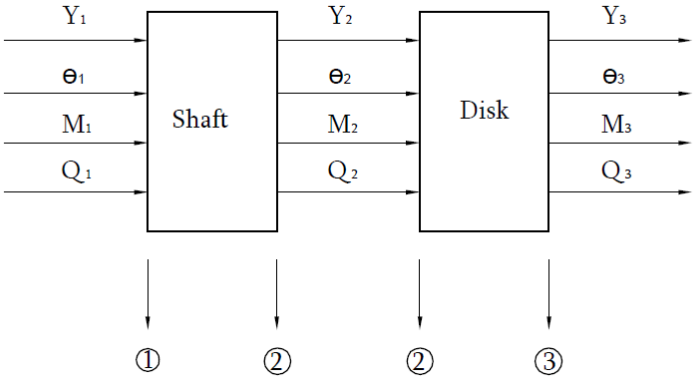

Fig. 3.5 Distributed–lumped shaft rotor model.

The transfer matrix for impulse loading is given by,

$$H(s)=\begin{bmatrix} 1 & 0 & 0 & 0 \\ 0 & 1 & 0 & 0 \\ 0 & -J\Omega s & 1 & 0 \\ ms^2 & 0 & 0 & 1 \end{bmatrix} \begin{bmatrix} 1 & \frac{l\gamma(1)}{\gamma(0)} & \frac{-\gamma^2(1)c(0)l^2}{2\gamma^2(0)} & \frac{-c(0)l^3\gamma^3(1)}{6\gamma^3(0)} \\ \frac{\gamma^3(1)\gamma(0)}{6l} & 1 & \frac{-c(0)l\gamma(1)}{\gamma(0)} & \frac{-\gamma^2(1)c(0)}{2\gamma^2(l)} \\ \frac{-\gamma^2(0)\gamma^2(1)}{2c(0)l^2} & \frac{-\gamma^3(0)\gamma(0)}{6lc(0)} & 1 & \frac{l\gamma(1)}{\gamma(0)} \\ \frac{-\gamma^3(c)\gamma(1)}{l^3c(0)} & \frac{-\gamma^2(0)\gamma^2(1)}{2l^2c(0)} & \frac{\gamma(1)\gamma^3(0)}{6l} & 1 \end{bmatrix}.$$

$$= \begin{bmatrix} 1 & \frac{l\gamma(1)}{\gamma(0)} & \frac{-\gamma^2(1)c(0)l^2}{2\gamma^2(0)} & \frac{-c(0)l^3\gamma^3(1)}{6\gamma^3(0)} \\ \frac{\gamma^3(1)\gamma(0)}{6l} & 1 & \frac{-c(0)l\gamma(1)}{\gamma(0)} & \frac{-\gamma^2(1)c(0)l^2}{2\gamma^2(l)} \\ \frac{-J\Omega s\gamma^3(1)\gamma(0)}{6l} - \frac{\gamma^2(c)\gamma^2(1)}{2c(0)l^2} & -J\Omega s - \frac{\gamma^3(0)\gamma(0)}{6lc(0)} & 1+\frac{J\Omega sc(0)l\gamma(1)}{\gamma(0)} & \frac{J\Omega s\gamma^2(1)l^2c(0)}{2\gamma^2(l)} + \frac{l\gamma(l)}{\gamma(0)} \\ ms^2 - \frac{\gamma^3(0)\gamma(1)}{l^3c(0)} & \frac{ms^2l\gamma(1)}{\gamma(0)} - \frac{\gamma^2(0)\gamma^2(1)}{2l^2c(0)} & \frac{-ms^2\gamma^2(1)c(0)l^2}{2\gamma^2(0)} + \frac{\gamma(0)\gamma^3(l)}{6l} & \frac{-ms^2c(0)l^3\gamma^3(1)}{6\gamma^3(0)} + 1 \end{bmatrix} \quad (3.5.2)$$

For a cantilever shaft an impulse of 1N is applied at the free end, the boundary conditions becomes,

$$\text{At } x = 0, Y_1 = 0, \theta_1 = 0 \text{ and} \quad (3.5.3)$$

$$\text{At } x = l, M_3 = 0, Q_3 = 1 \quad (3.5.4)$$

$$\therefore \begin{bmatrix} Y_3 \\ \theta_3 \\ 0 \\ 1 \end{bmatrix} = \begin{bmatrix} H_{11} & H_{12} \\ H_{21} & H_{22} \end{bmatrix} \begin{bmatrix} 0 \\ 0 \\ M_1 \\ Q_1 \end{bmatrix}$$

After partitioning, one can write

$$\begin{bmatrix} Y_3 \\ \theta_3 \end{bmatrix} = \begin{bmatrix} H_{12} \end{bmatrix} \begin{bmatrix} M_1 \\ Q_1 \end{bmatrix} \tag{3.5.5}$$

$$\begin{bmatrix} 0 \\ 1 \end{bmatrix} = \begin{bmatrix} H_{22} \end{bmatrix} \begin{bmatrix} M_1 \\ Q_1 \end{bmatrix} \tag{3.5.6}$$

$$\begin{bmatrix} M_1 \\ Q_1 \end{bmatrix} = \begin{bmatrix} H_{22} \end{bmatrix}^{-1} \begin{bmatrix} 0 \\ 1 \end{bmatrix} \tag{3.5.7}$$

Substituting equation (3.5.7) into equation (3.5.5), one can get

$$\begin{bmatrix} Y_3 \\ \theta_3 \end{bmatrix} = \begin{bmatrix} H_{12} \end{bmatrix} \begin{bmatrix} H_{22} \end{bmatrix}^{-1} \begin{bmatrix} 0 \\ 1 \end{bmatrix} \tag{3.5.8}$$

$$\text{Now} \begin{bmatrix} H_{22} \end{bmatrix}^{-1} = \frac{1}{|H_{22}|} \text{adj.}(H_{22})$$

$$H_{22} = \begin{pmatrix} 1 + \dfrac{J\Omega slc(0)\gamma(l)}{\gamma(0)} & \dfrac{J\Omega sl^2\gamma^2(l)}{2\gamma^2(0)} + \dfrac{l\gamma(l)}{\gamma(0)} \\ \dfrac{-ms^2l^2\gamma^2(l)c(0)}{2\gamma^2(0)} + \dfrac{\gamma(0).\gamma^3(l)}{6l} & 1 + \dfrac{-ms^2l^3\gamma^3(l)c(0)}{6\gamma^3(0)} \end{pmatrix}$$

$$\text{adj}H_{22} = \begin{pmatrix} 1 - \dfrac{ms^2l^3\gamma^3(l)c(0)}{6\gamma^3(0)} & -\dfrac{J\Omega sl^2\gamma^2(l)c(0)}{2\gamma^2(0)} - \dfrac{l\gamma(l)}{\gamma(0)} \\ \dfrac{ms^2l^2\gamma^2(l)c(0)}{2\gamma^2(0)} - \dfrac{\gamma(0).\gamma^3(l)}{6l} & 1 + \dfrac{J\Omega slc(0)\gamma(l)}{\gamma(0)} \end{pmatrix}$$

$$\det H_{22} = \left(1 + \frac{J\Omega slc(0)\gamma(l)}{\gamma(0)}\right)\left(1 - \frac{ms^2l^3\gamma^3(l)c(0)}{6\gamma^3(0)}\right) - \left(\frac{J\Omega sl^2\gamma^2(l)}{2\gamma^2(0)} + \frac{l\gamma(l)}{\gamma(0)}\right)\left(\frac{-ms^2l^2\gamma^2(l)c(0)}{2\gamma^2(0)} + \frac{\gamma(0).\gamma^3(l)}{6l}\right)$$

$$\det H_{22} = \frac{\left(mJ\Omega l^4\gamma^4(l)c(0)^2\right)s^3 + \left(4ml^3\gamma^3(l)\gamma(0)c(0)\right)s^2 + J\Omega slc(0)\gamma^3(0)[12\gamma(l) - \gamma^5(l)].s + 2\gamma^4(l)[6 - \gamma^4(l)]}{12\gamma^4(0)}$$

$$= \frac{\Delta s}{12\gamma^4(0)}$$

$$[H_{12}][\text{adj}H_{22}]\begin{bmatrix}0\\1\end{bmatrix} = \begin{bmatrix} -\frac{l^2\gamma^2(l)c(0)}{2\gamma^2(0)} & -\frac{l^3\gamma^3(l)c(0)}{6\gamma^3(0)} \\ -\frac{l\gamma(l)c(0)}{\gamma(0)} & -\frac{l^2\gamma^2(l)c(0)}{2\gamma^2(0)} \end{bmatrix}\begin{bmatrix} -\frac{J\Omega s l^2\gamma^2(l)c(0)}{2\gamma^2(0)} - \frac{l\gamma(l)}{\gamma(0)} \\ 1+\frac{J\Omega slc(0)\gamma(l)}{\gamma(0)} \end{bmatrix}$$

$$= \begin{bmatrix} \left(-\frac{l^2\gamma^2(l)c(0)}{2\gamma^2(0)}\right)\left(-\frac{J\Omega s l^2\gamma^2(l)c(0)}{2\gamma^2(0)} - \frac{l\gamma(l)}{\gamma(0)}\right) + \left(-\frac{l^3\gamma^3(l)c(0)}{6\gamma^3(0)}\right)\left(1+\frac{J\Omega slc(0)\gamma(l)}{\gamma(0)}\right) \\ \left(-\frac{l\gamma(l)c(0)}{\gamma(0)}\right)\left(-\frac{J\Omega s l^2\gamma^2(l)c(0)}{2\gamma^2(0)} - \frac{l\gamma(l)}{\gamma(0)}\right) + \left(-\frac{l^2\gamma^2(l)c(0)}{2\gamma^2(0)}\right)\left(1+\frac{J\Omega slc(0)\gamma(l)}{\gamma(0)}\right) \end{bmatrix}$$

$$= \begin{pmatrix} \frac{c(0)\gamma^3(l)l^3}{2\gamma^3(0)} + \frac{J\Omega sc(0)^2\gamma^4 l^4}{4\gamma^4(0)} - \frac{c(0)\gamma^3(l)l^3}{6\gamma^3(0)} - \frac{J\Omega sc()^2\gamma^4(l)l^4}{6\gamma^4(0)} \\ \frac{c(0)\gamma^2(l)l^2}{\gamma^2(0)} + \frac{J\Omega sc(0)^2\gamma^3(l)l^3}{2\gamma^3(0)} - \frac{c(0)\gamma^2(l)l^2}{2\gamma^2(0)} - \frac{J\Omega sc(0)^2\gamma^3(l)l^3}{2\gamma^3(0)} \end{pmatrix}$$

$$= \begin{pmatrix} \frac{6c(0)\gamma^3(l)\gamma(0)l^3 + 3J\Omega sc(0)^2\gamma^4(l)l^4 - 2c(0)\gamma^3(l)\gamma(0)l^3 - 2J\Omega sc(0)^2\gamma^4(l)l^4}{12\gamma^4(0)} \\ \frac{2c(0)\gamma^2(l)\gamma(0)l^2 + J\Omega sc(0)^2\gamma^3(l)l^3 - c(0)\gamma^2(l)\gamma(l)l^2 - J\Omega sc(0)^2\gamma^3(0)l^3}{2\gamma^3(0)} \end{pmatrix}$$

$$\begin{pmatrix} Y_3 \\ \theta_3 \end{pmatrix} = \frac{1}{\frac{12\gamma^4(0)}{\Delta s}} \begin{pmatrix} c(0)l^3\gamma^3(l)[J\Omega sc(0)l\gamma(l) + 4\gamma(0)] \\ 6c(0)\gamma^2(l)\gamma^2(0)l^2 \end{pmatrix}$$

$$\begin{pmatrix} Y_3 \\ \theta_3 \end{pmatrix} = \frac{1}{\Delta s} \begin{pmatrix} c(0)l^3\gamma^3(l)\ [J\Omega sc(0)l\gamma(l) + 4\gamma(0)] \\ 6c(0)\gamma^2(l)\gamma^2(0)l^2 \end{pmatrix}$$

$$\therefore Y_3 = \frac{c(0)l^3\gamma^3(l)\ [J\Omega sc(0)l\gamma(l) + 4\gamma(0)]}{[mJ\Omega l^4\gamma^4(l)c(0)^2]s^3 + [4ml^3\gamma^3(0)\gamma r(0)c(0)]s^2 + [J\Omega c(0)l\gamma^3(0)(12-\gamma^4(l)]s + 2\gamma^4(0)[6-\gamma^4(l)]} \quad (3.5.9)$$

Where,

$$\Delta s = [mJ\Omega l^4\gamma^4(l)c(0)^2]s^3 + [4ml^3\gamma^3(0)\gamma r(0)c(0)]s^2 + [J\Omega c(0)l\gamma^3(0)(12-\gamma^4(l)]s + 2\gamma^4(0)[6-\gamma^4(l)]$$

The equation (3.5.9) gives the transfer function of the cantilever non-uniform shaft rotor system which represents the ratio displacement to the force in Laplace domain. The impulse frequency response of the system is obtained by solving equation (3.5.9) in MATLAB. The response of this transfer function results into two plots, one giving magnitude versus frequency and the other giving phase versus frequency.

3.6 Summary

This chapter gives a detailed matrix calculations and expressions involved in transfer matrix method. In the present work Euler-Bernoulli beam theory along with transfer matrix method is adopted. Shaft model and disk model along with their model matrices are presented in systematic manner. Both, the shaft model matrix and the disk model are combined to get the expression for transfer matrix of a cantilever shaft-rotor system. The finite element approach is discussed in the next chapter.

CHAPTER-4

THEORETICAL ANALYSIS BY FINITE ELEMENT APPROACH

4.1 Introduction

The concept of the finite element analysis exists for centuries. The idea behind is to replace a complex problem with a simpler one that represents the true solution to a desirable degree of accuracy. It is likely that ancient mathematicians employed finite element like problem solving techniques to many physical problems. With the advent of the high speed computer FEA can now be applied to more broad and sophisticated problems. The very obvious indication of ancient mathematicians utilizing finite element techniques are found in early attempts to calculate value of π. Chinese literature written in the very beginning of the first century A.D. indicates that the Chinese were aware of certain geometric theorems. These theorems led a Chinese engineer Tsu Chung Chilk, to estimate π to be between 3.1415926 and 3.1415927 in 480 A.D. This was most likely done by representing the area of a circle with many inscribed and circumscribed rectangles, or finite elements. Archimedes also used the finite element technique to estimate the volume of various solids. These are very few of the more obvious early uses of the finite element technique. Today finite element approach is used to solve more complex problems of various backgrounds.

Rotating machinery is very extensively used in diverse engineering applications. The accurate prediction of dynamic characteristics, such as natural whirl frequencies, critical speeds, instability thresholds and response to mass unbalance, is very important in the design of any type of rotating machinery.

The utilization of finite element models in the field of rotor dynamics has yielded highly successful results. As stated earlier in literature review, Ruhl and Booker [12] and Nelson and McVaugh [14] contributed their works to rotor dynamics with finite element approach.

4.2 System configuration

A typical flexible shaft-rotor system to be analysed consists of a rotor composed of discrete discs, non-uniform rotor shaft segments with distributed mass and elasticity.

Such a system is illustrated in Fig. 4.1 along with two reference frames for describing the system motion. For the analysis of rotating structures, generally two types of reference frames, rotating and stationary are used. For stationary reference frame, the reference analysis system is attributed to the global coordinate system, which is a fixed one, and gyroscopic moments due to nodal rotations are added in the damping matrix. For rotating reference frame, entire model along with the reference coordinates, rotates at same rotational speed. The two frames [14], XYZ: $\mathfrak{I}$ and xyz: $\mathfrak{R}$ triads are the fixed ($\mathfrak{I}$) and rotating ($\mathfrak{R}$) references respectively with X and x collinear and coincident with the un-deformed rotor centre line. $\mathfrak{R}$ is defined relative to $\mathfrak{I}$ by a single rotation ωt about X, where ω denotes the whirl speed.

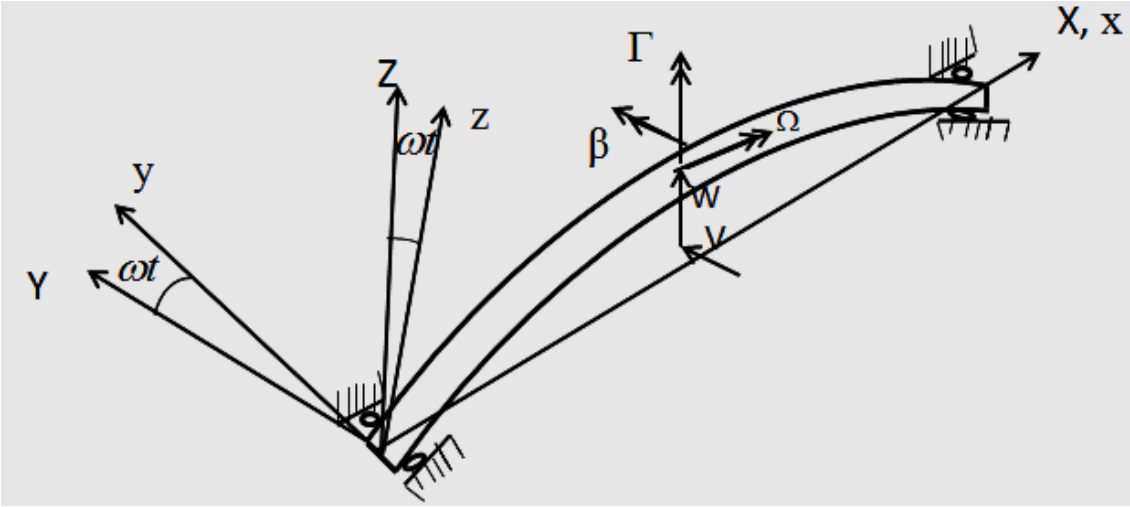

Fig. 4.1 Displacement variables and coordinate systems

A cross-section of the shaft, in a deformed state is defined relative to fixed references $\mathfrak{I}$ by translations V(x,t) and W(x,t) in the Y and Z directions to locate the elastic centreline and small angle rotations B(x,t) and Γ(x,t) in Y and Z directions to orient the plane of the cross-section.

A triad abc: C is obtained by the following rotations:

1. Rotation Γ about Z to obtain $a"b"c"$.

2. Rotation B about b″ to obtain $a'b'c'$.

3. Rotation φ about a′ to obtain the abc.

$$\begin{Bmatrix}\omega_a\\ \omega_b\\ \omega_c\end{Bmatrix}=\begin{bmatrix}-\sin B & 1 & 0\\ \cos B\sin\phi & 0 & \cos\phi\\ \cos B\cos\phi & 0 & -\sin\phi\end{bmatrix}\begin{Bmatrix}\dot{\Gamma}\\ \dot{\phi}\\ \dot{B}\end{Bmatrix} \tag{4.2.1}$$

For small deformations the (B, Γ), the rotations are approximately collinear with (X, Y) respectively. The spin angle φ, for a constant speed system with negligible torsional deformation, is Ωt, where Ω denotes the shaft-rotor spin speed.

4.3 Component equations

The component (disk and shaft) equations of motion can be found by using Lagrangian formulation (equation (4.3.1)). The Lagrangian (L) is defined as the difference between the element's kinetic energy and potential energy. Additionally, energy dissipation in the system due to internal damping or friction can be incorporated in Eq. (4.3.1). The shaft-rotor element equation of motion is developed by specifying the spatial shape functions and then treating the shaft-rotor element as an integration of infinite set ofdifferential elements.

$$\frac{d}{dt}\left(\frac{\partial L}{\partial \dot{q}}\right)-\frac{\partial L}{\partial q}=Q \tag{4.3.1}$$

4.3.1 Rigid disk

The rigid rotor disk has a total of four degrees of freedom. These are translation and rotation in Y and Z direction respectively, hence four displacement coordinates are associated with it. The kinetic energy of the disk with mass centre coincident with the elastic rotor centreline is given by the equation (4.3.2).

$$J_d=\frac{1}{2}\begin{Bmatrix}\dot{V}\\ \dot{W}\end{Bmatrix}^T\begin{bmatrix}m_d & 0\\ 0 & m_d\end{bmatrix}\begin{Bmatrix}\dot{V}\\ \dot{W}\end{Bmatrix}+\begin{Bmatrix}\dot{\omega}_a\\ \dot{\omega}_b\\ \dot{\omega}_c\end{Bmatrix}^T\begin{bmatrix}I_d & 0 & 0\\ 0 & I_d & 0\\ 0 & 0 & I_p\end{bmatrix}\begin{Bmatrix}\dot{\omega}_a\\ \dot{\omega}_b\\ \dot{\omega}_c\end{Bmatrix} \tag{4.3.2}$$

$$J_d=\frac{1}{2}\begin{Bmatrix}\dot{V}\\ \dot{W}\end{Bmatrix}^T\begin{bmatrix}m_d & 0\\ 0 & m_d\end{bmatrix}\begin{Bmatrix}\dot{V}\\ \dot{W}\end{Bmatrix}+\begin{Bmatrix}\dot{B}\\ \dot{\Gamma}\end{Bmatrix}^T\begin{bmatrix}I_d & 0\\ 0 & I_d\end{bmatrix}\begin{Bmatrix}\dot{B}\\ \dot{\Gamma}\end{Bmatrix}-\dot{\phi}\dot{\Gamma}BI_p \tag{4.3.3}$$

Since the disk is considered as a rigid body, therefore no strain energy is involved. The Lagrangian equation of motion of the disk for constant spin condition is given by equation (4.3.4). The forcing term includes external forces.

$$([M_T^d]+[M_R^d])\{\ddot{q}^d\}-\Omega[G^d]\{\dot{q}^d\}=\{Q^d\} \tag{4.3.4}$$

4.3.2 Finite rotor-shaft element

A typical finite rotor-shaft element is shown for illustration in Fig. 4.2. The element time dependent cross section displacements (V, W, B, Γ) are functions of position (x) along the axis of the element. The rotations (B, Γ) are related to the translations (V, W) by Eq. (4.3.5).

$$B=-\frac{\partial W}{\partial x};\quad \Gamma=\frac{\partial V}{\partial x} \tag{4.3.5}$$

The coordinates $(q_1^e, q_2^e, ..., q_8^e)$ are the time dependent end point displacements of the finite shaft-rotor element. The translations and rotations of a point internal to the element are chosen to obey the relations given by equation (4.3.6) and (4.3.7) respectively.

$$\begin{Bmatrix} V(x,t) \\ W(x,t) \end{Bmatrix} = [\psi(x)]\{q^e(t)\} \text{ and} \tag{4.3.6}$$

$$\begin{Bmatrix} B(x,t) \\ \Gamma(x,t) \end{Bmatrix} = [\Phi(x)]\{q^e(t)\} \tag{4.3.7}$$

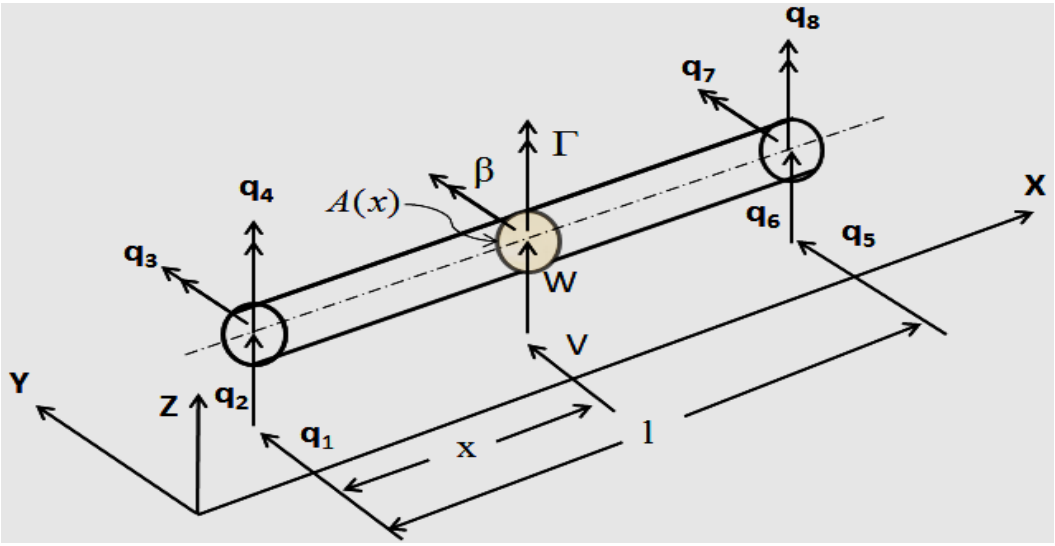

Fig. 4.2 Finite rotor shaft element

Each of the elements of the displacement function matrices represents the static displacement mode associated with unit displacement of one of the end point coordinates while all others fixed. These functions are given by Eq. (4.3.8).

The translational shape matrix is given by

$$[\psi(x)] = \begin{bmatrix} \psi_1 & 0 & 0 & \psi_2 & \psi_3 & 0 & 0 & \psi_4 \\ 0 & \psi_1 & -\psi_2 & 0 & 0 & \psi_3 & -\psi_4 & 0 \end{bmatrix} \tag{4.3.8}$$

The rotational shape matrix is given by

$$[\Phi(x)] = \begin{bmatrix} \lfloor \Phi_\beta \rfloor \\ \lfloor \Phi_\Gamma \rfloor \end{bmatrix} \begin{bmatrix} 0 & -\dot{\psi}_1 & \dot{\psi}_2 & 0 & 0 & -\dot{\psi}_3 & \dot{\psi}_4 & 0 \\ \dot{\psi}_1 & 0 & 0 & \dot{\psi}_2 & \dot{\psi}_3 & 0 & 0 & \dot{\psi}_4 \end{bmatrix} \tag{4.3.9}$$

Where, the shape functions are given by,

$$\psi_1 = 1 - 3\frac{x^2}{l^2} + 2\frac{x^3}{l^3} \tag{4.3.10}$$

$$\psi_2 = x - 2\frac{x^2}{l} + \frac{x^3}{l^2} \tag{4.3.11}$$

$$\psi_3 = 3\frac{x^2}{l^2} - 2\frac{x^3}{l^3} \tag{4.3.12}$$

$$\psi_4 = -\frac{x^2}{l} + \frac{x^3}{l^2} \tag{4.3.13}$$

For a differential rotor shaft element located at (x), elastic bending, axial load and kinetic energy are given by equations (4.3.14)-(4.3.16). These are expressed in terms of nodal displacements in equations (4.3.17)-(4.3.19). One can observe the flexural rigidity, mass per unit length and inertias are the functions of length as the shaft-rotor system considered here consists of non-uniform shaft.

$$dP_B^e = \frac{1}{2}\begin{Bmatrix} \ddot{V} \\ \ddot{W} \end{Bmatrix}^T \begin{bmatrix} EI(x) & 0 \\ 0 & EI(x) \end{bmatrix} \begin{Bmatrix} \ddot{V} \\ \ddot{W} \end{Bmatrix} dx \tag{4.3.14}$$

$$dP_A^e = -\frac{1}{2}\begin{Bmatrix} \dot{V} \\ \dot{W} \end{Bmatrix}^T \begin{bmatrix} P & 0 \\ 0 & P \end{bmatrix} \begin{Bmatrix} \dot{V} \\ \dot{W} \end{Bmatrix} dx \tag{4.3.15}$$

$$dT^e = \frac{1}{2}\begin{Bmatrix}\dot{V}\\ \dot{W}\end{Bmatrix}^T \begin{bmatrix}\mu(x) & 0\\ 0 & \mu(x)\end{bmatrix}\begin{Bmatrix}\dot{V}\\ \dot{W}\end{Bmatrix}dx + \frac{1}{2}\dot{\phi}\, I_p(x)dx + \frac{1}{2}\begin{Bmatrix}\dot{B}\\ \dot{\Gamma}\end{Bmatrix}^T \begin{bmatrix}I_d(x) & 0\\ 0 & I_d(x)\end{bmatrix}\begin{Bmatrix}\dot{B}\\ \dot{\Gamma}\end{Bmatrix}dx + \dot{\phi}\dot{\Gamma}\, I_p(x)dx \tag{4.3.16}$$

$$dP_B^e = \frac{1}{2}EI(x)\left\{q^e\right\}^T\left[\ddot{\psi}\right]^T\left[\ddot{\psi}\right]\left\{q^e\right\}dx \tag{4.3.17}$$

$$dP_A^e = -\frac{1}{2}P\left\{q^e\right\}^T\left[\dot{\psi}\right]^T\left[\dot{\psi}\right]\left\{q^e\right\}dx \tag{4.3.18}$$

$$dT^e = \frac{1}{2}\mu(x)\{\dot{q}^e\}^T\left[\dot{\psi}\right]^T\left[\dot{\psi}\right]\{\dot{q}^e\}dx + \frac{1}{2}\dot{\phi}\, I_p(x)dx + \frac{1}{2}I_d(x)\{\dot{q}^e\}^T\left[\Phi\right]^T\left[\Phi\right]\{\dot{q}^e\}dx + \dot{\phi}\, I_p(x)\{\dot{q}^e\}^T\left[\Phi_\Gamma\right]^T\left[\Phi_B\right]\{\dot{q}^e\}dx \tag{4.3.19}$$

The energy of the complete shaft-rotor element is obtained by integrating equation over the element length is given by Eq. (4.3.20).

$$P_B^e + P_A^e + T^e = \frac{1}{2}\left\{q^e\right\}^T([K_B^e]-[K_A^e])\left\{q^e\right\} + \frac{1}{2}\{\dot{q}^e\}^T([M_T^e]-[M_R^e])\{\dot{q}^e\} + \frac{1}{2}I_P^e\dot{\phi}^{\,2} + \dot{\phi}\{\dot{q}^e\}^T[N^e]\{\dot{q}^e\} \tag{4.3.20}$$

Where,

$$\left[M_T^e\right] = \int_0^l \rho A(x)\left[\psi\right]^T\left[\psi\right]dx \tag{4.3.21}$$

$$\left[M_R^e\right] = \int_0^l I_d(x)\left[\Phi\right]^T\left[\Phi\right]dx \tag{4.3.22}$$

$$\left[N_e\right] = \int_0^l I_p(x)\left[\phi_\Gamma\right]^T\left[\phi_\beta\right]dx \tag{4.3.23}$$

$$\left[K_B^e\right] = \int_0^l EI(x)\left[\psi''\right]^T\left[\psi''\right]dx \tag{4.3.24}$$

$$\left[K_A^e\right] = \int_0^l P\left[\psi'\right]^T \left[\psi'\right] dx \tag{4.3.25}$$

The Lagrangian equation of motion of the finite rotor shaft element under constant spin condition is given by Eq. (4.3.26). Gyroscopic matrix is given by Eq. (4.3.27).

$$([M_T^e]+[M_R^e])\{\ddot{q}^e\} - \Omega[G^e]\{\dot{q}^e\} + ([K_B^e]+[K_A^e])\{q^e\} = \{Q^e\} \tag{4.3.26}$$

$$[G^e] = ([N^e]-[N^e]^T) \tag{4.3.27}$$

4. 4 System equations of motion

The assembled equation of motion for complete system, consisting of component equations is given by Eq. (4.4.1). The mass matrix [M^s] contains the assemblage of both the translational and rotary effect of the shaft, the rigid disk mass and the diametric moment of inertia. The matrix [G^s] represents the gyroscopic moments and is skew symmetric in nature. The stiffness matrix [K^s] contains stiffness effects of rotor-shaft elements. The excitation matrix [Q^s] contains the excitation due to external forces.

$$[M^s]\{\ddot{q}^s\} + [G^s]\{\dot{q}^s\} + [K^s]\{q^s\} = \{Q^s\} \tag{4.4.1}$$

For efficiently and simple computing, equation (4.4.1) is expressed in terms of the first order state vector form in equation (4.4.2).

$$\begin{bmatrix} [0] & [M^s] \\ [M^s] & -\Omega[G^s] \end{bmatrix} \{\dot{z}\} + \begin{bmatrix} [-M^s] & [0] \\ [0] & [K^s] \end{bmatrix} \{z\} = \{Z\} \tag{4.4.2}$$

Where

$$\{z\} = \begin{Bmatrix} \{\dot{q}\} \\ \{q\} \end{Bmatrix}, \quad \{Z\} = \begin{Bmatrix} \{0\} \\ \{Q^s\} \end{Bmatrix} \tag{4.4.3}$$

4.5 Summary

This chapter describes the detail of the finite element formulation of the shaft-rotor system. The equation of motion of the rotating non-uniform shaft is derived using Lagrangian approach together with the finite-element method. Finite element model of rigid disk and finite shaft element has been presented. Element mass, stiffness and

gyroscopic matrices are found. Expression for the assembled equation of motion for complete shaft-rotor system is also presented. Results and discussions are discussed in the next chapter.

CHAPTER-5

RESULTS AND DISCUSSIONS

5.1 Transfer matrix approach

5.1.1 Profiled shaft-rotor system with multi disks

A cantilever profiled rotor-shaft system with two disks at different lengths is shown in Fig. 5.2. By replacing l_1, m_1, J_1 and l_2, m_2, J_2 instead of l, m and J as in Whalley and Ameer [2], for suffixes 1 and 2 respectively for the rotors-shafts and neglecting the bearing effects, as proceeded in the above sections, in the same way for the dual disk systems illustrated in Fig. 5.2. can be formulated as-

$$\boldsymbol{H(s) = R_2(s)F_2(s)R_1(s)F_1(s)} \qquad (5.1.1)$$

$(y_1(s), y_5(s))$, $(\theta_1(s), \theta_5(s))$, $(M_{y1}(s), M_{y5}(s))$ *and* $(Q_{y1}(s), Q_{y5}(s))$ are the deflections, slopes, bending moments and shear forces at the fixed and free end respectively. Distributed-lumped shaft rotor model for two shafts and two disks is shown in Fig. 5.1.

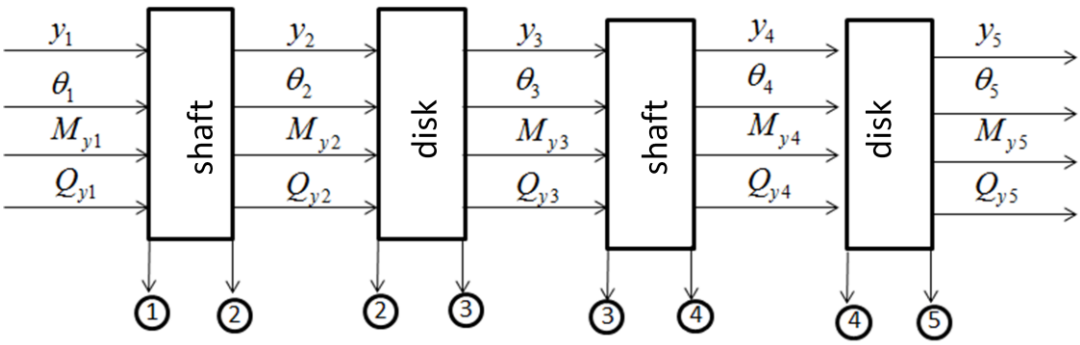

Fig. 5.1 Distributed-lumped shaft-rotor model for two shafts and disks.

Input-output vectors relationship for the model shown in Fig. 5.1 is given by,

$$\begin{bmatrix} y_5 \\ \theta_5 \\ M_{y5} \\ Q_{y5} \end{bmatrix} = H(s) \begin{bmatrix} y_1 \\ \theta_1 \\ M_{y1} \\ Q_{y1} \end{bmatrix}$$

Applying the boundary conditions for a cantilever shaft-rotor, and adding impulse of 1N on the free end, the above equation can be written as,

$$\begin{bmatrix} y_5 \\ \theta_5 \\ 0 \\ 1 \end{bmatrix} = \begin{bmatrix} H_{11} & H_{12} \\ H_{21} & H_{22} \end{bmatrix} \begin{bmatrix} 0 \\ 0 \\ M_{y1} \\ Q_{y1} \end{bmatrix}$$

Hence,

$$\begin{bmatrix} y_5 \\ \theta_5 \end{bmatrix} = H_{11} \begin{bmatrix} 0 \\ 0 \end{bmatrix} + H_{12} \begin{bmatrix} M_{y1} \\ Q_{y1} \end{bmatrix} = H_{12} \begin{bmatrix} M_{y1} \\ Q_{y1} \end{bmatrix}$$

Then,

$$\begin{bmatrix} 0 \\ 1 \end{bmatrix} = H_{21} \begin{bmatrix} 0 \\ 0 \end{bmatrix} + H_{22} \begin{bmatrix} M_{y1} \\ Q_{y1} \end{bmatrix} = H_{22} \begin{bmatrix} M_{y1} \\ Q_{y1} \end{bmatrix}$$

From the above Eqs., we get

$$\begin{bmatrix} y_5 \\ \theta_5 \end{bmatrix} = H_{12}.H_{22}^{-1} \begin{bmatrix} 0 \\ 1 \end{bmatrix}$$

And hence transfer function can be obtained from above expressions, which represents the ratio displacement to the force in Laplace domain. For numerical analysis following data are considered for the system illustrated in Fig. 5.2:

$m_1 = 0.6$ kg, $m_2 = 0.7$ kg,
$d_1 = 0.08$ m, $d_2 = 0.09$ m,
ρ=7800 kg/m^3, E=209x$10^9 Pa$
$\omega = 10000$ rpm and
$l_1 = l_2 = 0.075$ m, $r_0 = 0.005$ m

For example, applying the fixed-free boundary condition, the transfer function for NN=40 and rotational speed of 10000 rpm with 1 N vertically downward force on the disk is given as

$$\frac{1.667s^4 + 7.262\times10^4 s^3 + 6.839\times10^8 s^2 + 2.77\times10^{11} s + 1.726\times10^{15}}{s^6 + 4.357\times10^4 s^5 + 4.137\times10^8 s^4 + 2.308\times10^{11} s^3 + 1.223\times10^{15} s^2 + 7.014\times10^{16} s + 8.814\times10^{19}}$$

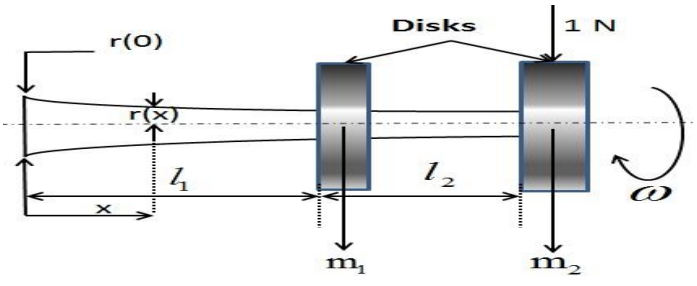

Fig. 5.2 Non-uniform shaft-rotor system with dual disk.

The profile equation for the shaft-rotor [2] is given by

$$r(x) = r_0(1 - NN(x^2)) \tag{5.1.2}$$

Bode plots for different profile values, rotating speeds and shaft-rotor lengths have been obtained and are shown in Fig. 5.3, Fig. 5.4 and Fig. 5.5 respectively and the results obtained are tabulated for better understanding.

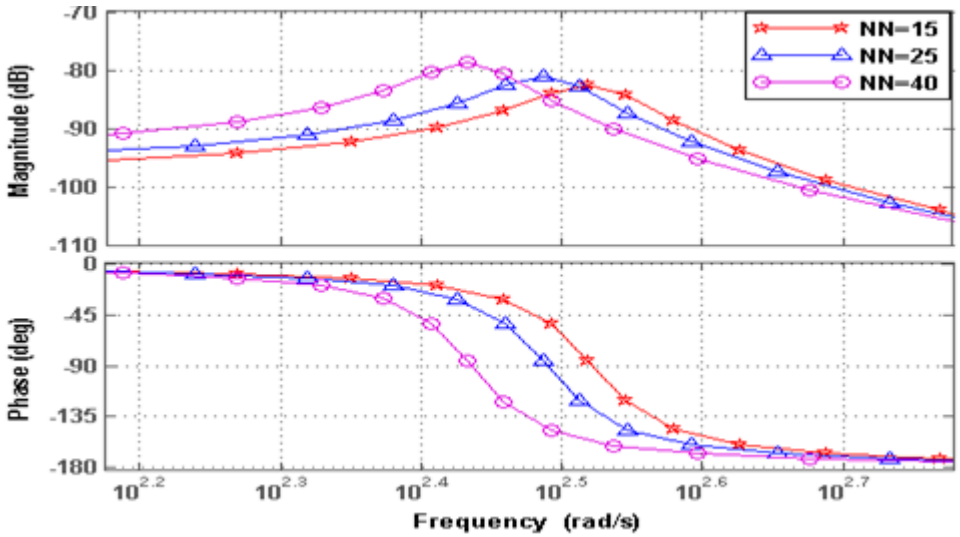

Fig. 5.3 Bode plot for varying profiles for shaft-rotor system illustrated in Fig. 5.2 for 10000 rpm and l_1=l_2=0.075 m .

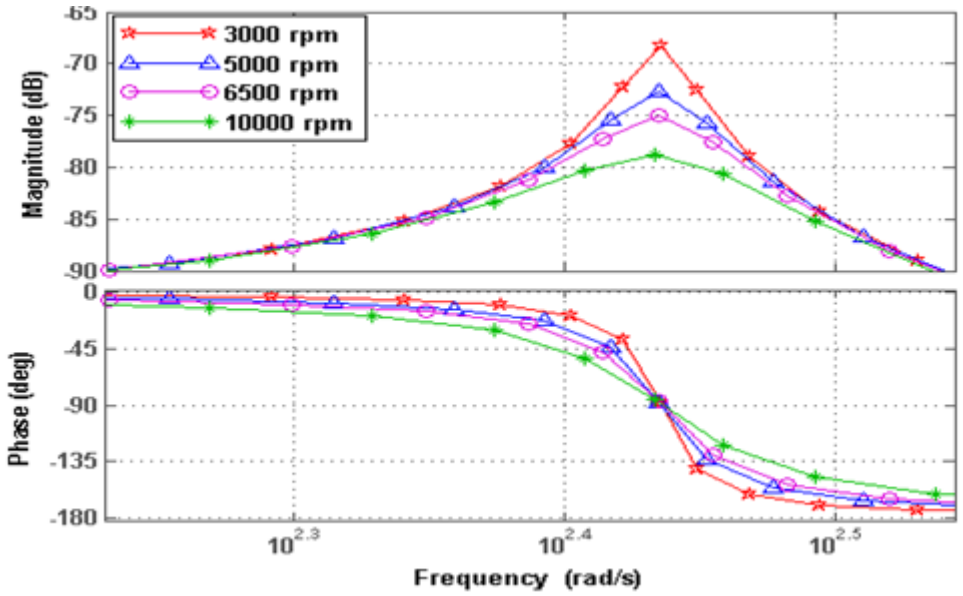

Fig. 5.4 Bode plot for different rotor speeds for shaft-rotor system illustrated in Fig. 5.2 for NN=25 and l_1=l_2=0.075 m.

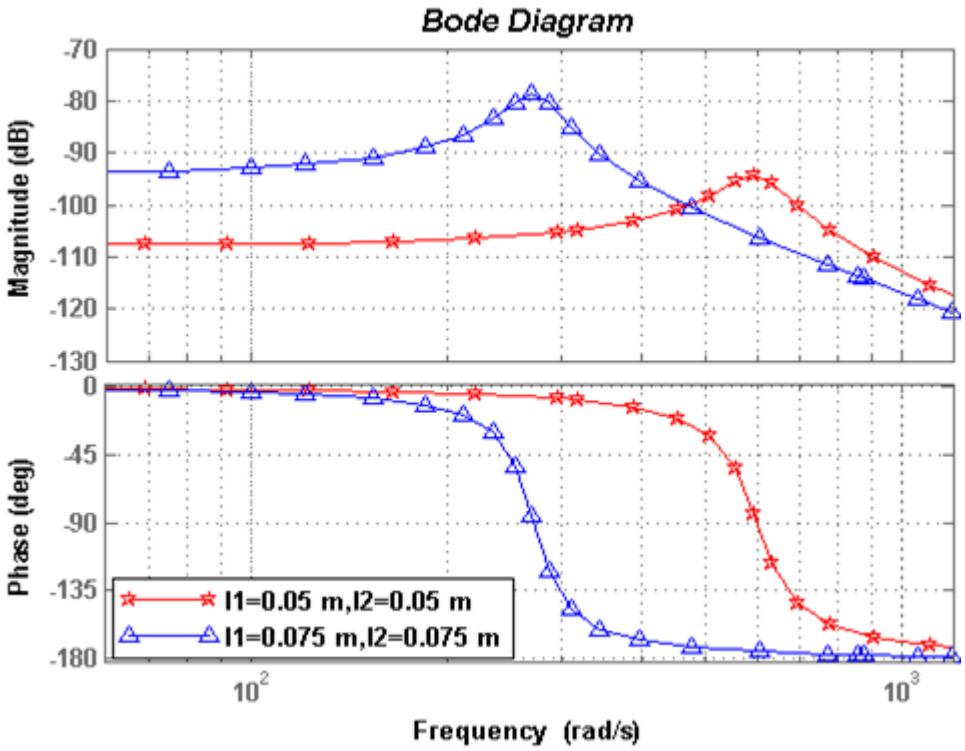

Fig. 5.5 Bode plot for different rotor lengths for shaft-rotor system illustrated in Fig. 5.2 for 10000 rpm and NN=25.

The x-axis of bode plot represents the frequency in rad/s, while y-axis represents the amplitude in dB. However they can be represented by other units. The whirling frequency is noted at the peaks in magnitude diagram of Bode plot. All the plots are obtained using MATLAB® software. It is observed that as the speed of rotor decreases the amplitude increases and vice-versa. Also, small change in shaft length has significant effect on critical frequency.

Table 5.1. Results obtained from Bode plots for shaft-rotor system illustrated in Fig. 5.2

l_1 (m)	l_2 (m)	Speed (rpm)	Value of NN	Critical Frequency (rad/sec)	Amplitude (dB)
0.050	0.050	10000	40	593	-94.4
0.075	0.075	10000	40	271	-78.7
0.075	0.075	10000	15	330	-82.5
0.075	0.075	10000	25	307	-81.1
0.075	0.075	3000	40	272	-68.3
0.075	0.075	5000	40	272	-72.7
0.075	0.075	6500	40	304	-75.0

For NN=40, at 11000 rpm, the step response, following an impulse of unit load (in Newton) at the free end, gives the characteristics shown in Fig. 5.6. This indicates that steady state conditions will be restored in approximately 0.157 s. At lesser rotational

speeds the effects would be much greater because of the reduction in the gyroscopic couple. In Fig. 5.6, at 5500 rpm the maximum overshoot remains almost unchanged, but its settling time is almost double than for that of 11000 rpm, i.e., 0.314 s, after the same impulse disturbance.

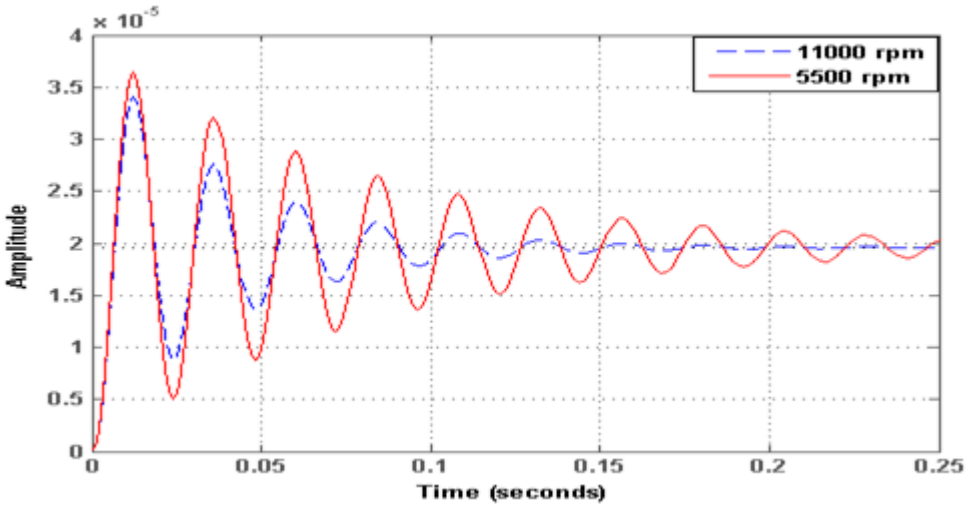

Fig. 5.6 Step Response for multi-disc profiled shaft-rotor system shown in Fig. 5.2.

5.1.2 Multi-profiled shaft rotor system

5.1.2 (a) Different profiled shafts and disks in series

A typical shaft-rotor system with two different profiled shafts with two disks at the end of each profiled shaft is shown in Fig. 5.7. Various parameters and their values for multi-profiled system shown in Fig. 5.7 have been given in Table 5.2.

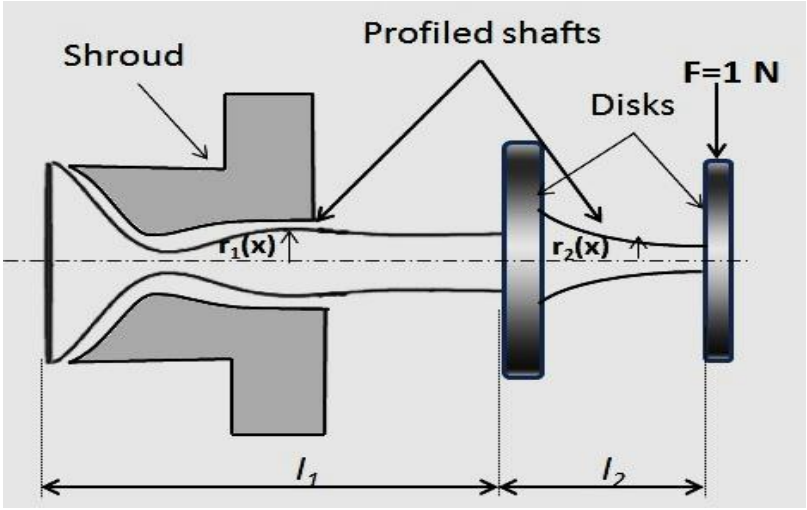

Fig. 5.7 Multi profiled shaft-rotor with two disks.

Table 5.2. Values for the multi-profiled shaft-rotor system illustrated in Fig. 5.7

Parameters	**Values**
Length of the shaft-rotors, l_1, l_2 (m)	0.2, 0.1
Mass of the disks, m_1, m_2(Kg)	20, 1
Diameters of the disks, D_1, D_2 (m)	0.2, 0.09
Young's Modulus of Elasticity, E (GPa)	209
Density of the material, ρ (Kg/m^3)	7800
Rotational Speed (rpm)	5000

The equation of radius for shaft 1 is given by,

$$r_1(x) = 0.01 + 0.027275e^{(-12.8x)}\sin(29.328x + 1.1593) - 0.00035x. \qquad (5.1.3)$$

And the equation of the radius of shaft 2 is given by,

$$r_2(x) = r_0(1 - NN(x^2)). \qquad (5.1.4)$$

As seen from Fig. 5.7, there are two different profiled shafts in the rotor system and two disks at the end of each profiled-shaft have been mounted. Equations for the profiles of each shaft are different and have been mentioned earlier. The illustrated system can be practically manufactured either by casting or some other production methods. Otherwise two different profiled shafts can be coupled together by some suitable coupling devices. However, any such coupling devices and their effects have not been considered in the present work. The model will be same as shown in Fig. 5.1. The transfer function for the values given in Table for profiled shaft-rotor system as illustrated in Fig. 5.7 is given by,

$$\frac{s^4 + 1.6097*10^7 s^3 + 1.1766*10^{13} s^2 + 4.6549*10^{19} s + 6.6205*10^{23}}{s^6 + 1.6097*10^7 s^5 + 1.1766*10^{13} s^4 + 4.6549*10^{19} s^3 + 6.6204*10^{23} s^2 + 4.4789*10^{25} s + 1.5968*10^{29}} \qquad (5.1.5)$$

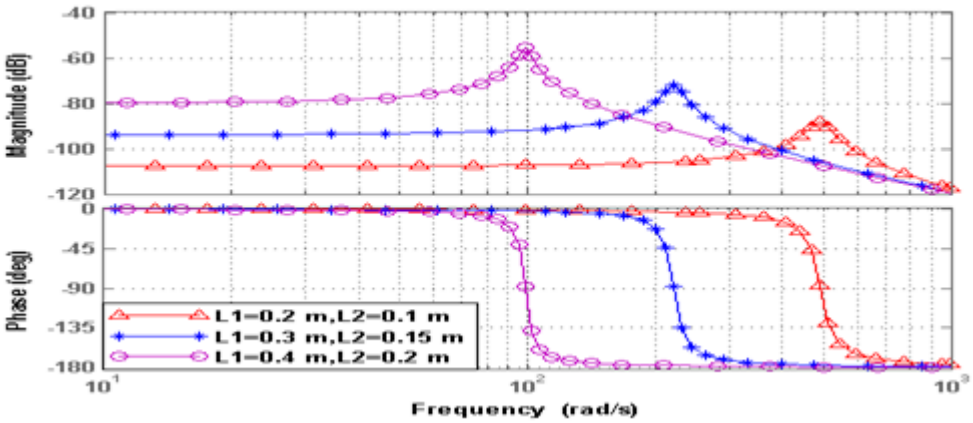

Fig. 5.8 Bode plot for varying lengths for multi-profiled shaft-rotor system at 5000 rpm.

The effect of different shaft lengths of rotating systems on frequency response calculation is significant. So, the study of changing length is considered to be of great use dealing with the resonance conditions. The Bode plot has been obtained for different lengths of the shaft-rotor segments at 5000 rpm and NN=15, as shown in Fig. 5.8. The plot shows the effect of different lengths while rotor-speed has been kept constant. The effect of change in lengths of the shaft part of the concerned rotor system (Fig. 5.7) is clearly notable from Fig. 5.8. As shown in the bode plot, when the shaft length is increased from 0.2 m and 0.1 m of lengths to 0.4 m and 0.2 m respectively, the critical frequency changes from 491 rad/s to 98.6 rad/s. While the amplitude increases from -87.9 dB to -55.4 dB respectively.

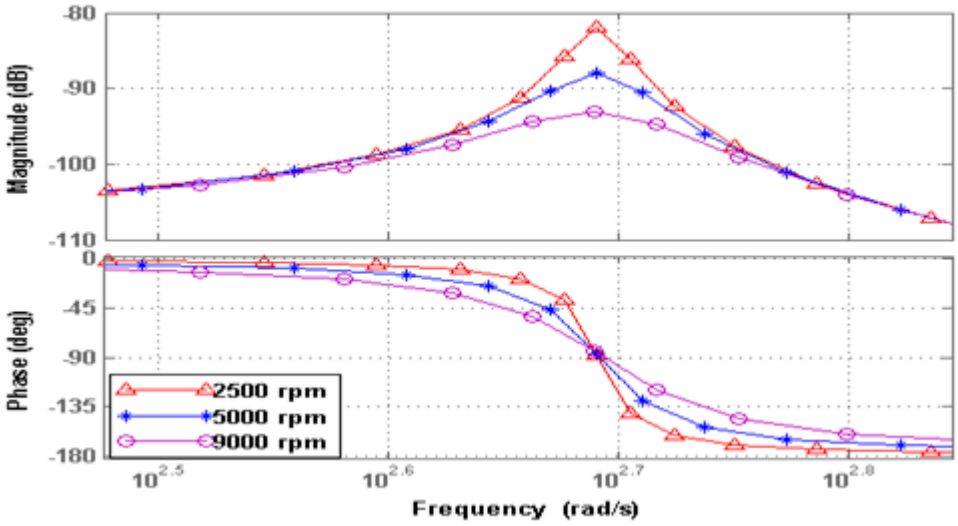

Fig. 5.9 Bode plot for varying rotor speedfor multi-profiled shaft-rotor system.

The Bode plot has been obtained for changing rotor speeds for 2500, 5000 and 9000 rpm as shown in Fig. 5.9. The lengths of the shafts have been kept constant i.e. l_1 = 0.2 m and l_2 = 0.1 m respectively. Also, the profile value of second profiled shaft is also kept as NN=15. It may be noticed that the effect of rotational speeds on the critical frequency is negligible, however the impact on amplitude can be felt via bode plot. As shown from the bode plot, when the rotational speed is increased from 2500 rpm to 9000 rpm, the whirling frequency remains constant at 491 rad/s but the magnitude decreases from -81.9 dB to -93 dB respectively.

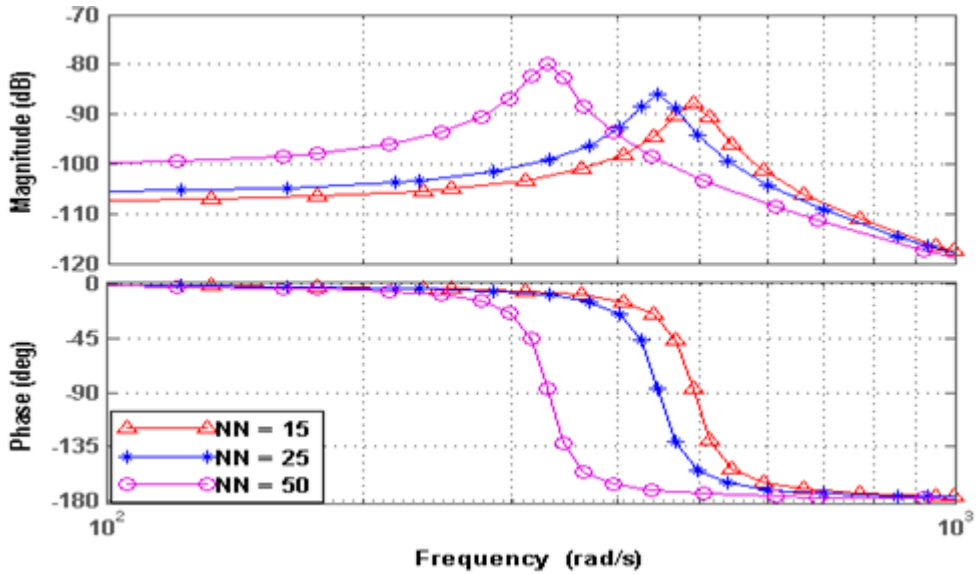

Fig. 5.10 Bode Plot for different profile values (NN) at 5000 rpm.

The Bode plot has been obtained for different profile values of the shaft-rotor system by changing the values of NN in the profile equation of the second shaft-rotor. The rotor speed and length of the shaft part of the rotor is kept constant at 5000 rpm and l_1 = 0.2 m and l_2 = 0.1 m respectively. As shown in Fig. 5.10, when the profile value NN for the second profile shaft is changed from 15 to 50, then the whirling frequency reduces from 491 rad/s to 330 rad/s respectively, while the magnitude increases from -87.9 dB to -79.9 dB respectively.

Table 5.3. Results obtained from Bode plots for multi-profiled shaft-rotor system shown in Fig. 5.7

l_1 (m)	l_2 (m)	Speed (rpm)	Value of NN	Critical Frequency (rad/sec)	Amplitude (dB)
0.20	0.10	5000	15	491	-87.9
0.20	0.10	5000	25	447	-86.0
0.20	0.10	5000	50	330	-79.9
0.30	0.15	5000	15	222	-71.8
0.40	0.20	5000	15	98.6	-55.4
0.20	0.10	2500	15	491	-81.9
0.20	0.10	9000	15	490	-93.0

For NN=15, at 9000 rpm, the step response, following an impulse of 1 N, gives the characteristics shown in Fig. 5.11. It shows the steady state conditions will be restored in approximately 0.0839s. At lesser rotational speeds the effects of this disturbance would be greater because of the reduction in the gyroscopic couple. In Fig. 5.11, at

4500 rpm the maximum overshoot remains unchanged, but settling time is almost double than for 9000 rpm, i.e., 0.167 s, after the same impulse.

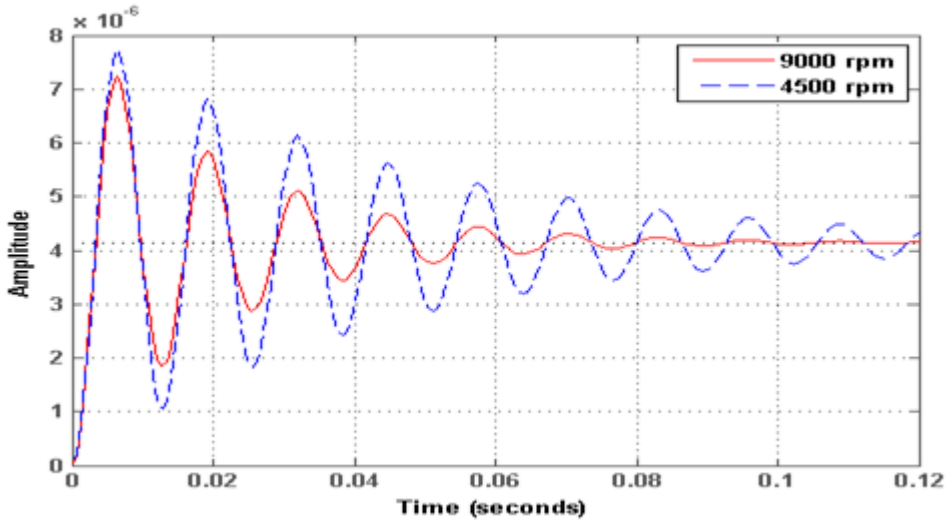

Fig. 5.11 Step response for multi-profiled shaft-rotor system

5.1.2 (b) Convergent-divergent shaft-rotor system

In this section, two profiled shafts in series have been taken into account. The cross-sectional area of the first shaft is reducing till the neck portion and then area of the second shaft gradually increases till the end of the shaft, where a disk is attached, as shown in Fig. 5.12 for illustration purpose. The ending radius of the convergent shaft portion is will be the starting radius for the divergent portion of the shaft-rotor. The transfer function will be obtained by,

$$\boldsymbol{H(s) = R(s)F_2(s)F_1(s)} \tag{5.1.6}$$

Where R(s) is the rigid disk matrix while the $F_1(s)$ and $F_2(s)$ are the modal matrix for the convergent and divergent portions of the shaft-rotor respectively.

The profile equation for the shaft-rotor is given by-

$$r(x) = r_0(1 \mp NN(x^2)) \tag{5.1.7}$$

The '$\mp$' sign indicates the decrement and then increment in the cross-sectional area of the shafts. A unit impulse is applied on the disk at the free end to produce excitations in the shaft-rotor system. Values of different parameters of the convergent-divergent shaft-rotor system are given in Table 5.4.

Table 5.4. Various parameters of convergent-divergent shaft-rotor system as shown in Fig. 5.12

Parameters	Values
Length of the shaft-rotor, l_1, l_2 (m)	0.1, 0.1
Mass of the disk, m (Kg)	0.75
Diameter of the disk, D (m)	0.09
Young's Modulus of Elasticity, E (GPa)	209
Density of the material, ρ (Kg/m^3)	7800
Rotational Speed, N (rpm)	10000
Profile Value, NN (Constant)	15

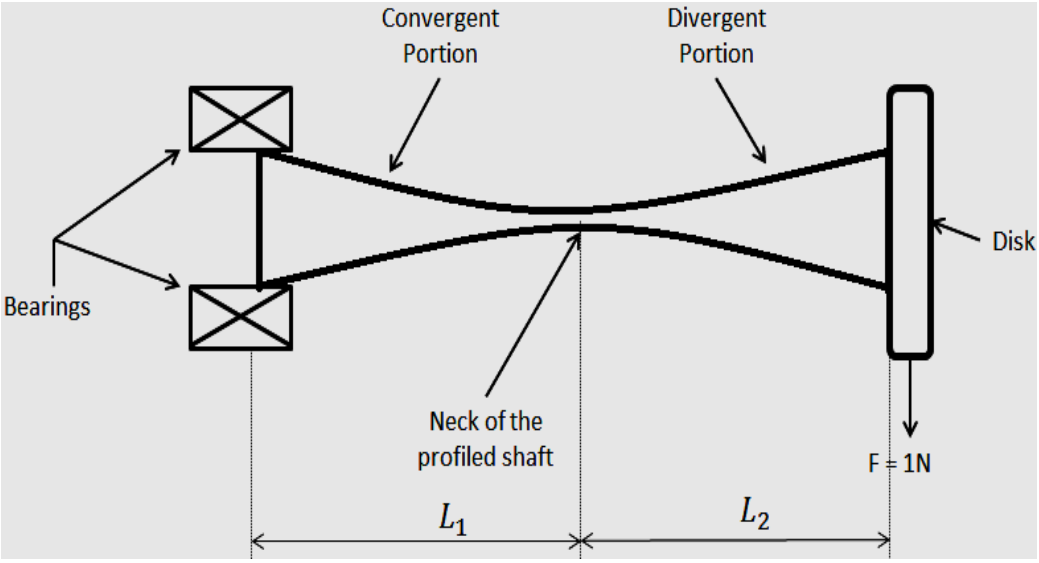

Fig. 5.12 Convergent divergent shaft rotor system with 1 N force on the disk.

Table 5.5. Neck radius for various profile values (NN) for convergent-shaft length of 0.1 m

Profile Value NN	Neck radius (m) of the shaft-rotor shown in Fig 4
15	0.0043
25	0.0037
40	0.0030

The transfer function obtained for the system shown in Fig. 5.12, for the values given in Table 5.4, is given as,

$$\frac{1.333\,s + 7090}{s^3 + 5317\,s^2 + 7.673\times10^5\,s + 1.044\times10^9}$$

Table 5.6. Computed values of compliance, mass per unit length and gamma parameter for shaft with l_1=0.1 m and l_2 =0.1 m and speed 10000 rpm

Profile Value (NN)	Compliance (C(x))			Mass per unit length (L(x))			Gamma Parameter ($\Gamma(x)$)		
	X=0	X=l1 (neck portion)	X=l2	X=0	X=l1 (neck portion)	X=l2	X=0	X=l1 (neck portion)	X=l2
15	0.00975	0.01867	0.01019	0.61261	0.44261	0.59921	0.17029	0.03015	0.02795
25	0.00975	0.03081	0.01331	0.6126	0.34459	0.52416	0.17029	0.03210	0.52416
40	0.00975	0.07521	0.01958	0.6126	0.22054	0.43226	0.17029	0.03589	0.03033

Bode plots for various lengths, profile value NN and rotor speed has been found with the help of MATLAB ® software shown in Figs. 5.13-5.15.

Table 5.7. Results obtained from Bode plots for convergent-divergent shaft-rotor system

l_1 (m)	l_2 (m)	Speed (rpm)	Value of NN	Critical Frequency (rad/sec)	Amplitude (dB)
0.10	0.10	10000	15	447	-91.3
0.10	0.10	10000	25	370	-91.0
0.10	0.10	10000	40	273	-89.9
0.15	0.15	10000	15	161	-76.4
0.20	0.20	10000	15	47	-62.4
0.10	0.10	1000	15	449	-71.3
0.10	0.10	2500	15	449	-79.3
0.10	0.10	4000	15	448	-83.4

Bode plot for different profile values (NN) of the convergent-divergent shaft-rotor system, with 0.1 m length for both convergent and divergent shaft portions respectively and rotational speed of 10,000 rpm is shown in Fig. 5.13.

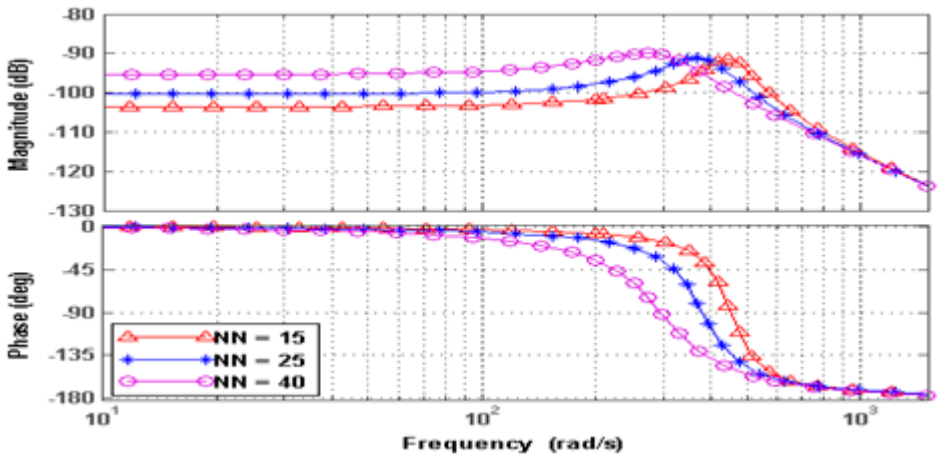

Fig. 5.13 Bode plot for varying profile values (NN) for convergent-divergent shaft-rotor system for L_1=0.1m and L_2=0.1m and 10000 rpm.

Bode plot for different lengths for both convergent and divergent shaft portions respectively of the convergent-divergent shaft-rotor system, with profile value NN of 15 and rotational speed of 10,000 rpm is shown in Fig. 5.14. It is seen that when the rotational speed increases the amplitude decreases.

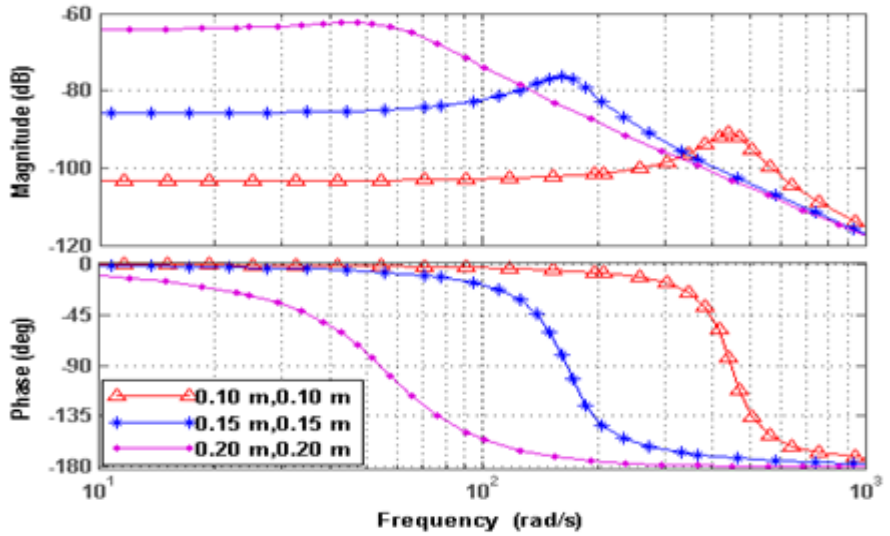

Fig. 5.14 Bode plot for different shaft lengths of convergent-divergent shaft-rotor with profile value (NN) =15 and 10000 rpm.

Bode plot for various rotational speeds (rpm) of the convergent-divergent shaft-rotor system, with 0.1 m length for both convergent and divergent shaft portions respectively and profile value (NN) of 15 is shown in Fig. 5.15.

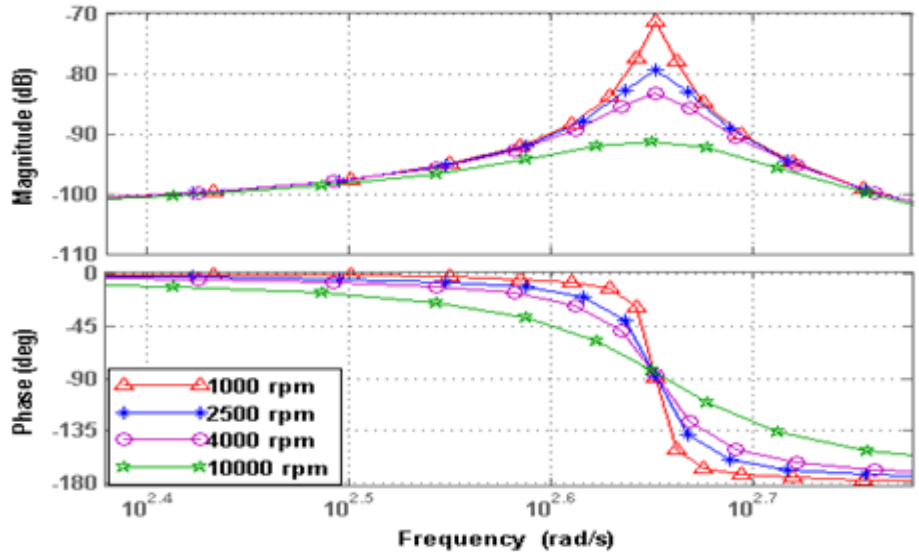

Fig. 5.15 Bode plot for varying rotor speeds for convergent-divergent shaft-rotor system for L_1=0.1 m, L_2=0.1 m and NN=15.

5.1.3 Hollow profiled shaft rotor system

5.1.3 (a) Hollow shaft-rotor with uniform thickness

A tubular or hollow profiled shaft with uniform thickness and a disk at free end is illustrated in Fig. 5.16, and values of various parameters of the system are given in Table 5.8. One can observe that the thickness remains constant throughout the shaft, while the inner bore gradually changes till the end of the shaft-rotor system.

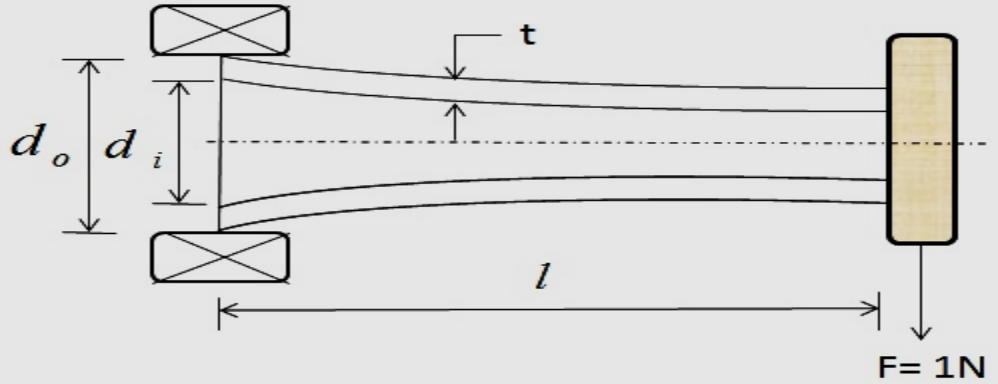

Fig. 5.16 Tubular profiled shaft with uniform thickness t and force of 1 N on the disk

Table 5.8. Values of various parameters for the system illustrated in Fig. 5.16

Parameters	Values
Length of the shaft-rotor, l (m)	0.1
r_0 (m)	0.005
Mass of the disk, m (Kg)	0.7443
Diameter of the disk, D (m)	0.09
Young's Modulus of Elasticity, E (GPa)	209
Density of the material, ρ (Kg/m^3)	7800
Rotational Speed, N (rpm)	10000
Thickness of the tubular shaft, t (m)	0.002
Profile value, NN (Constant)	25

After applying the boundary conditions for cantilever beam, we get deflection at the free end of the system, so we will ultimately get the transfer function, where the profile equation of the shaft-rotor is given by,

$$r(x) = r_0(1 - NN(x^2)). \tag{5.1.8}$$

For example, transfer function for NN=25, l=0.1m, t=0.002 m, E=209x10^9 Pa, m=0.7443 Kg, D=0.09 and rotational speed of 10000 rpm is given by,

$$\frac{1.344\,s + 1.025\times10^4}{s^3 + 7626\,s^2 + 8.608\times10^5\,s + 1.641\times10^9}. \tag{5.1.9}$$

Bode plot has been obtained for different profiles of the shaft-rotor system by changing the profile values of NN in Eq. (5.1.8) of the shaft, as shown in Fig. 5.17. Critical frequencies obtained for tubular profiled shafts are tabulated in Table 5.9.

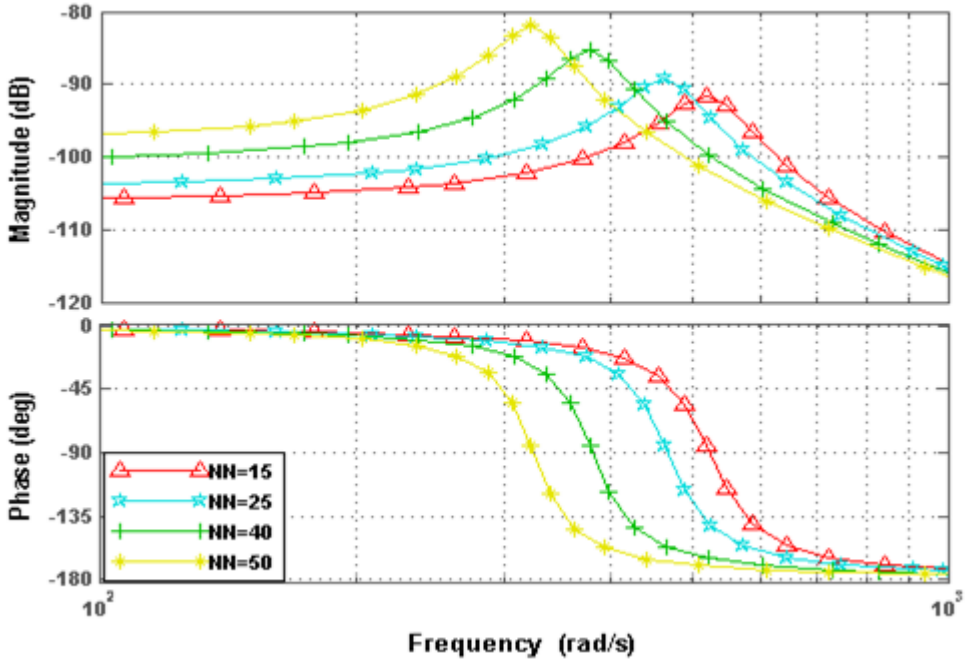

Fig. 5.17 Bode plot for different profile values (NN) for tubular profiled shaft-rotor for shaft-length of 0.1 m and rotating speed of 10000 rpm.

Table 5.9. Critical frequencies for rotating tubular shaft-rotor system for different profile values (NN)

Value of NN	**Critical Frequency(rad/s)**
15	518
25	463
40	378
50	322

The study of changing length is considered to be of great use dealing with the resonance conditions. Bode plot has been obtained for different lengths of the shaft-rotor segments as shown in Fig. 5.18.

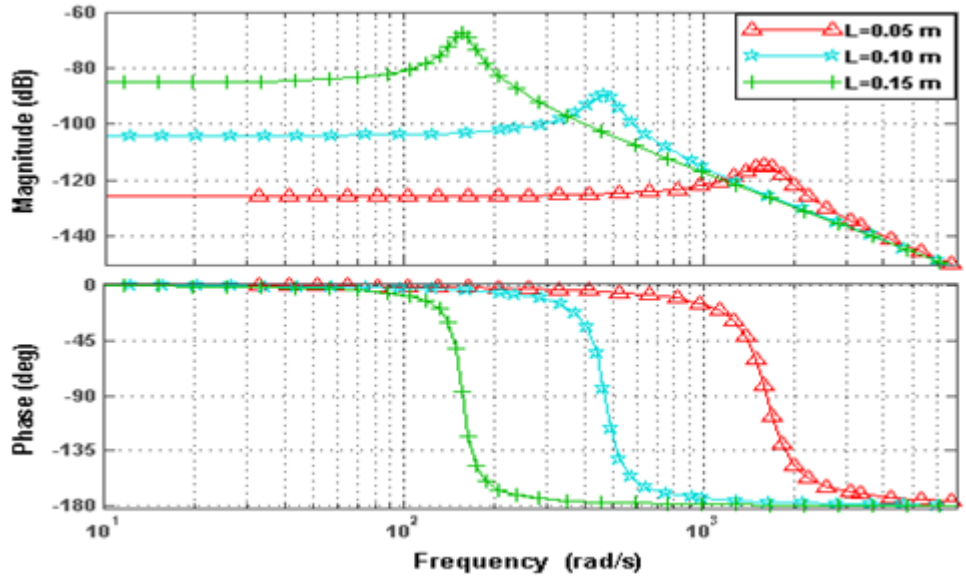

Fig. 5.18 Bode plot for different shaft lengths for tubular profiled shaft-rotor for profile value (NN) of 25 and rotating speed of 10000 rpm.

The Bode plot has been obtained for changing rotor speeds for 2000, 4000, 6000 and 10000 rpm as shown in Fig. 5.19. It may be noticed that the effect of rotational speeds on the critical frequency is negligible, however the impact on amplitude can be observed from bode plot.

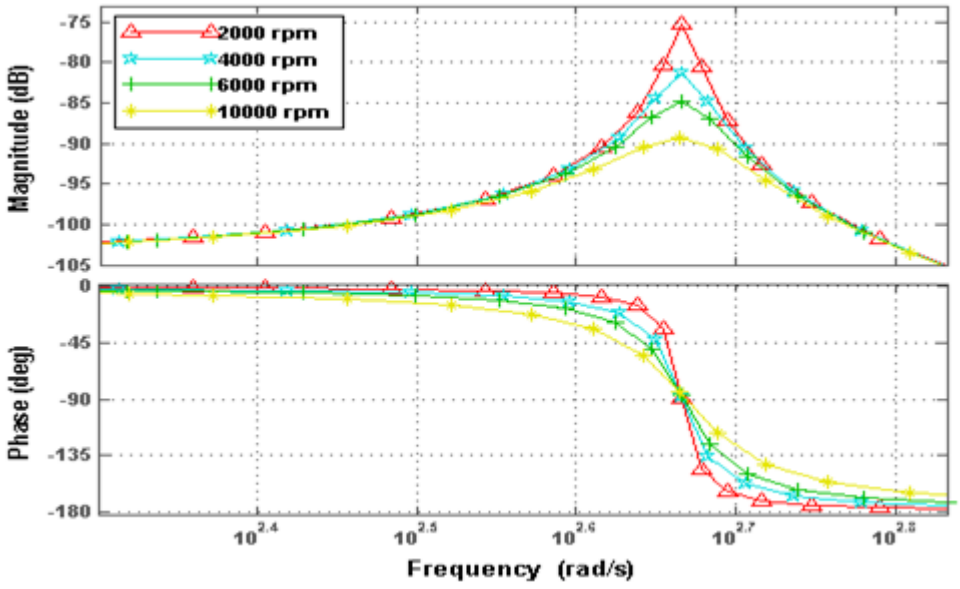

Fig. 5.19 Bode plot for different rotational speeds for tubular profiled shaft-rotor for shaft-length of 0.1 m and profile value (NN) of 25.

For NN=25, at 10000 rpm, the step response, following an impulse of 1 N, gives the characteristics shown in Fig 5.20. It shows the steady state conditions will be restored

in approximately 0.0891 s. At lesser rotational speeds the effects of this disturbance would be greater because of the reduction in the gyroscopic couple. In Fig. 5.20, at 5000 rpm the maximum overshoot remains unchanged, but settling time is almost double than for 10000 rpm, i.e., 0.183 s, after the same impulse disturbance, and hence is the effect of gyroscopic couple.

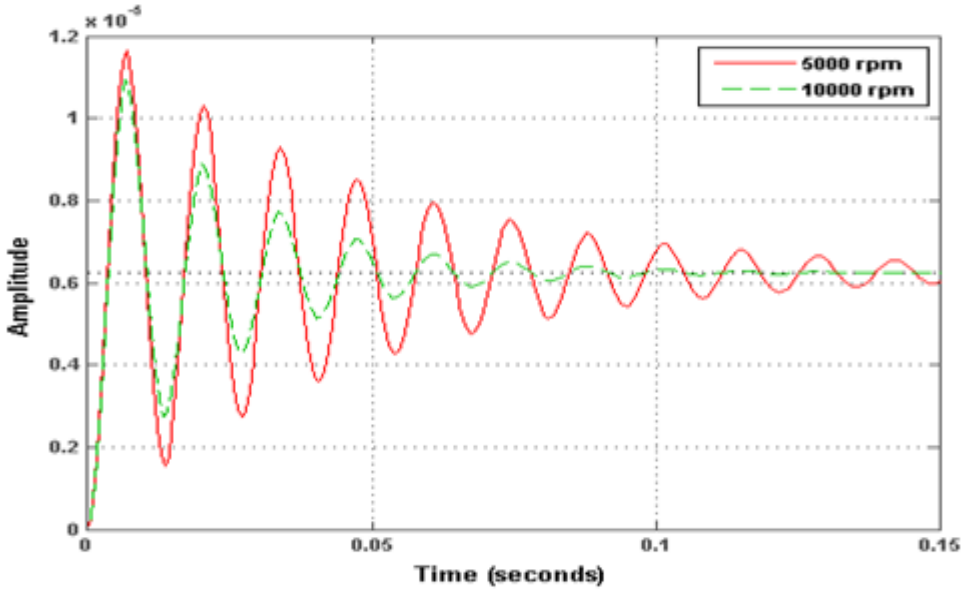

Fig. 5.20 Step response for an impulse of 1 N at two different speeds for tubular profiled shaft-rotor system shown in Fig. 5.16.

5.1.3 (b) Hollow shaft-rotor with uniform bore

A typical hollow profiled shaft with uniform bore and a disk at free end is illustrated in Fig. 5.21 and various parameters and their values are given in Table 5.10. One can observe that the bore remains constant throughout the shaft, while the thickness gradually changes till the end of the shaft-rotor system. For example, transfer function for NN=25, l=0.1m, d_i=0.002 m, E=209x10^9 Pa, m=0.7443 Kg, D=0.09 and rotational speed of 10000 rpm is given by,

$$\frac{1.344\,s + 1.217\times10^4}{s^3 + 9059s^2 + 1.097\times10^6 s + 2.483\times10^9} \qquad (5.1.10)$$

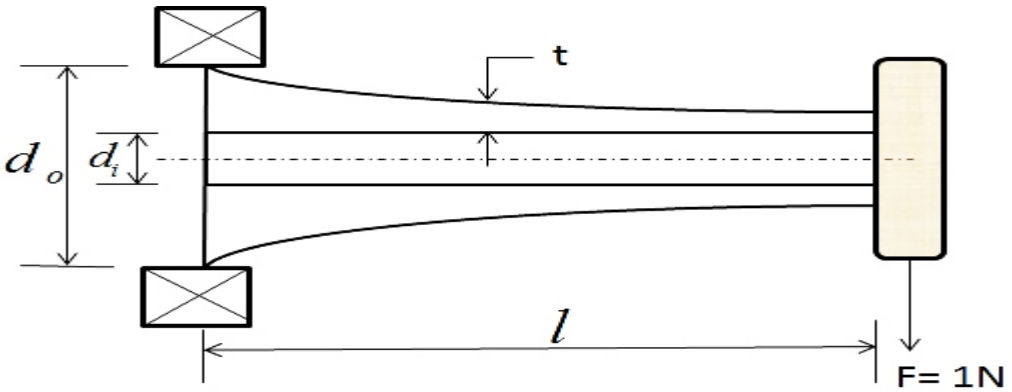

Fig. 5.21 Hollow profiled shaft with uniform bore and force of 1 N on the disk

Table 5.10. Values of various parameters for the system illustrated in Fig. 5.21

Parameters	**Values**
Length of the shaft-rotor, l (m)	0.1
Mass of the disk, m (Kg)	0.7443
r_0 (m)	0.005
Diameter of the disk, D (m)	0.09
Young's Modulus of Elasticity, E (GPa)	209
Density of the material, ρ (Kg/m^3)	7800
Rotational Speed, N (rpm)	10000
Inner radius of hollow shaft, r_i (m)	0.001
Profile Value, NN (Constant)	25

Bode plot has been obtained for different profiles of the shaft-rotor system by changing the profile values of NN in Eq. (5.1.8) of the shaft, as shown in Fig. 5.22.

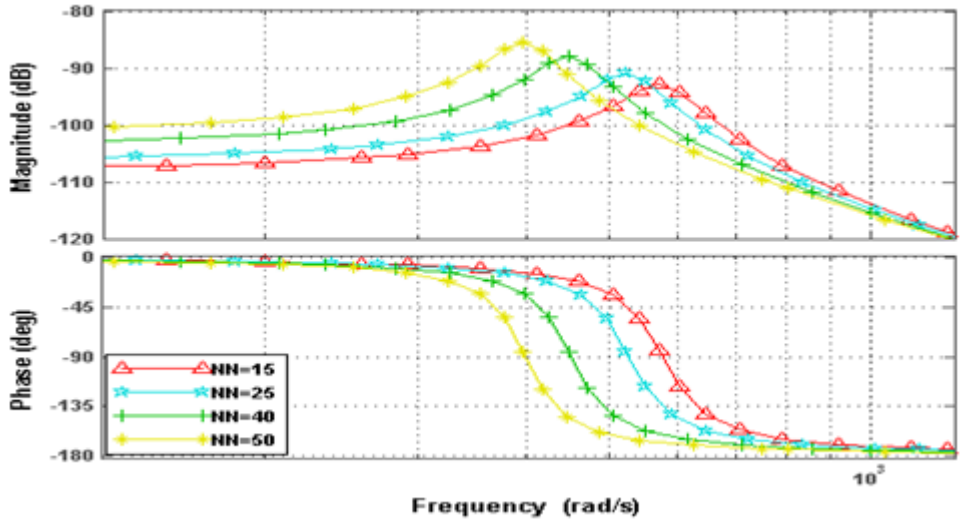

Fig. 5.22 Bode plot for different NN values for hollow profiled shaft-rotor for length of 0.1 m and rotating speed of 10000 rpm.

Table 5.11. Critical frequencies for hollow profiled shaft-rotor system for different profile values (NN)

Value of NN	Critical Frequency (Hollow Shaft) (rad/s)
15	570
25	522
40	448
50	397

The study of changing shaft-rotor length is considered to be of great use dealing with the resonance conditions. Bode plot has been obtained for different lengths of the shaft-rotor segments as shown in Fig. 5.23.

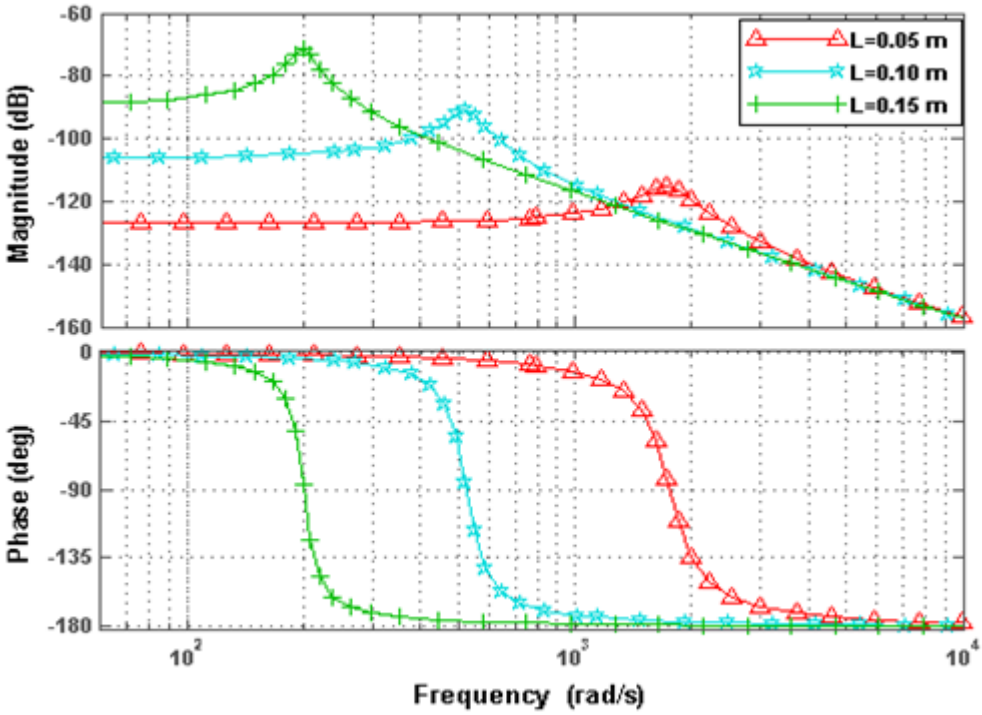

Fig. 5.23 Bode plot for different shaft lengths for hollow profiled shaft-rotor for profile value (NN) of 25 and rotating speed of 10000 rpm.

The Bode plot has been obtained for changing rotor speeds for 2000, 4000, 6000 and 10000 rpm as shown in Fig. 5.24. It may be noticed that the effect of rotational speeds on the critical frequency is negligible, however the effect on amplitude can be felt via bode plot.

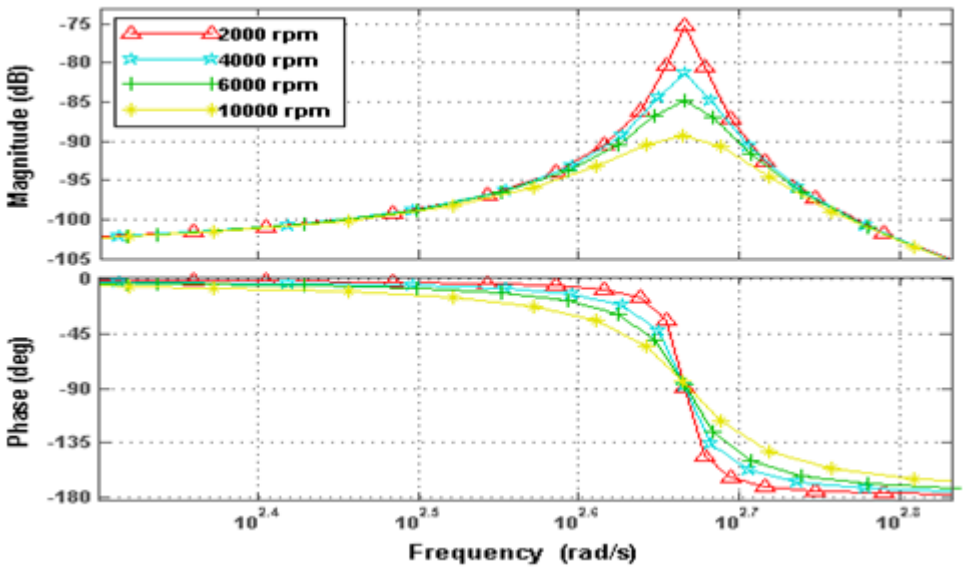

Fig. 5.24 Bode plot for different rotational speeds for hollow profiled shaft-rotor for length of 0.1 m and rotating profile value (NN) of 25.

For NN=25, at 10000 rpm, the step response, following an impulse of 1 N, gives the characteristics shown in Fig 5.25 It shows the steady state conditions will be restored in approximately 0.0846 s. At lesser rotational speeds the effects of this disturbance would be greater because of the reduction in the gyroscopic couple. In Fig.5.25, at 5000 rpm the maximum overshoot remains unchanged, but settling time is almost double than for 10000 rpm, i.e., 0.169 s, after the same impulse disturbance, and hence is the effect of gyroscopic couple.

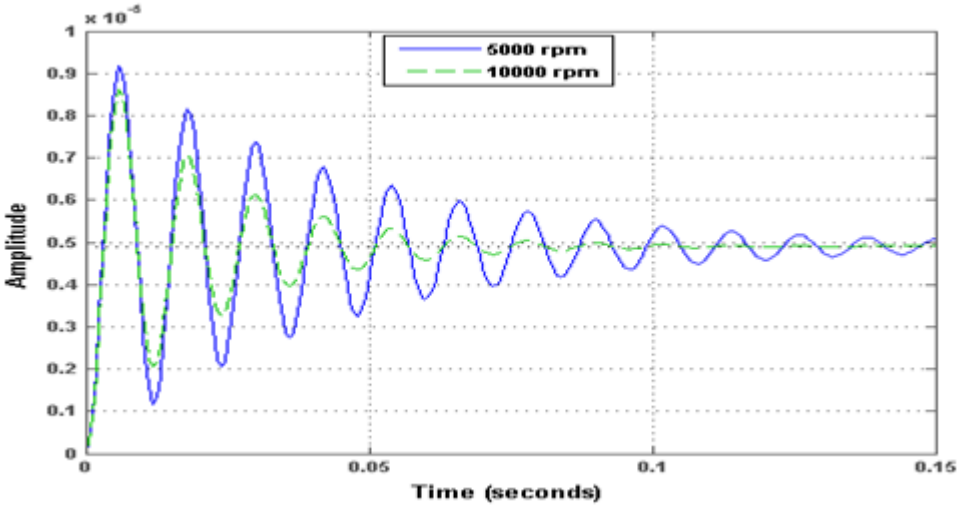

Fig. 5.25 Step response for an impulse force at two different speeds for hollow profiled shaft-rotor system shown in Fig. 5.21.

5.1.4 Linear tapered shaft rotor system

5.1.4 (a) Hollow shaft-rotor with uniform thickness

A cantilever tapered shaft-rotor with uniform thickness t and a disk at the free end with a downward force 'P' on the disk as shown in Fig. 5.26. The values of various parameters are tabulated in Table 5.12.

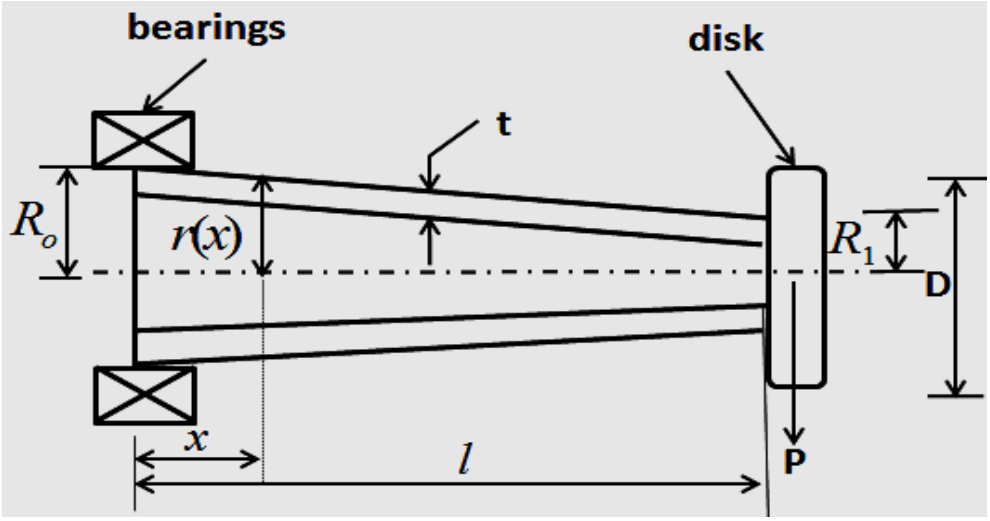

Fig. 5.26 Hollow tapered shaft-disk with uniform thickness.

The profile equation of the shaft-rotor or the radius, which is the function of shaft's length, is given by,

$$r(x) = R_0 + \left(\frac{R_1 - R_0}{l}\right)x \tag{5.1.11}$$

Where R_0 and R_1 are the starting and ending radius of the tapered shaft respectively.

Table 5.12. Various parameters of the hollow shaft-rotor system shown in Fig. 5.26 and their values

Parameters	**Values**
Length of the shaft-rotor, l (m)	0.1
Mass of the disk, m (Kg)	0.7443
Diameter of the disk, D (m)	0.09
Young's Modulus of Elasticity, E (GPa)	209
Density of the material, ρ (Kg/m^3)	7800
Rotational Speed, N (rpm)	10000
Thickness of the hollow shaft, t (m)	0.002
Beginning radius , R_0 (m)	0.0050
End radius, R_1 (m)	0.0037

Transfer function for tubular shaft with constant thickness as shown in Fig. 5.26 for the values given in Table 5.12 is computed, and is given by,

$$\frac{1.344\,s+1.016\times10^{4}}{s^{3}+7564\,s^{2}+8.401\times10^{5}\,s+1.589\times10^{9}}. \qquad (5.1.12)$$

Bode plots for different lengths and rotating speed have been plotted using MATLAB® software, as shown in Fig. 5.27 and Fig. 5.28.

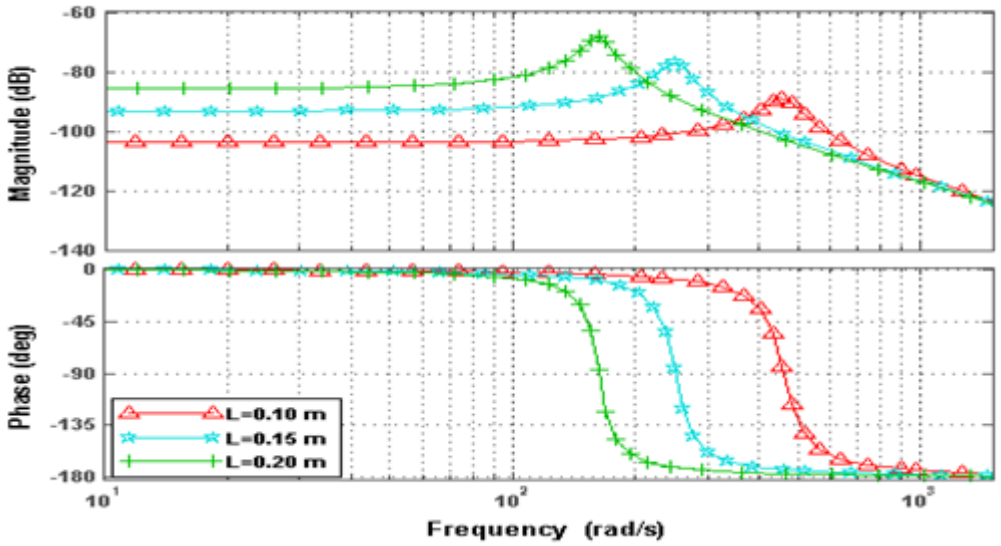

Fig. 5.27 Bode plot for different lengths for hollow tapered shaft-rotor with uniform thickness and rotating speed of 10000 rpm.

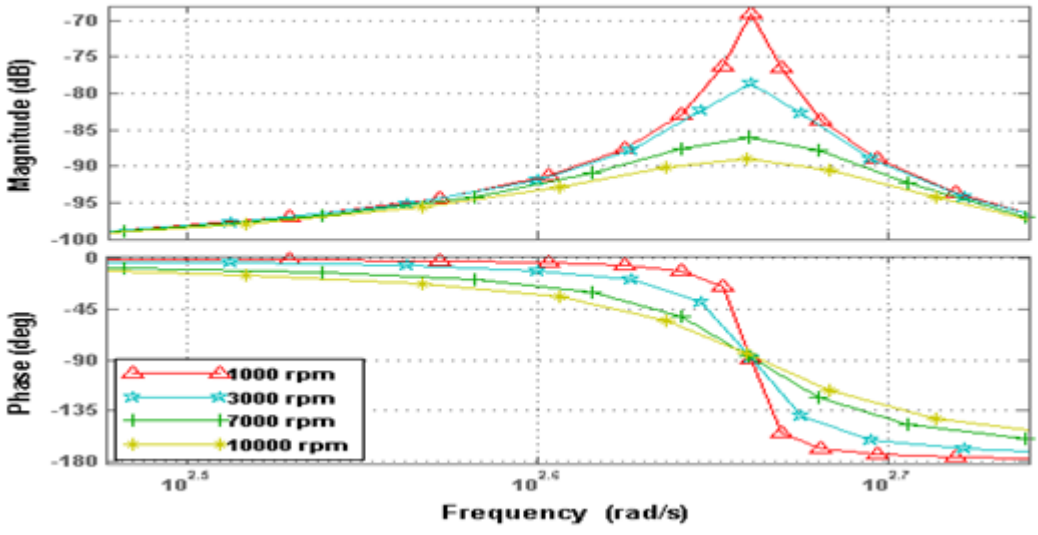

Fig. 5.28 Bode plot for various speeds for hollow tapered shaft-rotor with uniform thickness and length of 0.1 m.

5.1.4 (b) Hollow shaft-rotor with uniform bore

A typical cantilever hollow tapered shaft with uniform bore and a disc at the free end is shown in Fig. 5.29. The values of various parameters are given in Table 5.13.

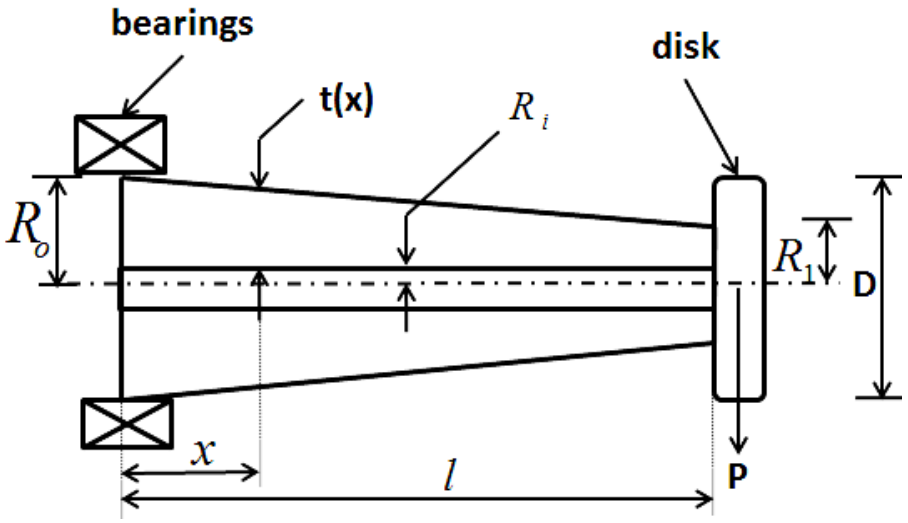

Fig. 5.29 Hollow tapered shaft-disk with uniform bore and vertically downward force P on the disk.

The profile equation of the tapered shaft-rotor or the radius which is the function of shaft's length is given by,

$$r(x) = R_0 + \left(\frac{R_1 - R_0}{l}\right)x \tag{5.1.13}$$

Table 5.13. Various parameters of the system shown in Fig. 5.29 and their values

Parameters	**Values**
Length of the shaft-rotor, l (m)	0.1
Mass of the disk, m (Kg)	0.7443
Diameter of the disk, D (m)	0.09
Young's Modulus of Elasticity, E (GPa)	209
Density of the material, ρ (Kg/m^3)	7800
Rotational Speed, N (rpm)	10000
Inner Radius of hollow shaft, R_i (m)	0.001
Beginning radius , R_0 (m)	0.0050
End radius, R_1 (m)	0.0037
Impulse force, P (N)	1

The transfer function for hollow shaft with uniform bore, for values given in Table 5.13 is given by

$$\frac{1.344\,s+1.217\times10^{4}}{s^{3}+9059\,s^{2}+1.097\times10^{6}\,s+2.483\times10^{9}}. \qquad (5.1.14)$$

The Bode plots for different lengths and rotating speed have been plotted using MATLAB® software, as shown in Fig. 5.30 and Fig. 5.31 respectively.

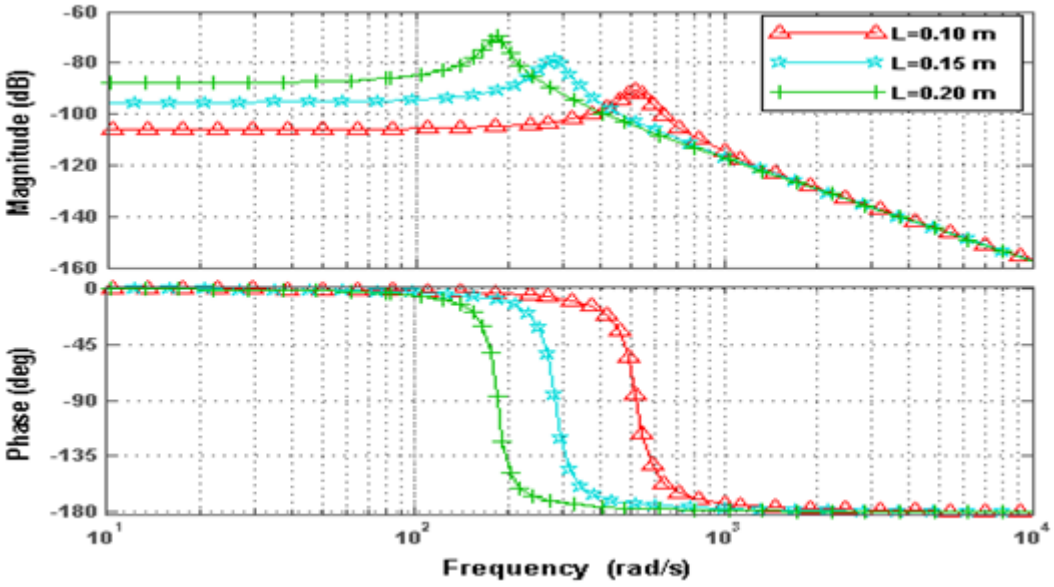

Fig. 5.30 Bode plot for various lengths for hollow tapered shaft-rotor with uniform bore at 10000 rpm.

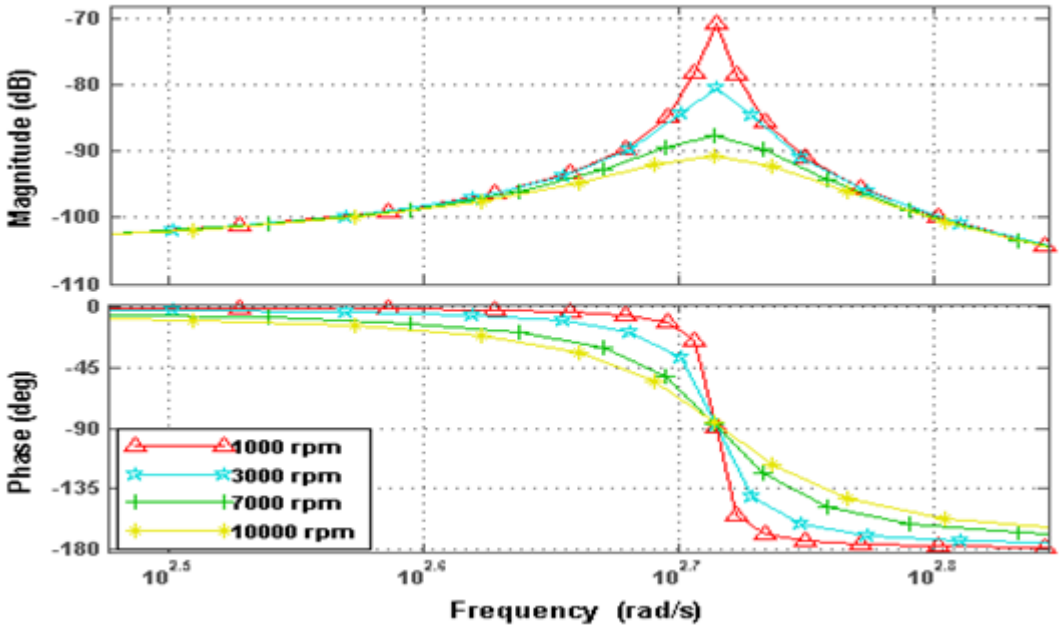

Fig. 5.31 Bode plot for different speeds for hollow tapered shaft-rotor with uniform bore and l=0.1 m.

5.2 Finite element approach

5.2.1 Profiled Shaft Rotor

A finite profiled shaft element is shown in Fig. 5.32. Applying FEM, we get mass, gyroscopic and stiffness matrices. The various parameters of the profiled-shaft-rotor system are given in Table 5.14. Values of radius at different locations are given in Table 5.15. Effects of bearing elements are neglected.

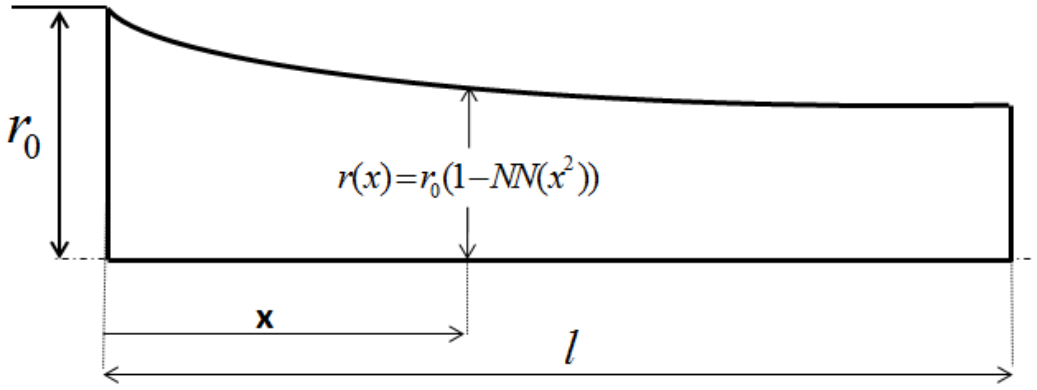

Fig. 5.32 Profiled shaft finite element

Table 5.14. Values of various parameters for the shaft-rotor system illustrated in Fig. 5.32

Parameters	**Values**
Length of the shaft-rotor, l (m)	0.1
Initial radius, r_o (m)	0.005
Mass of the disk, m (Kg)	0.7443
Diameter of the disk, D (m)	0.09
Young's Modulus of Elasticity, E (GPa)	209
Density of the material, ρ (Kg/m^3)	7800
Rotational Speed, N (rpm)	10000

Table 5.15. Values for radius at different locations of the profiled-shaft illustrated in Fig. 5.32 for NN=25 and r_o = 0.005 m

x (m)	**r(x) (mm)**
0.01	4.9875
0.02	4.9500
0.03	4.8875
0.04	4.8000
0.05	4.6875
0.06	4.5500
0.07	4.3875
0.08	4.2000
0.09	3.9875
0.10	3.7500

From Eqs. (4.3.21)-(4.3.24) we get stiffness, translational and rotational mass and gyroscopic matrices. Since there is no axial pull considered, hence $\left[K_A^e\right]$ is neglected. Stiffness matrix is given by,

$$K_p = \begin{bmatrix} k_{p11} & & & & & & & \\ k_{p21} & k_{p22} & & & & & & \\ k_{p31} & k_{p32} & k_{p33} & & & sym. & & \\ k_{p41} & k_{p42} & k_{p43} & k_{p44} & & & & \\ k_{p51} & k_{p52} & k_{p53} & k_{p54} & k_{p55} & & & \\ k_{p61} & k_{p62} & k_{p63} & k_{p64} & k_{p65} & k_{p66} & & \\ k_{p71} & k_{p72} & k_{p73} & k_{p74} & k_{p75} & k_{p76} & k_{p77} & \\ k_{p81} & k_{p82} & k_{p83} & k_{p84} & k_{p85} & k_{p86} & k_{p87} & k_{p88} \end{bmatrix} \tag{5.2.1}$$

Elements of stiffness matrix are given by,

$$k_{p11} = \frac{\pi E r_0^4 (259NN^4l^8 - 1210NN^3l^6 + 2178NN^2l^4 - 1848NNl^2 + 1155)}{385l^3}$$

$$k_{p41} = \frac{\pi E r_0^4 \left(469NN^4l^8 - 2145NN^3l^6 + 3762NN^2l^4 - 3234NNl^2 + 3465\right)}{2310l^2}$$

$$k_{p81} = \frac{\pi E r_0^4 \left(1085NN^4l^8 - 5115NN^3l^6 + 9306NN^2l^4 - 7854NNl^2 + 3465\right)}{2310l^2}$$

$$k_{p33} = \frac{\pi E r_0^4 (217NN^4l^8 - 990NN^3l^6 + 1782NN^2l^4 - 1848NNl^2 + 3465)}{3465l}$$

$$k_{p73} = \frac{\pi E r_0^4 (973NN^4l^8 - 4455NN^3l^6 + 7722NN^2l^4 - 6006NNl^2 + 3465)}{6930l}$$

$$k_{p77} = \frac{\pi E r_0^4 (1141NN^4l^8 - 5445NN^3l^6 + 10098NN^2l^4 - 8778NNl^2 + 3465)}{3465l}$$

$$k_{p21} = k_{p42} = k_{p82} = k_{p31} = 0,$$
$$k_{p43} = k_{p53} = k_{p83} = k_{p64} = k_{p74} = 0$$

$$k_{p52} = k_{p53} = k_{p65} = k_{p75} = 0,$$
$$k_{p61} = k_{p65} = k_{p86} = k_{p71} = k_{p87} = 0$$

$$k_{p22} = k_{p55} = k_{p66} = k_{p11},\ k_{p51} = k_{p62} = -k_{p11},\ k_{p63} = k_{p41}$$

$$k_{p32} = k_{p54} = -k_{p41},\ k_{p76} = k_{p81},\ k_{p72} = k_{p85} = k_{p72} = -k_{p81},\ k_{p44} = k_{p33},\ k_{p84} = k_{p73}.$$

The translational mass matrix is given by,

$$M_{pt} = \begin{bmatrix} m_{pt11} & & & & & & & \\ m_{pt21} & m_{pt22} & & & & & & \\ m_{pt31} & m_{pt32} & m_{pt33} & & sym. & & & \\ m_{pt41} & m_{pt42} & m_{pt43} & m_{pt44} & & & & \\ m_{pt51} & m_{pt52} & m_{pt53} & m_{pt54} & m_{pt55} & & & \\ m_{pt61} & m_{pt62} & m_{pt63} & m_{pt64} & m_{pt65} & m_{pt66} & & \\ m_{pt71} & m_{pt72} & m_{pt73} & m_{pt74} & m_{pt75} & m_{pt76} & m_{pt77} & \\ m_{pt81} & m_{pt82} & m_{pt83} & m_{pt84} & m_{pt85} & m_{pt86} & m_{pt87} & m_{pt88} \end{bmatrix} \quad (5.2.2)$$

Elements of translational mass matrix are given by,

$$m_{pt11} = \frac{\pi\rho l r_0^2 \left(45NN^2l^4 - 418NNl^2 + 2574\right)}{6930}$$

$$m_{pt41} = -\frac{\pi\rho l^2 r_0^2 \left(23NN^2l^4 - 187NNl^2 + 726\right)}{13860}$$

$$m_{pt51} = \frac{\pi\rho l r_0^2 (207NN^2l^4 - 1012NNl^2 + 1782)}{13860}$$

$$m_{pt81} = -\frac{\pi\rho l^2 r_0^2 \left(75NN^2l^4 - 418NNl^2 + 858\right)}{27720}$$

$$m_{pt33} = -\frac{\pi\rho l^3 r_0^2 \left(3NN^2l^4 - 22NNl^2 + 66\right)}{6930}$$

$$m_{pt63} = -\frac{\pi\rho l^2 r_0^2 \left(119NN^2l^4 - 550NNl^2 + 858\right)}{27720}$$

$$m_{pt73} = -\frac{\pi\rho l^3 r_0^2 \left(21NN^2l^4 - 110NNl^2 + 198\right)}{27720}$$

$$m_{pt76} = \frac{\pi\rho l^2 r_0^2 \left(210NN^2l^4 - 715NNl^2 + 726\right)}{13860}$$

$$m_{pt77} = \frac{\pi\rho l^3 r_0^2 \left(14NN^2l^4 - 55NNl^2 + 66\right)}{6930}$$

$$m_{pt21} = m_{pt42} = m_{pt82} = m_{pt31} = m_{pt43} = 0,$$
$$m_{pt53} = m_{pt83} = m_{pt64} = m_{pt74} = 0$$

$$m_{pt52} = m_{pt53} = m_{pt75} = m_{pt61} = 0,$$
$$m_{pt65} = m_{pt86} = m_{pt71} = m_{pt87} = 0$$

$$m_{pt22} = m_{pt55} = m_{pt66} = m_{pt11},$$
$$m_{pt51} = m_{pt62}, \quad m_{pt32} = -m_{pt41}, m_{pt63} = m_{pt54}$$

$$m_{pt72} = -m_{pt81},\ m_{pt44} = m_{pt33},$$
$$m_{pt84} = m_{pt73},\ m_{pt85} = -m_{pt76}$$

The rotational mass matrix is given by,

$$M_{pr} = \begin{bmatrix} m_{pr11} & & & & & & & \\ m_{pr21} & m_{pr22} & & & & & & \\ m_{pr31} & m_{pr32} & m_{pr33} & & & sym. & & \\ m_{pr41} & m_{pr42} & m_{pr43} & m_{pr44} & & & & \\ m_{pr51} & m_{pr52} & m_{pr53} & m_{pr54} & m_{pr55} & & & \\ m_{pr61} & m_{pr62} & m_{pr63} & m_{pr64} & m_{pr65} & m_{pr66} & & \\ m_{pr71} & m_{pr72} & m_{pr73} & m_{pr74} & m_{pr75} & m_{pr76} & m_{pr77} & \\ m_{pr81} & m_{pr82} & m_{pr83} & m_{pr84} & m_{pr85} & m_{pr86} & m_{pr87} & m_{pr88} \end{bmatrix} \qquad (5.2.3)$$

Elements of rotational mass matrix are,

$$m_{pr11} = \frac{\pi\rho {r_0}^4 \left(105NN^4l^8 - 728NN^3l^6 + 2145NN^2l^4 - 3432NNl^2 + 3003\right)}{10010l}$$

$$m_{pr41} = \frac{\pi\rho {r_0}^4 \left(357NN^4l^8 - 2366NN^3l^6 + 6435NN^2l^4 - 8580NNl^2 + 3003\right)}{120120}$$

$$m_{pr51} = -\frac{\pi\rho {r_0}^4 \left(105NN^4l^8 - 728NN^3l^6 + 2145NN^2l^4 - 3432NNl^2 + 3003\right)}{10010l}$$

$$m_{pr81} = -\frac{\pi\rho {r_0}^4 \left(-735NN^4l^8 + 3640NN^3l^6 - 6435NN^2l^4 + 3432NNl^2 + 3003\right)}{120120}$$

$$m_{pr33} = \frac{\pi\rho l {r_0}^4 \left(77NN^4l^8 - 494NN^3l^6 + 1287NN^2l^4 - 1716NNl^2 + 3003\right)}{90090}$$

$$m_{pr63} = \frac{\pi\rho {r_0}^4 \left(357NN^4l^8 - 2366NN^3l^6 + 6435NN^2l^4 - 8580NNl^2 + 3003\right)}{120120}$$

$$m_{pr73} = -\frac{\pi\rho l {r_0}^4 \left(693NN^4l^8 - 3458NN^3l^6 + 6435NN^2l^4 - 5148NNl^2 + 3003\right)}{360360}$$

$$m_{pr76} = \frac{\pi\rho {r_0}^4 \left(-735NN^4l^8 + 3640NN^3l^6 - 6435NN^2l^4 + 3432NNl^2 + 3003\right)}{120120}$$

$$m_{pr77} = \frac{\pi\rho l {r_0}^4 \left(2520NN^4l^8 - 11284NN^3l^6 + 19305NN^2l^4 - 15444NNl^2 + 6006\right)}{180180}$$

$$m_{pr21} = m_{pr42} = m_{pr82} = m_{pr31} = m_{pr43} = m_{pr53} = m_{pr83} = m_{pr64} = m_{pr74} = 0$$

$$m_{pr52} = m_{pr53} = m_{pr75} = m_{pr61} = m_{pr65} = m_{pr86} = m_{pr71} = m_{pr87} = 0$$

$m_{pr22} = m_{pr55} = m_{pr66} = m_{pr11},\ m_{pr51} = m_{pr62},\ \ m_{pr32} = -m_{pr41},\ m_{pr63} = m_{pr54}$

$m_{pr72} = -m_{pr81},\ m_{pr44} = m_{pr33},\ m_{pr84} = m_{pr73},\ m_{pr85} = -m_{pr76}$

The gyroscopic matrix for the profiled shaft-rotor finite element is given by,

$$G_p = \begin{bmatrix} g_{p11} & & & & & & & \\ g_{p21} & g_{p22} & & & & & & \\ g_{p31} & g_{p32} & g_{p33} & & & \textit{skewsym.} & & \\ g_{p41} & g_{p42} & g_{p43} & g_{p44} & & & & \\ g_{p51} & g_{p52} & g_{p53} & g_{p54} & g_{p55} & & & \\ g_{p61} & g_{p62} & g_{p63} & g_{p64} & g_{p65} & g_{p66} & & \\ g_{p71} & g_{p72} & g_{p73} & g_{p74} & g_{p75} & g_{p76} & g_{p77} & \\ g_{p81} & g_{p82} & g_{p83} & g_{p84} & g_{p85} & g_{p86} & g_{p87} & g_{p88} \end{bmatrix} \qquad (5.2.4)$$

Elements of gyroscopic matrix are given by,

$$g_{p21} = \frac{\pi\rho r_0^4\left(2145NN^2l^4 - 3432NNl^2 - 728NN^3l^6 + 105NN^4l^8 + 3003\right)}{5005l}$$

$$g_{p31} = -\frac{\pi\rho r_0^4\left(6435NN^2l^4 - 8580NNl^2 - 2366NN^3l^6 + 357NN^4l^8 + 3003\right)}{60060}$$

$$g_{p71} = -\frac{\pi\rho r_0^4\left(3432NN^2l^4 - 6435NNl^2 + 3640NN^3l^6 - 735NN^4l^8 + 3003\right)}{60060}$$

$$g_{p43} = \frac{\pi\rho lr_0^4\left(1287NN^2l^4 - 1716NNl^2 - 494NN^3l^6 + 77NN^4l^8 + 3003\right)}{45045}$$

$$g_{p83} = -\frac{\pi\rho lr_0^4\left(6435NN^2l^4 - 5148NNl^2 - 3458NN^3l^6 + 693NN^4l^8 + 3003\right)}{180180}$$

$$g_{p87} = \frac{\pi\rho lr_0^4\left(19305NN^2l^4 - 15444NNl^2 - 11284NN^3l^6 + 2520NN^4l^8 + 6006\right)}{90090}$$

$g_{p52} = g_{p65} = g_{p21},\ g_{pe61} = -g_{p21},\ g_{p42} = g_{p53} = g_{p64} = g_{p31}$

$g_{p82} = g_{p71},\ g_{p86} = g_{p75} = -g_{p71},\ g_{p75} = -g_{p83}$

$g_{p11} = g_{p41} = g_{p51} = g_{p81} = g_{p22} = 0,$
$g_{p32} = g_{p62} = g_{p72} = g_{p33} = g_{p63} = 0$

$g_{p73} = g_{p44} = g_{p54} = g_{p84} = g_{ue55} = 0,$
$g_{p85} = g_{p66} = g_{p76} = g_{p77} = g_{p88} = 0$

Discretizing the tapered shaft into six elements of equal length, as shown in Fig. 5.33 and then assembling the element matrices, we get the assembled mass, gyroscopic and stiffness matrices. Equation of motion for the complete system is given by,

$$\left[M_p^s\right]\left\{\ddot{q}^s\right\}-\Omega\left[G_p^s\right]\left\{\dot{q}^s\right\}+\left[K_p^s\right]\left\{q^s\right\}=\left\{Q_p^s\right\} \qquad (5.2.5)$$

$\left[M_p^s\right]$ contains assemblage of both the translational and rotational mass matrices.

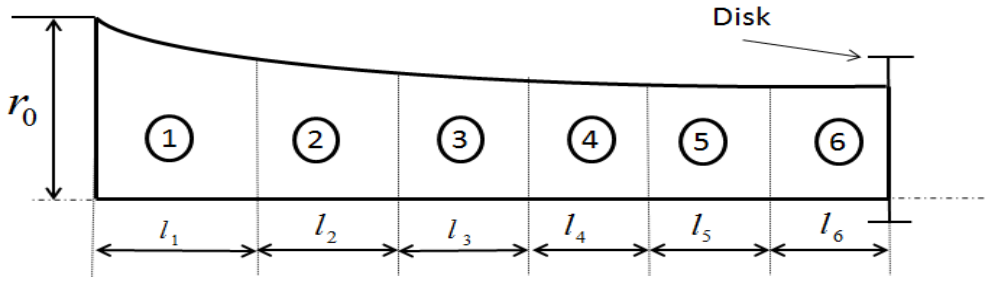

Fig. 5.33.Discretization of profiled shaft into six elements of equal length (0.1/6 m).

The cantilever boundary condition on the system's equation of motion has been applied. MATLAB® program is used to find the bode plot for a unit impulse of 1N acting vertically downward on disk at 7th node of the discretized shaft element for different values of profile value NN as shown in Figure 5.34. For authenticity, the results obtained are compared with that of Whalley and Ameer [2] approach, as shown in Table 5. 16.

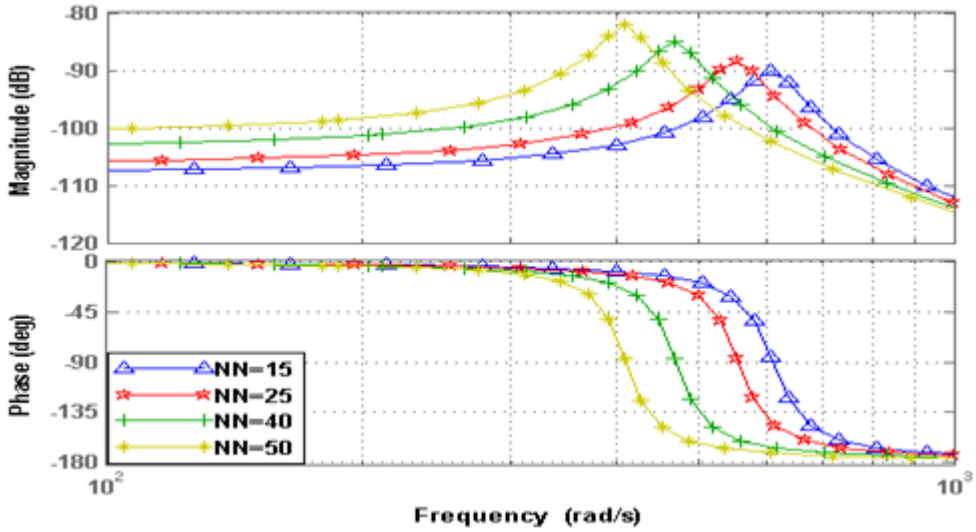

Fig. 5.34 Bode plot for an impulse of 1 N for profiled-shaft rotor [2] obtained by finite element approach.

Table 5.16. Results obtained from FEA is compared with that of Whalley and Ameer[2] approach

Profile Value NN	Critical frequency Whalley's approach [2] (rad/s)	Critical frequency obtained using FEM (rad/s)	Error %
15	583.043	608	4.105
25	531.55	554	4.223
40	456.43	469	2.754
50	394.29	409	3.731

Table 5.17. Convergence study of the profiled shaft-rotor system rotating at 10000 rpm and profile value NN of 25

No of Finite Shaft Elements	Critical frequency obtained using FEM (rad/s)
4	557
6	554
8	554
12	554

5.2.2 Hollow tapered shaft-rotors with uniform thickness

Applying finite element approach on the system shown in Fig. 5.26, we get mass, gyroscopic and stiffness matrices from Eqs. (4.3.21-4.3.24). A finite hollow tapered shaft element is shown in Fig. 5.35.

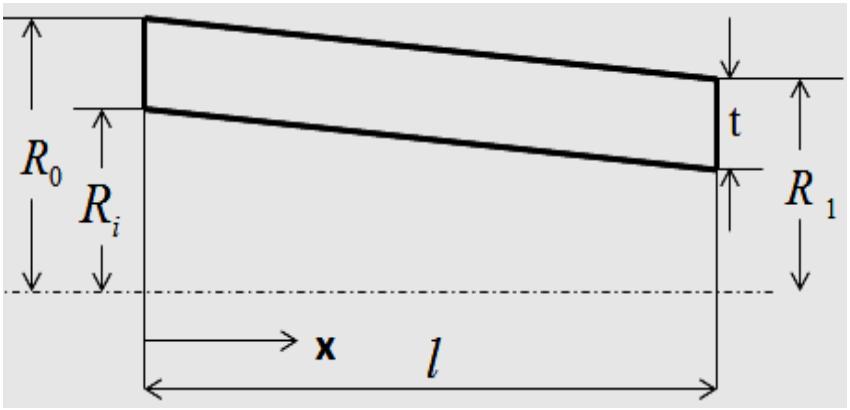

Fig. 5.35 Hollow tapered shaft finite element with uniform thickness t

The stiffness matrix for hollow tapered shaft-element with uniform thickness is given by,

$$K_n = \begin{bmatrix} k_{n11} & & & & & & & \\ k_{n21} & k_{n22} & & & & & & \\ k_{n31} & k_{n32} & k_{n33} & & & sym. & & \\ k_{n41} & k_{n42} & k_{n43} & k_{n44} & & & & \\ k_{n51} & k_{n52} & k_{n53} & k_{n54} & k_{n55} & & & \\ k_{n61} & k_{n62} & k_{n63} & k_{n64} & k_{n65} & k_{n66} & & \\ k_{n71} & k_{n72} & k_{n73} & k_{n74} & k_{n75} & k_{n76} & k_{n77} & \\ k_{n81} & k_{n82} & k_{n83} & k_{n84} & k_{n85} & k_{n86} & k_{n87} & k_{n88} \end{bmatrix} \quad (5.2.6)$$

Where elements of the stiffness matrices are,

$$k_{n11} = \frac{3\pi Et(7R_0^3 + 3R_0^2R_1 - 12R_0^2t + 3R_0R_1^2 - 6R_0R_1t + 10R_0t^2 + 7R_1^3 - 12R_1^2t + 10R_1t^2 - 5t^3)}{5l^3}$$

$$k_{n41} = \frac{\pi Et(30R_0^3 + 12R_0^2R_1 - 51R_0^2t + 6R_0R_1^2 - 18R_0R_1t + 40R_0t^2 + 12R_1^3 - 21R_1^2t + 20R_1t^2 - 15t^3)}{10l^2}$$

$$k_{n81} = \frac{\pi Et(12R_0^3 + 6R_0^2R_1 - 21R_0^2t + 12R_0R_1^2 - 18R_0R_1t + 20R_0t^2 + 30R_1^3 - 51R_1^2t + 40R_1t^2 - 15t^3)}{10l^2}$$

$$k_{n33} = \frac{\pi Et(11R_0^3 + 5R_0^2R_1 - 19R_0^2t + 2R_0R_1^2 - 7R_0R_1t + 15R_0t^2 + 2R_1^3 - 4R_1^2t + 5R_1t^2 - 5t^3)}{5l}$$

$$k_{n73} = \frac{\pi Et(8R_0^3 + 2R_0^2R_1 - 13R_0^2t + 2R_0R_1^2 - 4R_0R_1t + 10R_0t^2 + 8R_1^3 - 13R_1^2t + 10R_1t^2 - 5t^3)}{10l}$$

$$k_{n77} = \frac{\pi Et(2R_0^3 + 2R_0^2R_1 - 4R_0^2t + 5R_0R_1^2 - 7R_0R_1t + 5R_0t^2 + 11R_1^3 - 19R_1^2t + 15R_1t^2 - 5t^3)}{5l}$$

$$k_{n21} = k_{n42} = k_{n82} = k_{n31} = 0,$$
$$k_{n43} = k_{n53} = k_{n83} = k_{n64} = k_{n74} = 0$$

$$k_{n52} = k_{n53} = k_{n65} = k_{n75} = k_{n61} = 0,$$
$$k_{n65} = k_{n86} = k_{n71} = k_{n87} = 0$$

$$k_{n22} = k_{n55} = k_{n66} = k_{n11},\ k_{n51} = k_{n62} = -k_{n11},$$
$$k_{n63} = k_{n41},\ k_{n32} = k_{n54} = -k_{n41}$$

$$k_{n76} = k_{n81},\ k_{n72} = k_{n85} = -k_{n81},\ k_{n44} = k_{n33},\ k_{n84} = k_{n73}$$

The translational mass matrix is given by

$$M_{nt} = \begin{bmatrix} m_{nt11} & & & & & & & \\ m_{nt21} & m_{nt22} & & & & & & \\ m_{nt31} & m_{nt32} & m_{nt33} & & & sym. & & \\ m_{nt41} & m_{nt42} & m_{nt43} & m_{nt44} & & & & \\ m_{nt51} & m_{nt52} & m_{nt53} & m_{nt54} & m_{nt55} & & & \\ m_{nt61} & m_{nt62} & m_{nt63} & m_{nt64} & m_{nt65} & m_{nt66} & & \\ m_{nt71} & m_{nt72} & m_{nt73} & m_{nt74} & m_{nt75} & m_{nt76} & m_{nt77} & \\ m_{nt81} & m_{nt82} & m_{nt83} & m_{nt84} & m_{nt85} & m_{nt86} & m_{nt87} & m_{nt88} \end{bmatrix} \quad (5.2.7)$$

Where elements of translational mass matrix are given by,

$$m_{nt11} = \frac{\pi\rho lt(20R_0 + 6R_1 - 13t)}{35}$$

$$m_{nt41} = \frac{\pi\rho tl^2(15R_0 + 7R_1 - 11t)}{210}$$

$$m_{nt51} = \frac{9\pi\rho lt(R_0 + R_1 - t)}{70}$$

$$m_{nt81} = \frac{-(\pi\rho tl^2(14R_0 + 12R_1 - 13t))}{420}$$

$$m_{nt33} = \frac{\pi\rho l^3 t(5R_0 + 3R_1 - 4t)}{420}$$

$$m_{nt63} = \frac{-(\pi\rho l^2 t(12R_0 + 14R_1 - 13t))}{420}$$

$$m_{nt73} = \frac{-(\pi\rho l^3 t(R_0 + R_1 - t))}{140}$$

$$m_{nt76} = \frac{\pi\rho l^2 t(7R_0 + 15R_1 - 11t)}{210}$$

$$m_{nt77} = \frac{\pi\rho l^3 t(3R_0 + 5R_1 - 4t)}{420}$$

$$m_{nt21} = m_{nt42} = m_{nt82} = m_{nt31} = 0,$$
$$m_{nt43} = m_{nt53} = m_{nt83} = m_{nt64} = m_{nt74} = 0$$

$$m_{nt52} = m_{nt53} = m_{nt75} = m_{nt61} = 0,$$
$$m_{nt65} = m_{nt86} = m_{nt71} = m_{nt87} = 0$$

$$m_{nt22} = m_{nt55} = m_{nt66} = m_{nt11},\ m_{nt51} = m_{nt62},$$
$$m_{nt32} = -m_{nt41},\ m_{nt63} = m_{nt54}$$

$$m_{nt72} = -m_{nt81},\ m_{nt44} = m_{nt33},$$
$$m_{nt84} = m_{nt73},\ m_{nt85} = -m_{nt76}$$

Rotational mass matrix is given by:

$$M_{nr} = \begin{bmatrix} m_{nr11} & & & & & & & \\ m_{nr21} & m_{nr22} & & & & & & \\ m_{nr31} & m_{nr32} & m_{nr33} & & & sym. & & \\ m_{nr41} & m_{nr42} & m_{nr43} & m_{nr44} & & & & \\ m_{nr51} & m_{nr52} & m_{nr53} & m_{nr54} & m_{nr55} & & & \\ m_{nr61} & m_{nr62} & m_{nr63} & m_{nr64} & m_{nr65} & m_{nr66} & & \\ m_{nr71} & m_{nr72} & m_{nr73} & m_{nr74} & m_{nr75} & m_{nr76} & m_{nr77} & \\ m_{nr81} & m_{nr82} & m_{nr83} & m_{nr84} & m_{nr85} & m_{nr86} & m_{nr87} & m_{nr88} \end{bmatrix} \quad (5.2.8)$$

Where elements of rotational mass matrix are given by

$$m_{nr11} = \frac{3\pi\rho t^2(8R_0^2 + 12R_0R_1 - 14R_0t + 8R_1^2 - 14R_1t + 7t^2)}{70l}$$

$$m_{nr41} = \frac{\pi\rho t^2(-8R_0^2 + 6R_0R_1 + 20R_1^2 - 28R_1t + 7t^2)}{280}$$

$$m_{nr51} = \frac{-(3\pi\rho t^2(8R_0^2 + 12R_0R_1 - 14R_0t + 8R_1^2 - 14R_1t + 7t^2))}{70l}$$

$$m_{nr33} = \frac{\pi\rho t^2 l(18R_0^2 + 6R_0R_1 - 21R_0t + 4R_1^2 - 7R_1t + 7t^2)}{210}$$

$$m_{nr63} = \frac{\pi\rho t^2(-8R_0^2 + 16R_0R_1 + 20R_1^2 - 28R_1t + 7t^2)}{280}$$

$$m_{nr73} = \frac{-(\pi\rho t^2 l(12R_0^2 + 4R_0R_1 - 14R_0t + 12R_1^2 - 14R_1t + 7t^2))}{840}$$

$$m_{nr76} = \frac{\pi\rho t^2(20R_0^2 + 16R_0R_1 - 28R_0t - 8R_1^2 + 7t^2)}{280}$$

$$m_{nr77} = \frac{\pi\rho t^2 l(4R_0^2 + 6R_0R_1 - 7R_0t + 18R_1^2 - 21R_1t + 7t^2)}{210}$$

$$m_{nr21} = m_{nr42} = m_{nr82} = m_{nr31} = m_{nr43} = 0,$$
$$m_{nr53} = m_{nr83} = m_{nr64} = m_{nr74} = 0$$

$$m_{nr52} = m_{nr53} = m_{nr75} = m_{nr61} = 0,$$
$$m_{nr65} = m_{nr86} = m_{nr71} = m_{nr87} = 0$$

$$m_{nr22} = m_{nr55} = m_{nr66} = m_{nr11}, \; m_{nr51} = m_{nr62},$$
$$m_{nr32} = -m_{nr41}, m_{nr63} = m_{nr54}$$

$$m_{nr81} = m_{nr76}, \; m_{nr72} = -m_{nr76}, \; m_{nr44} = m_{nr33}, \; m_{nr84} = m_{nr73}, \; m_{nr85} = -m_{nr76}$$

The gyroscopic matrix is given by

$$G_{ne} = \begin{bmatrix} g_{ne11} & & & & & & & \\ g_{ne21} & g_{ne22} & & & & & & \\ g_{ne31} & g_{ne32} & g_{ne33} & & \textit{skewsym.} & & & \\ g_{ne41} & g_{ne42} & g_{ne43} & g_{ne44} & & & & \\ g_{ne51} & g_{ne52} & g_{ne53} & g_{ne54} & g_{ne55} & & & \\ g_{ne61} & g_{ne62} & g_{ne63} & g_{ne64} & g_{ne65} & g_{ne66} & & \\ g_{ne71} & g_{ne72} & g_{ne73} & g_{ne74} & g_{ne75} & g_{ne76} & g_{ne77} & \\ g_{ne81} & g_{ne82} & g_{ne83} & g_{ne84} & g_{ne85} & g_{ne86} & g_{ne87} & g_{ne88} \end{bmatrix} \qquad (5.2.9)$$

Where the elements of the gyroscopic matrix are given by

$$g_{ne21} = \frac{3\pi\rho t^2(8R_0^2 + 12R_0R_1 - 14R_0t + 8R_1^2 - 14R_1t + 7t^2)}{35l}$$

$$g_{ne31} = \frac{-(\pi\rho t^2(-8R_0^2 + 16R_0R_1 + 20R_1^2 - 28R_1t + 7t^2))}{140}$$

$$g_{ne71} = \frac{-(\pi\rho t^2(20R_0^2 + 16R_0R_1 - 28R_0t - 8R_1^2 + 7t^2))}{140}$$

$$g_{ne43} = \frac{\pi\rho lt^2(18R_0^2 + 6R_0R_1 - 21R_0t + 4R_1^2 - 7R_1t + 7t^2)}{105}$$

$$g_{ne83} = \frac{-(\pi\rho lt^2(12R_0^2 + 4R_0R_1 - 14R_0t + 12R_1^2 - 14R_1t + 7t^2))}{420}$$

$$g_{ne87} = \frac{\pi\rho lt^2(4R_0^2 + 6R_0R_1 - 7R_0t + 18R_1^2 - 21R_1t + 7t^2)}{105}$$

$$g_{ne52} = g_{ne65} = g_{ne21},\ g_{ne61} = -g_{ne21},$$
$$g_{ne42} = g_{ne53} = g_{ne64} = g_{ne31}$$

$$g_{ne82} = g_{ne71},\ g_{ne86} = g_{ne75} = -g_{ne71},\ g_{ne75} = -g_{ne83}$$

$$g_{ne11} = g_{ne41} = g_{ne51} = g_{ne81} = g_{ne22} = g_{ne32} = 0,$$
$$g_{ne62} = g_{ne72} = g_{ne33} = g_{ne63} = 0$$

$$g_{ne73} = g_{ne44} = g_{ne54} = g_{ne84} = g_{ne55} = g_{ne85} = 0,$$
$$g_{ne66} = g_{ne76} = g_{ne77} = g_{ne88} = 0$$

Discretizing the tapered shaft into six elements as shown in Fig. 5.36 and then assembling the element matrices, we get the assembled mass, gyroscopic and stiffness matrices. Equation of motion for the complete shaft-rotor system is given by,

$$\left[M_n^s\right]\{\ddot{q}^s\} - \Omega\left[G_n^s\right]\{\dot{q}^s\} + \left[K_n^s\right]\{q^s\} = \{Q_n^s\}. \qquad (5.2.10)$$

Where $\left[M_n^s\right]$ is the assembled mass matrix containing both the translational and rotational mass matrices.

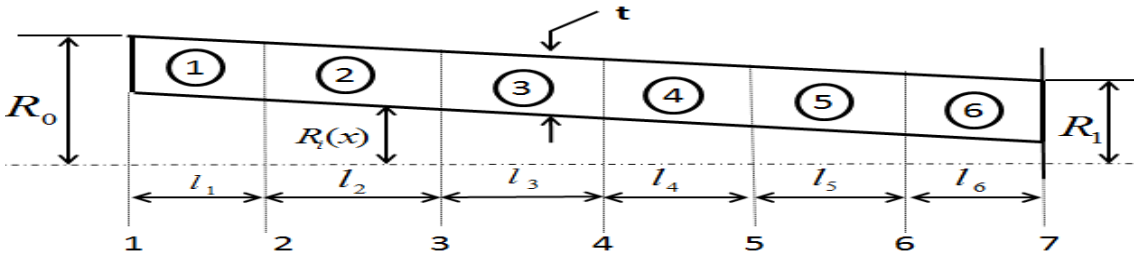

Fig. 5.36 Discretized shaft element with six elements of equal length (0.1/6 m).

The assembled equation of motion is arranged in first order state vector form for simplicity in computations.

$$\begin{bmatrix} [0] & [M_n^s] \\ [M_n^s] & -\Omega[G_n^s] \end{bmatrix} \{\dot{z}\} + \begin{bmatrix} [-M_n^s] & [0] \\ [0] & [K_n^s] \end{bmatrix} \{z\} = \{Z\} \qquad (5.2.11)$$

Where

$$\{z\} = \begin{Bmatrix} \{\dot{q}\} \\ \{q\} \end{Bmatrix}, \quad \{Z\} = \begin{Bmatrix} \{0\} \\ \{Q_n^s\} \end{Bmatrix} \qquad (5.2.12)$$

The shaft-rotor has been discretized into six elements of equal length.

MATLAB® program is used to find the bode plot for different values of shaft-length and rotor-speed as shown in Fig. 5.37 and Fig. 5.38 and are found to be in good agreement with bode plots found using TMM as shown in Fig. 5.27 and Fig. 5.28.

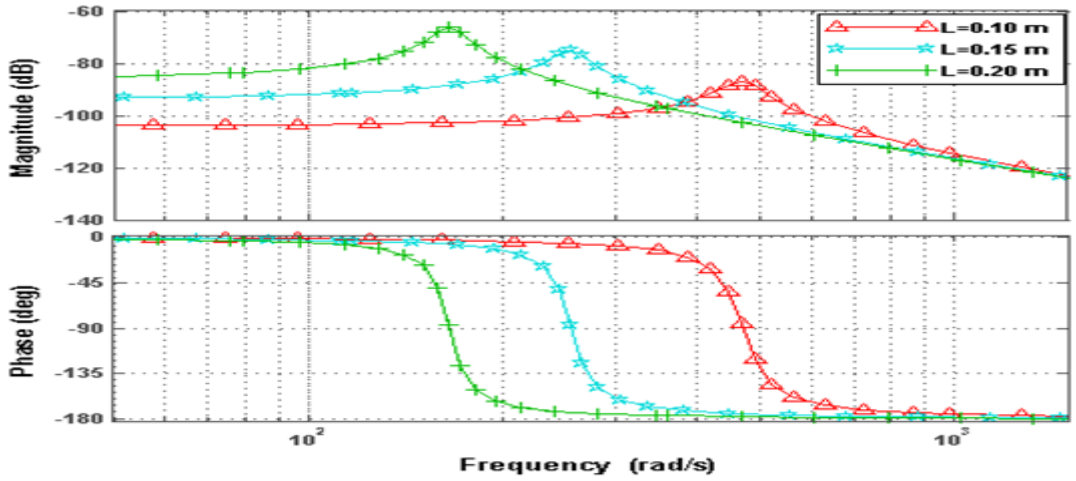

Fig. 5.37 Bode plot for different shaft lengths (FEA) for hollow tapered shaft-rotor with uniform thickness and rotating speed of 10000 rpm.

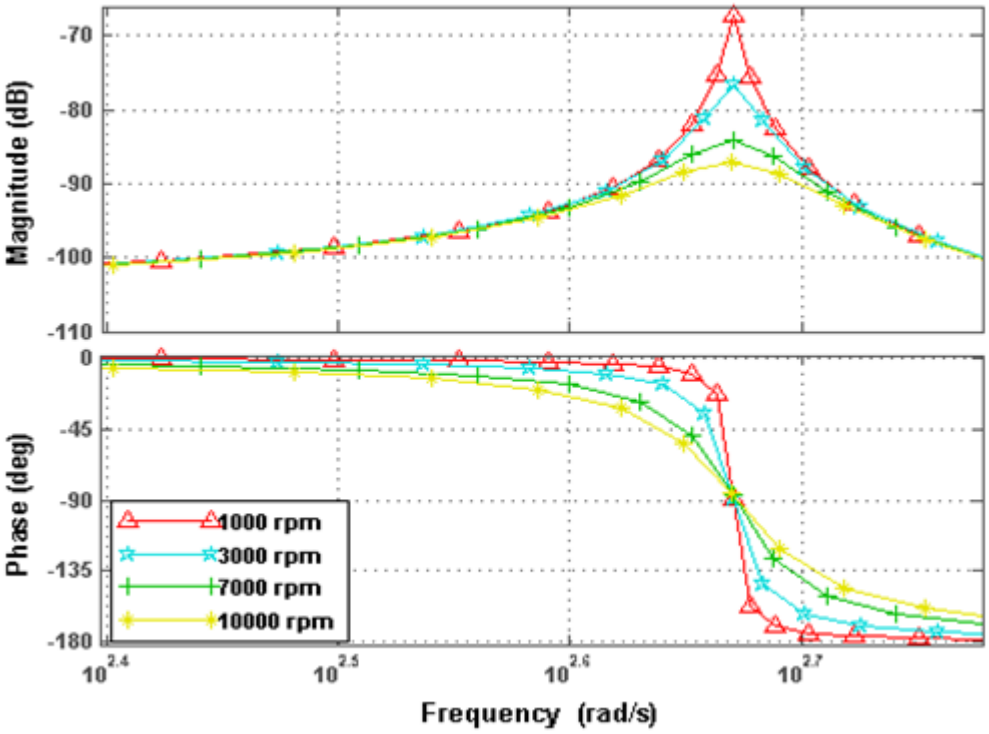

Fig. 5.38 Bode plot for various rotor-speeds (FEA) for hollow tapered shaft-rotor with uniform thickness and length of 0.1 m.

Table 5.18. Comparison of Bode plots obtained using Whalley and Ameer [2] approach and FEA for different rotor speeds and shaft lengths of a hollow tapered shaft-rotor system with uniform thickness, t

Length of tapered shaft-rotor (m)	Rotational speed (rpm)	Critical frequency using Whalley and Ameer [2] approach (rad/s)	Critical frequency using FEM (rad/s)
0.10	1000	458	469
0.10	3000	458	468
0.10	7000	458	468
0.10	10000	457	468
0.15	10000	249	255
0.20	10000	162	166

5.2.3 Hollow tapered shaft-rotors with uniform bore

Applying FEM on the same system, as shown in Fig. 5.29 we get mass, gyroscopic and stiffness matrices from Eqs. (4.3.21)- (4.3.24). A finite hollow tapered shaft element is shown in Fig. 5.39.

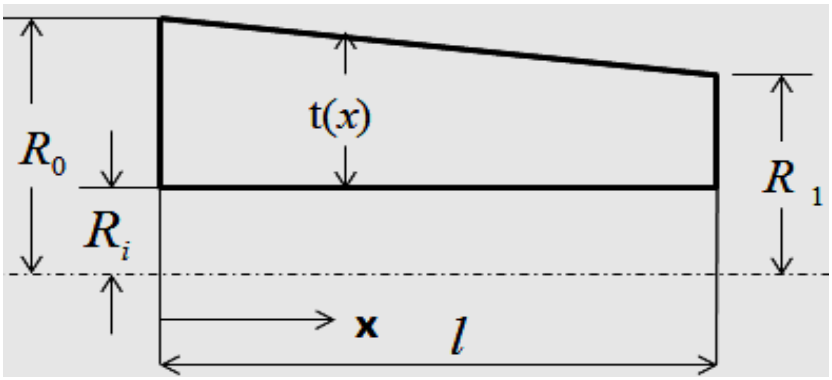

Fig. 5.39 Hollow tapered shaft finite element with uniform bore.

The stiffness matrix for hollow tapered shaft with uniform bore is given by

$$K_u = \begin{bmatrix} k_{u11} & & & & & & & \\ k_{u21} & k_{u22} & & & & & & \\ k_{u31} & k_{u32} & k_{u33} & & & sym. & & \\ k_{u41} & k_{u42} & k_{u43} & k_{u44} & & & & \\ k_{u51} & k_{u52} & k_{u53} & k_{u54} & k_{u55} & & & \\ k_{u61} & k_{u62} & k_{u63} & k_{u64} & k_{u65} & k_{u66} & & \\ k_{u71} & k_{u72} & k_{u73} & k_{u74} & k_{u75} & k_{u76} & k_{u77} & \\ k_{u81} & k_{u82} & k_{u83} & k_{u84} & k_{u85} & k_{u86} & k_{u87} & k_{u88} \end{bmatrix} \quad (5.2.13)$$

Where elements of the stiffness matrices are given by,

$$k_{u11} = \frac{3\pi E(11R_0^4 + 5R_0^3R_1 + 3R_0^2R_1^2 + 5R_0R_1^3 + 11R_1^4 - 35R_i^4)}{35l^3}$$

$$k_{u41} = \frac{\pi E(47R_0^4 + 22R_0^3R_1 + 9R_0^2R_1^2 + 8R_0R_1^3 + 19R_1^4 - 105R_i^4)}{70l^2}$$

$$k_{u81} = \frac{\pi E(19R_0^4 + 8R_0^3R_1 + 9R_0^2R_1^2 + 22R_0R_1^3 + 47R_1^4 - 1105R_i^4)}{70l^2}$$

$$k_{u33} = \frac{\pi E(17R_0^4 + 9R_0^3R_1 + 4R_0^2R_1^2 + 2R_0R_1^3 + 3R_1^4 - 35R_i^4)}{35l}$$

$$k_{u73} = \frac{\pi E(13R_0^4 + 4R_0^3R_1 + R_0^2R_1^2 + 4R_0R_1^3 + 13R_1^4 - 35R_i^4)}{70l}$$

$$k_{u77} = \frac{\pi E(3R_0^4 + 2R_0^3R_1 + 4R_0^2R_1^2 + 9R_0R_1^3 + 17R_1^4 - 35R_i^4)}{35l}$$

$$k_{u21} = k_{u42} = k_{u82} = k_{u31} = 0,$$
$$k_{u43} = k_{u53} = k_{u83} = k_{u64} = k_{u74} = 0$$

$$k_{u52} = k_{u53} = k_{u65} = k_{u75} = 0,$$
$$k_{u61} = k_{u65} = k_{u86} = k_{u71} = k_{u87} = 0$$

$$k_{u22} = k_{u55} = k_{u66} = k_{u11},\ k_{u51} = k_{u62} = -k_{u11},\ \boldsymbol{k_{u63} = k_{u41}}$$

$$k_{u32} = k_{u54} = -k_{u41},\ \boldsymbol{k_{u76} = k_{u81}},\ k_{u72} = k_{u85} = k_{u72} = -k_{u81}$$

$$k_{u44} = k_{u33},\ k_{u84} = k_{u73}$$

Translation mass matrix is given by,

$$M_{ut} = \begin{bmatrix} m_{ut11} & & & & & & & \\ m_{ut21} & m_{ut22} & & & & & & \\ m_{ut31} & m_{ut32} & m_{ut33} & & & \textit{sym.} & & \\ m_{ut41} & m_{ut42} & m_{ut43} & m_{ut44} & & & & \\ m_{ut51} & m_{ut52} & m_{ut53} & m_{ut54} & m_{ut55} & & & \\ m_{ut61} & m_{ut62} & m_{ut63} & m_{ut64} & m_{ut65} & m_{ut66} & & \\ m_{ut71} & m_{ut72} & m_{ut73} & m_{ut74} & m_{ut75} & m_{ut76} & m_{ut77} & \\ m_{ut81} & m_{ut82} & m_{ut83} & m_{ut84} & m_{ut85} & m_{ut86} & m_{ut87} & m_{ut88} \end{bmatrix} \quad (5.2.14)$$

Where elements of translational mass matrix are given by,

$$m_{ut11} = \frac{\pi\rho l(145R_0^2 + 70R_0R_1 + 19R_1^2 - 234R_i^2)}{630}$$

$$m_{ut41} = \frac{\pi\rho l^2(65R_0^2 + 50R_0R_1 + 17R_1^2 - 132R_i^2)}{2520}$$

$$m_{ut51} = \frac{(\pi\rho l(23R_0^2 + 35R_0R_1 + 23R_1^2 - 81R_i^2)}{630}$$

$$m_{ut81} = \frac{-(\pi\rho l^2(25R_0^2 + 34R_0R_1 + 19R_1^2 - 78R_i^2))}{2520}$$

$$m_{ut33} = \frac{\pi\rho l^3(5R_0^2 + 5R_0R_1 + 2R_1^2 - 12R_i^2)}{1260}$$

$$m_{ut63} = \frac{-(\pi\rho l^2(19R_0^2 + 34R_0R_1 + 25R_1^2 - 78R_i^2))}{2520}$$

$$m_{ut73} = \frac{-(\pi\rho l^3(5R_0^2 + 8R_0R_1 + 5R_1^2 - 18R_i^2))}{2520}$$

$$m_{ut76} = \frac{\pi\rho l^2(17R_0^2 + 50R_0R_1 + 65R_1^2 - 132R_i^2)}{2520}$$

$$m_{ut77} = \frac{\pi\rho l^3(2R_0^2 + 5R_0R_1 + 5R_1^2 - 12R_i^2)}{1260}$$

$$m_{ut21} = m_{ut42} = m_{ut82} = m_{ut31} = m_{ut43} = 0,$$
$$m_{ut53} = m_{ut83} = m_{ut64} = m_{ut74} = 0$$

$$m_{ut52} = m_{ut53} = m_{ut75} = m_{ut61} = 0,$$
$$m_{ut65} = m_{ut86} = m_{ut71} = m_{ut87} = 0$$

$$m_{ut22} = m_{ut55} = m_{ut66} = m_{ut11},$$
$$m_{ut51} = m_{ut62}, \quad m_{ut32} = -m_{ut41}, m_{ut63} = m_{ut54}$$

$$m_{ut72} = -m_{ut81}, \; m_{ut44} = m_{ut33},$$
$$m_{ut84} = m_{ut73}, \; m_{ut85} = -m_{ut76}$$

The rotational mass matrix is given by:

$$M_{ur} = \begin{bmatrix} m_{ur11} & & & & & & & \\ m_{ur21} & m_{ur22} & & & & & & \\ m_{ur31} & m_{ur32} & m_{ur33} & & & sym. & & \\ m_{ur41} & m_{ur42} & m_{ur43} & m_{ur44} & & & & \\ m_{ur51} & m_{ur52} & m_{ur53} & m_{ur54} & m_{ur55} & & & \\ m_{ur61} & m_{ur62} & m_{ur63} & m_{ur64} & m_{ur65} & m_{ur66} & & \\ m_{ur71} & m_{ur72} & m_{ur73} & m_{ur74} & m_{ur75} & m_{ur76} & m_{ur77} & \\ m_{ur81} & m_{ur82} & m_{ur83} & m_{ur84} & m_{ur85} & m_{ur86} & m_{ur87} & m_{ur88} \end{bmatrix} \quad (5.2.15)$$

Where the elements of the rotational mass matrix are given by,

$$m_{ur11} = \frac{\pi\rho(5R_0^4 + 10R_0^3R_1 + 12R_0^2R_1^2 - 24R_0^2R_i^2 + 10R_0R_1^3 - 36R_0R_1R_i^2 + 5R_1^4 - 24R_1^2R_i^2 + 42R_i^4)}{140l}$$

$$m_{ur41} = \frac{\pi\rho(-5R_0^4 + 6R_0^2R_1^2 + 8R_0^2R_i^2 + 8R_0R_1^3 - 16R_0R_1R_i^2 + 5R_1^4 - 20R_1^2R_i^2 + 14R_i^4)}{560}$$

$$m_{ur51} = \frac{-(\pi\rho(5R_0^4 + 10R_0^3R_1 + 12R_0^2R_1^2 - 24R_0^2R_i^2 + 10R_0R_1^3 - 36R_0R_1R_i^2 + 5R_1^4 - 24R_1^2R_i^2 + 42R_i^4))}{140l}$$

$$m_{ur81} = \frac{\pi\rho(5R_0^4 + 8R_0^3R_1 + 6R_0^2R_1^2 - 20R_0^2R_i^2 - 16R_0R_1R_i^2 - 5R_1^4 + 8R_1^2R_i^2 + 14R_i^4)}{560}$$

$$m_{ur33} = \frac{\pi\rho l(15R_0^4 + 5R_0^3R_1 + 3R_0^2R_1^2 - 36R_0^2R_i^2 + 3R_0R_1^3 - 12R_0R_1R_i^2 + 2R_1^4 - 8R_1^2R_i^2 + 28R_i^4)}{840}$$

$$m_{ur63} = \frac{\pi\rho(-5R_0^4 + 6R_0^2R_1^2 + 8R_0^2R_i^2 + 8R_0R_1^3 - 16R_0R_1R_i^2 + 5R_1^4 - 20R_1^2R_i^2 + 14R_i^4)}{560}$$

$$m_{ur73} = \frac{-(\pi\rho l(5R_0^4 + 2R_0^3R_1 - 12R_0^2R_i^2 + 2R_0R_1^3 - 4R_0R_1R_i^2 + 5R_1^4 - 12R_1^2R_i^2 + 14R_i^4))}{1680}$$

$$m_{ur76} = \frac{\pi\rho(5R_0^4 + 8R_0^3R_1 + 6R_0^2R_1^2 - 20R_0^2R_i^2 - 16R_0R_1R_i^2 - 5R_1^4 + 8R_1^2R_i^2 + 14R_i^4)}{560}$$

$$m_{ur77} = \frac{\pi\rho l(2R_0^4 + 3R_0^3R_1 + 3R_0^2R_1^2 - 8R_0^2R_i^2 + 5R_0R_1^3 - 12R_0R_1R_i^2 + 15R_1^4 - 36R_1^2R_i^2 + 28R_i^4)}{840}$$

$$m_{ur21} = m_{ur42} = m_{ur82} = m_{ur31} = m_{ur43} = m_{ur53} = m_{ur83} = m_{ur64} = m_{ur74} = 0$$

$$m_{ur52} = m_{ur53} = m_{ur75} = m_{ur61} = m_{ur65} = m_{ur86} = m_{ur71} = m_{ur87} = 0$$

$$m_{ur22} = m_{ur55} = m_{ur66} = m_{ur11},\ m_{ur51} = m_{ur62},\ m_{ur32} = -m_{ur41},\ m_{ur63} = m_{ur54}$$

$$m_{ur72} = -m_{ur81},\ m_{ur44} = m_{ur33},\ m_{ur84} = m_{ur73},\ m_{ur85} = -m_{ur76}$$

The gyroscopic matrix is given by,

$$G_{ue} = \begin{bmatrix} g_{ue11} & & & & & & & \\ g_{ue21} & g_{ue22} & & & & & & \\ g_{ue31} & g_{ue32} & g_{ue33} & & & \textit{skewsym.} & & \\ g_{ue41} & g_{ue42} & g_{ue43} & g_{ue44} & & & & \\ g_{ue51} & g_{ue52} & g_{ue53} & g_{ue54} & g_{ue55} & & & \\ g_{ue61} & g_{ue62} & g_{ue63} & g_{ue64} & g_{ue65} & g_{ue66} & & \\ g_{ue71} & g_{ue72} & g_{ue73} & g_{ue74} & g_{ue75} & g_{ue76} & g_{ue77} & \\ g_{ue81} & g_{ue82} & g_{ue83} & g_{ue84} & g_{ue85} & g_{ue86} & g_{ue87} & g_{ue88} \end{bmatrix} \qquad (5.2.16)$$

Where the elements of the gyroscopic matrix are given by,

$$g_{ue21} = \frac{\pi\rho(5R_0^4 + 10R_0^3R_1 + 12R_0^2R_1^2 - 24R_0^2R_i^2 + 10R_0R_1^3 - 36R_0R_1R_i^2 + 5R_1^4 - 24R_1^2R_i^2 + 42R_i^4)}{70l}$$

$$g_{ue31} = \frac{-(\pi\rho(-5R_0^4 + 6R_0^2R_1^2 + 8R_0^2R_i^2 + 8R_0R_1^3 - 16R_0R_1R_i^2 + 5R_1^4 - 20R_1^2R_i^2 + 14R_i^4))}{280}$$

$$g_{ue71} = \frac{-(\pi\rho(5R_0^4 + 8R_0^3R_1 + 6R_0^2R_1^2 - 20R_0^2R_i^2 - 16R_0R_1R_i^2 - 5R_1^4 + 8R_1^2R_i^2 + 14R_i^4))}{280}$$

$$g_{ue43} = \frac{\pi\rho l(15R_0^4 + 5R_0^3R_1 + 3R_0^2R_1^2 - 36R_0^2R_i^2 + 3R_0R_1^3 - 12R_0R_1R_i^2 + 2R_1^4 - 8R_1^2R_i^2 + 28R_i^4)}{420}$$

$$g_{ue83} = \frac{-(\pi\rho l(5R_0^4 + 2R_0^3R_1 - 12R_0^2R_i^2 + 2R_0R_1^3 - 4R_0R_1R_i^2 + 5R_1^4 - 12R_1^2R_i^2 + 14R_i^4))}{840}$$

$$g_{ue87} = \frac{\pi\rho l(2R_0^4 + 3R_0^3R_1 + 3R_0^2R_1^2 - 8R_0^2R_i^2 + 5R_0R_1^3 - 12R_0R_1R_i^2 + 15R_1^4 - 36R_1^2R_i^2 + 28R_i^4)}{420}$$

$$g_{ue52} = g_{ue65} = g_{ue21},\ g_{ue61} = -g_{ue21},\ g_{ue42} = g_{ue53} = g_{ue64} = g_{ue31}$$

$$g_{ue82} = g_{ue71},\ g_{ue86} = g_{ue75} = -g_{ue71},\ g_{ue75} = -g_{ue83}$$

$$g_{ue11} = g_{ue41} = g_{ue51} = g_{ue81} = g_{ue22} = 0,$$
$$g_{ue32} = g_{ue62} = g_{ue72} = g_{ue33} = g_{ue63} = 0$$

$$g_{ue73} = g_{ue44} = g_{ue54} = g_{ue84} = g_{ue55} = 0,$$
$$g_{ue85} = g_{ue66} = g_{ue76} = g_{ue77} = g_{ue88} = 0$$

Proceeding as in section 5.2.2, and then using MATLAB® program to obtain the bode plots for various shaft-length and rotor-speed as shown in Fig. 5.40 and Fig. 5.41 and are found to be in good agreement with bode plots found using TMM as shown in Fig. 5.30 and Fig. 5.31.

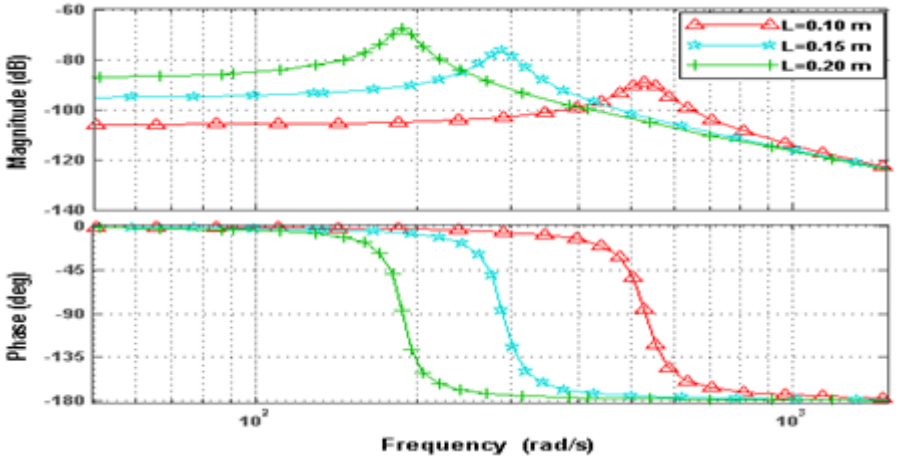

Fig. 5.40 Bode plot for different shaft lengths (FEA) for hollow tapered shaft-rotor with uniform bore at 10000 rpm.

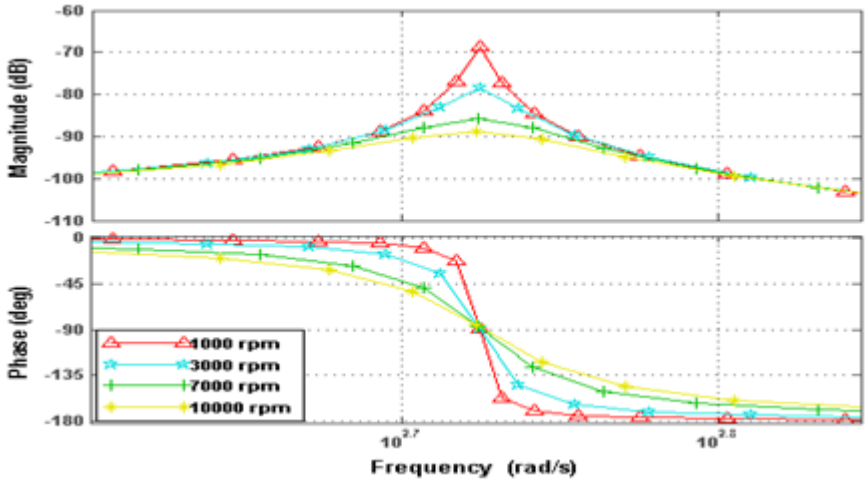

Fig. 5.41 Bode Plot for different rotating speeds (FEA) for hollow tapered shaft-rotor with uniform bore and l=0.1 m.

The results obtained from finite element approach are compared with that of Whalley and Ameer [2] approach and are tabulated in Table 5.18.

Table 5.19. Comparison of bode plots obtained using Whalley and Ameer [2] approach and FEA for different rotor speeds and shaft lengths of hollow tapered shaft-rotor with uniform bore

Length of tapered shaft-rotor (m)	Rotational speed (rpm)	Critical frequency using Whalley and Ameer [2] approach (rad/s)	Critical frequency using FEM (rad/s)
0.10	1000	519	530
0.10	3000	519	530
0.10	7000	518	530
0.10	10000	517	529
0.15	10000	282	288
0.20	10000	183	187

5.3 Summary

Transfer matrix method, as stated in chapter 3, includes complexity in calculations of frequency response. However, once the transfer matrix has been found, it is easier to find the frequency response. The length of the shaft is a vital parameter that affects the frequency response of the shaft-rotor system. As shown in Figs. 5.5, 5.8, 5.14, 5.18, 5.23, 5.27, 5.30, 5.37 and 5.40, there is increase in amplitude of vibration for increased value of shaft length, with the reduction in the whirling speed of shaft. The system exhibits this behaviour due to bending effect of the shaft and stiffness change. For changing lengths, there are large differences in frequencies even for small increase in lengths.

Effects of rotational speed on frequency response is clearly shown by bode plots in Figs. 5.4, 5.9, 5.15, 5.19, 5.24, 5.28, 5.31, 5.38 and 5.41. For an impulse input, the amplitude of vibration becomes larger for lower values of shaft speed and decreases with increase in speed. The phase angle changes abruptly for lower value of shaft speeds than higher speeds. This is due to the fact that there is reduction in gyroscopic couple as the rotational speed of the shaft decreases thereby giving larger amplitude of vibration. Step responses for shaft-rotors with different configurations are shown in Figs. 5.6, 5.11, 5.20 and 5.25. One can clearly observe that at lower rotational speeds, the disturbance is much greater owing to the reduction in the gyroscopic couple. Maximum overshoot almost remains unchanged; however the settling times for higher speeds are shorter. Results obtained from finite element approach are compared with the results obtained using Whalley and Ameer [2] approach, as shown for three different cases, in Tables 5.16 - 5.18, and are found to be in good agreement. Specific conclusions drawn and the scope for further research from the results are discussed in chapter-6.

CHAPTER-6

CONCLUSION AND SCOPE FOR FURTHER RESEARCH WORK

Conclusion

Shaft geometry plays one of the important roles in dynamic characteristics of rotating systems. The present chapter summarizes the important conclusions drawn from the theoretical analyses by TMM and FEM results. Vibration analysis with the help of bode plots has been done for shaft-rotor systems with various geometries and arrangements. Following conclusions can be drawn out from the results discussed in chapter 5:

- Shaft profiling, a commonly adopted design method enabling system deflection, mass and inertia minimisation. Shaft geometry plays one of the important roles in dynamic characteristics of rotating systems.
- Raw material cost is also reduced due to profiling of the shafts.
- There is increase in amplitude of vibration for increased value of shaft length, while reducing the whirling speed of shaft. The system exhibits this behaviour due to bending effect of the shaft and stiffness change. For changing lengths, there are large differences in frequencies even for small increase in lengths.
- For an impulse input, the amplitude of vibration becomes larger for lower values of shaft speed and decreases with increase in speed. The phase angle changes abruptly for lower value of shaft speeds than higher speeds. Rotating speeds have very little effect on the critical frequencies; however with increasing speed, amplitudes are lowered due to gyroscopic effect.

Scope for Further Research

The present work is based on estimating the critical frequencies of non-uniform shaft-rotors based on Euler-Bernoulli beam theory. Moreover, various vital parameters such as rotational speeds and shaft lengths affecting the frequency response of shaft-rotor system have been discussed in details. However, the present study can be extended for further research as pointed out below.

- Timoshenko beam theory can be used for vibration analysis instead of using Euler-Bernoulli beam theory.
- Effects of bearings may be included in the problem.
- Rotors with crack may be analyzed.
- The same analysis can be used for simply-supported and other such boundary conditions.
- Geared systems and their effects can be included in the problem.
- Other rotary elements can be mounted instead of discs and further calculations can be made.
- Functionally Graded Material and Composite Shafts can be analysed with the help of finite element models.

References

1. Genta G., Dynamics of Rotating Systems, *Mechanical Engineering Series*, Springer, New York, 2005.
2. Whalley R., Abdul Ameer A., "Whirling prediction with geometrical shaft profiling", *Applied Mathematical Modelling*, vol. 33, pp.3166-3177, 2009.
3. Myklestad N. O., "New Method of Calculating Natural Modes of Coupled Bending-Torsion Vibration of Beams", *Trans. ASME*, pp. 61-67, 1945.
4. Prohl M. A., "A General Method for Calculating Critical Speeds of Flexible Rotors", *Trans. ASME*, vol. 66, pp. A-142-A-148, 1945.
5. Jeffcott H., "The Lateral Vibration of Loaded Shaft in Neighbourhood of a Whirling Speed - The Effect of Want of balance" *Phil. Mag*., vol. 37, pp. 304-314, 1919.
6. Dunkerley, S., "On the whirling and vibration of shafts", *Philosophical Transactions, vol.*A , pp. 185-279, 1894.
7. Myklestad N. O., "A new method for calculating natural modes of uncoupled bending vibration of airplane wings", *J. Aeronaut. Sci.*, pp. 153–162, 1944.
8. Lund J. W., "Stability and Damped Critical Speeds of a Flexible Rotor in Fluid-Film Bearings", *J. of Engineering for Industry, Trans. ASME*, Series B, vol. 96(2) , pp. 509-517, 1974.
9. Murphy B. T., Vance, J. M., "An improved method for calculating critical speeds and rotor dynamic stability of turbo machinery", ASME *Journal of Engineering for Power*, vol. 105, pp. 591-595, 1983.
10. El-Marhomy AbdAlla, EldinNasar, Sattar Abdel, "Stability analysis of rotor-bearing systems via Routh-Hurwitz criterion", *Journal of Applied Energy*, vol. 77, pp. 287–308, 2004.
11. Hsieh, Sheng-Chung, Chen Juhn-Horng, Lee An-Chen , "A modified transfer matrix method for the coupling lateral and torsional vibrations of symmetric rotor-bearing systems", *Journal of Sound and Vibration*, vol. 289, pp. 294–333, 2006.
12. Ruhl R. L., J. F. Booker., "A Finite Element Model for Distributed Parameter Turborotor Systems", *J. Eng. for Industry*, vol. 94(1), pp. 126-133, 1972.
13. Thorkildsen T., "Solution of a distributed mass and unbalanced rotor system using a consistent mass matrix approach", *MSE Engineering Report*, Arizona State University, 1972.
14. Nelson H. D., McVaugh J.M., "The dynamics of rotor-bearing systems using finite elements", *Trans. ASME J.Eng.*, vol. 98, pp. 593–600, 1976.

15. Nelson H. D., “A Finite Rotating Shaft Element Using Timoshenko Beam Theory”, J. Mech. Des., vol. 102(4), pp. 793-803, 1980.

16. Chen L.W. and Ku D. M., “Finite element analysis of natural whirl speeds of rotating shafts”, Comput.& Structures, vol. 40, pp. 741-747, 1991.

17. Nevzat Ozguven H. and Levent Ozkan Z., “Whirl speeds and unbalance response of multibearing rotors using finite elements”, J. Vibration Acoustics, vol. 106, pp. 72-79, 1984.

18. Zorzi E.S. and Nelson H.D., “Finite Element Simulation of Rotor-Bearing Systems with Internal Damping”, Journal of Engineering for Power, Transactions of the ASME, vol. 99, pp. 71-76, 1977.

19. Rouch K.E., Kao J.S, “Dynamic reduction in rotor dynamics by the finite element method”, *Trans. ASME, J. Mech. Design,* vol. 102 , pp. 360–367, 1980.

20. Kim Y.D., Lee C.W., “Finite element analysis of rotor bearing systems using a modal transformation matrix”, J. *Sound Vibration*, vol. 111 (3), pp. 441–456, 1986.

21. Kalita Madhumita., Kakoty S.K.., “Analysis of whirl speeds for rotor-bearing systems supported on fluid film bearings”, *Mechanical Systems and Signal Processing*, vol. 18(6), pp. 1369–1380, 2004.

22. Khulief Y.A., Mohiuddin M.A., “On the dynamic analysis of rotors using modal reduction”, *Finite Elements in Analysis and Design*, vol. 26, pp.41-55, 1997.

23. Khulief Y.A., Al-Naserb H., “Finite element dynamic analysis of drillstrings”, *Finite Elements in Analysis and Design*, vol. 41, pp. 1270–1288, 2005.

24. Laszlo Forrai,”A Finite Element Model for Stability Analysis of Symmetrical Rotor Systems with internal Damping”, *Journal of computational and applied mechanics*, vol.1, pp. 37-47, 2000.

25. Aleyaasin M., Ebrahimi M., “Flexural vibration of rotating shafts by frequency domain hybrid modelling”, Compute. *Struct*., vol. 79 (39) , pp. 319–331, 2000.

26. Aleyaasin M., Ebrahimi M., “Vibration analysis of distributed-lumped rotor systems”, *Comput. Methods Appl. Mech. Engg*.vol. 189, pp. 545-558, 2000.

27. Lee C. W., Katz R., Ulsov A. G. and Scott R. A., “Modal analysis of a distributed parameter rotating shaft”, *Journal of Sound and Vibration*, vol. 122(1), pp. 119-130, 1988.

28. Katz R., Lee C. W., Ulsoy A. G. and Scott R. A., “The dynamic response of a rotating shaft subject to a moving load”, *Journal of Sound and Vibration*, vol. 122(1), pp. 131-148, 1988.

29. Katz R., “The dynamic response of a rotating shaft subject to an axially moving and rotating load”, *Journal of Sound and vibration*, vol. 246(5), pp. 757-775, 2001.

30. Ku D. M., “Vibration analysis of distributed-lumped rotor systems”, *Comput. Methods Appl. Mech. Engrg*., vol. 189, pp. 545-558, 2000.

31. Greenhill L. M., Bickford W. B. and Nelson H. D., “A conical beam finite element for rotor dynamics analysis”, *Journal of Vibration, Acoustics, Stress, and Reliability in Design*, vol. 107, pp. 421-430, 1985.

32. Genta G., Gugliotta A., “A conical element for finite element rotor dynamics”, *Journal of Sound and Vibration*, vol. 120, pp. 175-182, 1988.

33. Agostini, C.E., Capello Souza, E.A., “Complex modal analysis of a vertical rotor by finite elements method”, *Proceedings of the 9th Brazilian Conference on Dynamics Control and their Applications* (*DINCON’10*), Serra Negra, pp. 2178-3667, June 07-11, 2010.

34. Gmur T.C. and Rodrigues J.D., “Shaft finite elements for rotor dynamics analysis”, *J. Vibration Acoustics*, vol. 113, pp. 482-493, 1991.

35. Mohiuddin M.A., Khulief Y.A., “Modal characteristics of rotors using a conical shaft finite element”, *Comput. Methods Appl. Mech. Engrg*.vol. 115, pp. 125-144, 1994.

36. Mohiuddin M. A., Khulief Y. A., “Modal characteristics of cracked rotor using a conical shaft finite element”, *Computer Methods in Applied Mechanics and Engineering*, vol. 162, pp. 223-247, 1998.

37. Edney S. L., Fox H.J. and Williams E.J., “Tapered Timoshenko finite elements for rotor dynamics analysis”, *Journal of Sound and Vibration*, vol. 137(3), pp. 463-481, 1990.

38. Fertis Demester G., Mechanical and Structural Vibrations, John Wiley and Sons Inc., 1995.

39. Rao J.S., Rotor Dynamics, New Age International Publishers, New Delhi, pp. 146–266.

40. Groover G. K., Mechanical Vibrations, Seventh Edition, Nem Chand & Bros., Roorkee, India, 2001.

41. Cem Ece Mehmet, Aydogdu Metin and Taskin Vedat, “Vibration of a variable cross-section beam”, *Mechanics Research Communications*, vol. 34, pp. 78–84, 2007.

42. Tong X., Tabarrok B., Yeh K. Y., “Vibration analysis of Timoshenko beams with non-homogeneity and varying cross-section”, *Journal of Sound and Vibration*, vol. 186(5), pp. 821-835, 1995.

43. Abrate Serge, “Vibration of non-uniform rods and beams”, *Journal of Sound and Vibration*, vol. 185(4), pp. 703-716, 1995.

44. De Rosa M. A. and Auciello N. M., “Free vibrations of tapered beams with flexible ends”, *Compurers&Strucrures*, vol. 60(2), pp. 197-202, 1996.

45. Attarnejad R., Shahba A. and Eslaminia M., “Dynamic basic displacement functions for free vibration analysis of tapered beams”, *Journal of Vibration and Control*, vol. 17(14) , pp. 2222–2238, 2011.

46. Grossi R. 0., Bhat R. B., “A note on vibrating tapered beams”, *Journal of Sound and Vibration*, vol. 147(l), pp. 174-178, 1991.

47. Auciello N. M., Ercolano A., “Exact solution for the transverse vibration of a beam a part of which is a taper beam and other part is a uniform beam”, *Int. J. Solids Structures*, vol. 34(17), pp. 2115-2129, 1997.

48. Larisse Klein, “Transverse vibrations of non-uniform beams”, *Journal of Sound and Vibration*, vol. 37(4), pp .491-505, 1974.

49. Lee S.Y., Ke H.Y and Kuo Y.H., “Analysis of non-uniform beam vibration”, *Journal of Sound and Vibration*, vol. 142(l), pp. 15-29, 1990.

50. Lee S.Y., Ke H.Y., “Free vibrations of a non-uniform beam with general elastically restrained boundary conditions”, *Journal of Sound and Vibration*, vol. 136(3), pp. 425-437, 1990.

51. Laura P. A. A., Valerga de Greco B., Utjes J.C., Carnicer R., “Numerical experiments on free and forced vibrations of beams of non-uniform cross-section”, *Journal of Sound and Vibration*, vol. 120(3), pp. 587-596, 1988.

52. Zheng D. Y., Cheung Y. K., Au F. T. K. and Cheng Y. S., “vibration of multi-span non-uniform beams under moving loads by using modified beam vibration functions”, *Journal of Sound and Vibration*, vol. 212(3), pp. 455-467, 1998.

53. Dugush Y. A. and Eisenberger M., “Vibrations of non-uniform continuous beams under moving loads”, *Journal of Sound and vibration*, vol. 254(5), pp. 911-926, 2002.

54. Esmailzadeh F. and Ohadi A. R., “Vibration and stability analysis of non-uniform timoshenko beams under axial and distributed tangential loads”, *Journal of Sound and vibration*, vol. 236(3), pp. 443-456, 2000.

55. Li Q. S., “Free vibration analysis of non-uniform beams with an arbitrary number of cracks and concentrated masses”, *Journal of Sound and vibration*, vol. 252(3), pp. 509-525, 2002.

56. Kumar B. M. and Sujith R. I., “Exact solutions for the longitudinal vibration of non-uniform rods”, *Journal of Sound and Vibration*, vol. 207(5), pp. 721-729, 1997.

57. Li Q. S., “exact solutions for free longitudinalvibrations of non-uniform rods”, *Journal of Sound and Vibration*, vol. 234(1), pp. 1-19, 2000.

58. Irie T., Yamada G. and Takahashi I., “Vibration and stability of a non-uniform Timoshenko beam subjected to a follower force”, *Journal of Sound and Vibration*, vol. 70(4), pp. 503-512, 1980.

59. Rouch K. E., Kao J. S., “A tapered beam finite element for rotor dynamics analysis”, *Journal of Sound and Vibration*, vol. 66, pp. 119-140, 1979.

60. Abramowitz and Stegun, Handbook of Mathematical Functions with Formulas, Graphs, and Mathematical Tables, 1970.

Publications

International journals:

1. "Vibration Analysis of Multi-Disk Profiled Shaft-Rotor System", *International Journals of Advances in Management, Technology & Engineering Sciences (IJAMTES)*, vol. II, Issue 8(III), May 2013.
2. "Vibration Analysis of Hollow Tapered Shaft-Rotor", *Advances in Acoustics and Vibrations*, Hindawi Pub. Corp., Volume 2014, Article ID 410851, 14 pages.
3. "Vibration Analysis of Multi-disc Multi-profiled Shaft-rotor Systems", *Applied Mechanics and Materials*, Trans Tech Pub., vol. 612, 2014.

International conferences:

1. "Profiled Shaft and Rotor Dynamics", *1st International and 16th National Conference on Machines and Mechanisms (iNaCoMM2013)*, Dec 18-20 2013, IIT Roorkee.
2. "Vibration Analysis of Multi-Disk Profiled Shaft-Rotor System", *International Conference on Changes & Challenges in Commerce, Engineering, Technology and Social Sciences*, 25th May, 2013 , MCCIA, Pune.
3. "Vibration Analysis of Tubular Profiled Shafts", *International Conference on Design, Manufacturing and Mechatronics [ICDMM 2014]*, 09-10 Jan, 2014, Trinity College of Engineering and Research, Pune.
4. "Vibration Analysis of Hollow Profiled Shafts", *International Conference on Design, Manufacturing and Mechatronics [ICDMM 2014]*, 09-10 Jan, 2014, Trinity College of Engineering and Research, Pune.
5. "Vibration Analysis of Convergent-Divergent Shaft-Rotor System ", *International Conference on Design, Manufacturing and Mechatronics [ICDMM 2014]*, 09-10 Jan, 2014, Trinity College of Engineering and Research, Pune.
6. "Vibration Analysis of Multi-disc Multi-profiled Shaft-rotor Systems ", *International Conference on Design, Manufacturing and Mechatronics [ICDMM 2014]*, 09-10 Jan, 2014, Trinity College of Engineering and Research, Pune.

National Conferences:

1. "Rotor Dynamics and Hollow Tapered Shafts", *11th National Conference on Industrial Problems on Machines and Mechanisms (IPRoMM-2014)*, February 26-27, 2014, ITS Noida